Max-Planck-Institut
für Meteorologie

MAX-PLANCK-GESELLSCHAFT

International Max Planck Research School
on Earth System Modelling

Connections of low level jets and mesoscale convective systems in South America

Armelle Reca C. Remedio

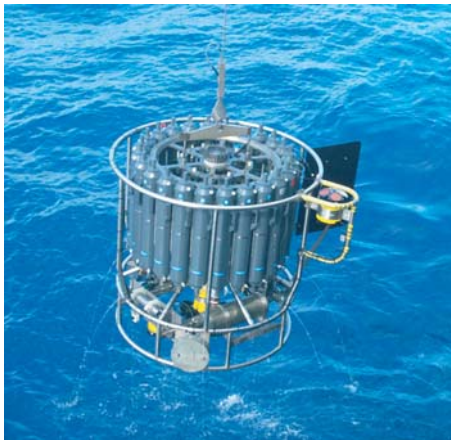

Berichte zur Erdsystemforschung 141/2013

Reports on Earth System Science

Hinweis

Die Berichte zur Erdsystemforschung werden vom Max-Planck-Institut für Meteorologie in Hamburg in unregelmäßiger Abfolge herausgegeben.

Sie enthalten wissenschaftliche und technische Beiträge, inklusive Dissertationen.

Die Beiträge geben nicht notwendigerweise die Auffassung des Instituts wieder.

Die "Berichte zur Erdsystemforschung" führen die vorherigen Reihen "Reports" und "Examensarbeiten" weiter.

Notice

The Reports on Earth System Science are published by the Max Planck Institute for Meteorology in Hamburg. They appear in irregular intervals.

They contain scientific and technical contributions, including Ph. D. theses.

The Reports do not necessarily reflect the opinion of the Institute.

The "Reports on Earth System Science" continue the former "Reports" and "Examensarbeiten" of the Max Planck Institute.

Anschrift / Address

Max-Planck-Institut für Meteorologie
Bundesstrasse 53
20146 Hamburg
Deutschland

Tel.: +49-(0)40-4 11 73-0
Fax: +49-(0)40-4 11 73-298
Web: www.mpimet.mpg.de

Layout:

Bettina Diallo, PR & Grafik

Titelfotos:
vorne:
Christian Klepp - Jochem Marotzke - Christian Klepp
hinten:
Clotilde Dubois - Christian Klepp - Katsumasa Tanaka

Berichte zur Erdsystemforschung 141/2013

Connections of low level jets and mesoscale convective systems in South America

Armelle Reca C. Remedio

Manolo Fortich, Bukidnon, Philippinen

Hamburg 2013

Reports on Earth System Science 141/2013

ISSN 1614-1199

Armelle Reca C. Remedio
Max-Planck-Institut für Meteorologie
Bundesstrasse 53
20146 Hamburg

Als Dissertation angenommen
vom Department Geowissenschaften der Universität Hamburg

auf Grund der Gutachten von
Prof. Dr. Hartmut Graßl
und
Dr. Daniela Jacob

Hamburg, den 1. Juli 2013
Prof. Dr. Jürgen Oßenbrügge
Leiter des Departments für Geowissenschaften

ISSN 1614-1199

Connections of low level jets and mesoscale convective systems in South America

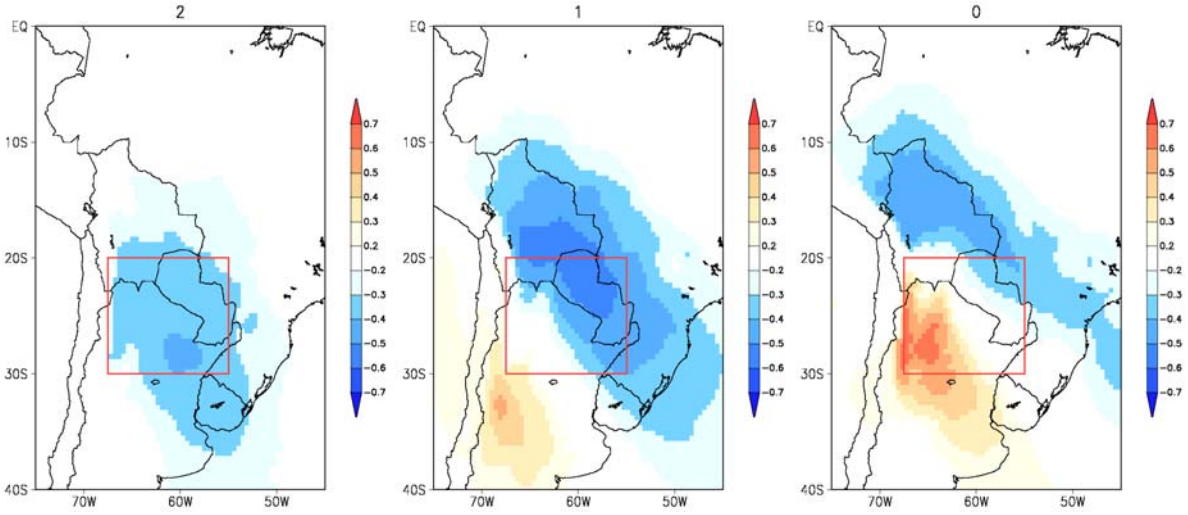

Armelle Reca C. Remedio

Hamburg 2013

"There can never be any real opposition between religion and science;
for the one is the complement of the other.
Every serious and reflective person realizes, I think,
that the religious element in his nature must be recognized
and cultivated if all the powers of the human soul are
to act together in perfect balance and harmony. And indeed it was
not by accident that the greatest thinkers of all ages
were deeply religious souls."
Max Planck (1858-1947)

Abstract

The majority of the human population and socio-economic resources in South America are located in La Plata Basin. During austral summer, large mesoscale convective systems (MCSs) are associated with strong low level jets (LLJs) that develop east of the Andes mountain range. Over the basin, the mature phase of MCS brings excessive amounts of rainfall that cause severe weather events such as thunderstorms, hail, and flooding. Due to its dire consequences, it is crucial to understand the relationship between LLJs and MCSs. The study aims to assess the long term role of the MCSs and LLJs in South America by characterizing their spatial and temporal characteristics and quantifying the correlation between these two systems.

The state-of-the-art tool used for analyzing the processes of LLJs and MCSs is the three-dimensional, hydrostatic, regional climate model REMO. The model's horizontal grid resolution in the rotated coordinated system is 0.44° (about 50 km) and the domain covers the entire continent with 31 vertical levels. The default model version is REMO2009, which has been modified due to the overestimation of the surface temperature over the Amazon basin during austral spring. Short sensitivity tests are performed using REMO2009 with varying values and coverage of the permanent wilting point parameter, which influences the water holding capacity of the vegetation in the selected region. The setup in which the permanent wilting point parameter is set to 10% in the forested regions exhibits the most realistic decrease of surface temperature ($\sim$3 K) in terms of affected regions. This modified REMO is able to simulate the climatic features of South America, thus it is used as a reasonable tool for the analysis.

Using observational datasets from stations, reanalyses, and satellite estimates with varying horizontal resolution, and the high resolution REMO simulation data, the spatial and temporal characteristics of LLJs and MCSs are investigated. During austral summer, the LLJs modulate the climate by transporting warm and moist air from the Amazon to the La Plata Basin. At the exit region of the LLJs, the MCSs initiate and develop, which bring heavy precipitation events. Regions with high frequency of LLJ and MCS occurrences are identified and the mean contribution of LLJs and heavy precipitation events associated with MCSs are from 30–50% and about 30%, respectively, relative to the summer mean. Evaluating the lead-lag correlation between the meridional wind speed and area-averaged precipitation over the La Plata Basin for several summer periods (e.g. summers with normal years,

ENSO warm, and cold phase years), a significant but weak negative correlation is calculated in both observations and simulation data two days before the anomalous rainfall. The negative correlation (∼–0.6, p=0.01) located near Bolivia strengthens the day before (Day 1) while a positive correlation (∼0.7, p=0.01) appears in central Argentina. These correlation values indicate a convergence of warm, moist air from the north and the cold, dry air from the southeast, which produce the heavy precipitation events the following day (Day 0). The significantly high correlation of anomalous meridional wind speeds the day before heavy precipitation events are good precursors for monitoring the severe weather events over the La Plata Basin.

Contents

1 Introduction

1.1 Climate in South America

The prominent topographic features in South America are the Amazon Basin and the Andes mountain range. Containing the dense rainforest and the world's largest river, the Amazon Basin provides a major source of water resources. The long (about 7,000 km extending from the northern tip to the southern tip of the continent) and narrow (with maximum heights reaching up to 6000 m) Andes Mountains act as a natural barrier for low level circulation patterns and aid in the poleward advection of moisture (Hobbs et al., 1998; Garreaud et al., 2009). These two topographic features make the continent immensely rich in biodiversity and the climate to vary from tropical, subtropical, and to polar climates near Antarctica.

Apart from the physical continental features, the climate of South America is also modulated by dominant atmospheric circulations over the continent. Figure 1.1 shows the location of two semi-permanent anti-cyclonic structures over the Atlantic and Pacific Ocean. Over the central part of the continent, the Bolivian High is present during austral summer due to deep convective activities. The low-level flow below the Bolivian High is responsible for the advection of moisture and heat from the Amazon Basin to the La Plata Basin, the second largest river basin (in terms of area) in the continent and the fifth[1] in the world. The trade winds also bring moisture from the Atlantic Ocean. Due to the diminishing land mass further south in the continent, the magnitude of the winds reaches up to 40 m/s, hence, they are often called as the "Roaring 40s" in the Southern Ocean.

Other large-scale circulations relevant in Figure 1.1 are the Intertropical Convergence Zone (ITCZ) and the South Atlantic Convergence Zone (SACZ), which are responsible for the region's rainy season (Vera et al., 2006b; Carvalho et al., 2004). The ITCZ is migratory and tends to be displaced northwards during the cold season (June to August) in the southern hemisphere. During the austral winter, the SACZ is responsible for the wintertime precipitation over the subtropical region. The cli-

[1]The five largest river basins in the world (according to area) are the: Amazon, Congo, Nile, Mississippi and La Plata. Source: Collins World Atlas, 2011.

mate variability of the region is also susceptible to the El Niño Southern Oscillations or ENSO, which brings severe floodings (droughts) during the warm (cold) phase (Grimm and Tedeschi, 2009).

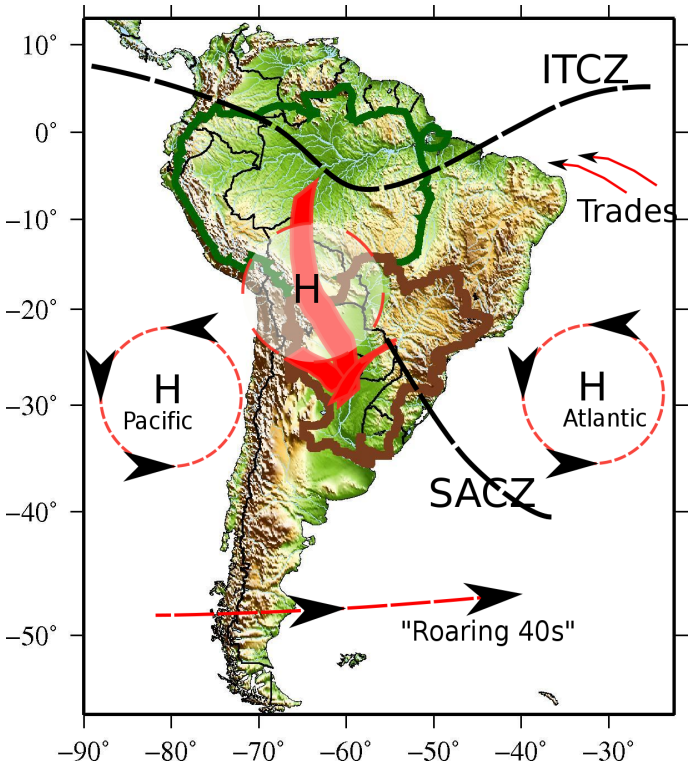

Figure 1.1: Schematic diagram of significant upper- and low-level atmospheric circulation features over the South American continent. The Bolivian High, which is the anticylconic upper-air circulation over Bolivia, 6 is depicted aloft the low level jet path (bold red arrow). The Amazon and La Plata Basins are delineated in green and brown lines, respectively. After Satyamurty et al. (1998).

The majority of the human population in South America resides in the La Plata Basin. The principal cities of the continent including Asunción, Brasilia, Sâo Paulo, Buenos Aires, and Montevideo are located within the vicinity of the basin. The economic resources of this basin are mainly agriculture and hydroelectric power production (Barros et al., 2006), which are largely dependent on the available water resources. Because of the basin's socio-economic significance, studies have considered La Plata as a system highly sensitive to climate variability and change e.g. Berbery et al. (2011).

The precipitation regimes over the La Plata basin are categorized into two parts depending on the location. The northern sector is influenced by the SACZ (Figure 1.1) while the southern sector has generally uniform precipitation but is fre-

quently affected by frontal systems (Cavalcanti, 2012). During austral summer, large mesoscale convective systems develop over the La Plata Basin and bring excessive amounts of rainfall that cause severe weather events suchs as flooding. These systems are associated with the low level flow that develops east of the Andes mountain range.

1.2 Mesoscale convective systems and low level jets

Understanding the relationship of mesoscale convective systems (MCSs) and low level jets (LLJs) is of great interest in South America. LLJs transport heat and moisture from the Amazon Basin down to the La Plata Basin (Marengo et al., 2004). At the exit region of LLJs, convective systems become more organized and form MCSs. MCSs are the main contributors of summertime precipitation and they also produce severe weather events such as lightning, flooding, hail, and storms (Houze, 2004).

Figure 1.2 illustrates the interaction between LLJs and MCSs over South America. Low-level winds passing through the Amazons are deflected by the orographic barrier. The low-level flow advects warm and moist air, which favor the organization of convection into MCSs. The occurrence of LLJs coupled with the downstream of a weak midlevel trough produce these severe convective weather events such as strong winds, hail, tornadoes, lightning, and flooding (Velasco and Fritsch, 1987; Zipser et al., 2004; Salio et al., 2007). Because of the long-lasting and contiguous regions of precipitation, MCSs are responsible for a large proportion of rainfall in tropical and warmer mid-latitudes. Furthermore, the organization and structure of these systems are quite complex but they generally involve two major processes that produce precipitation, the convective and stratiform one. These variabilities in the MCSs structures coupled with the extent and longevity of the systems lead to the variation of the upper level flow response to the MCSs. Thus, it is important to further understand and evaluate MCSs as the link between atmospheric convection and the large-scale atmospheric circulation.

Due to the significant occurrences of LLJs and MCSs and their possible devastating consequences in South America, two international research initiatives were under-

taken: the South American LLJ Experiment (SALLJEX)[2] and the CLARIS-LPB[3], A Europe-South America Network for Climate Change Assessment and Impact Studies in the La Plata Basin. The goals of the two projects are mentioned in the following sub-sections.

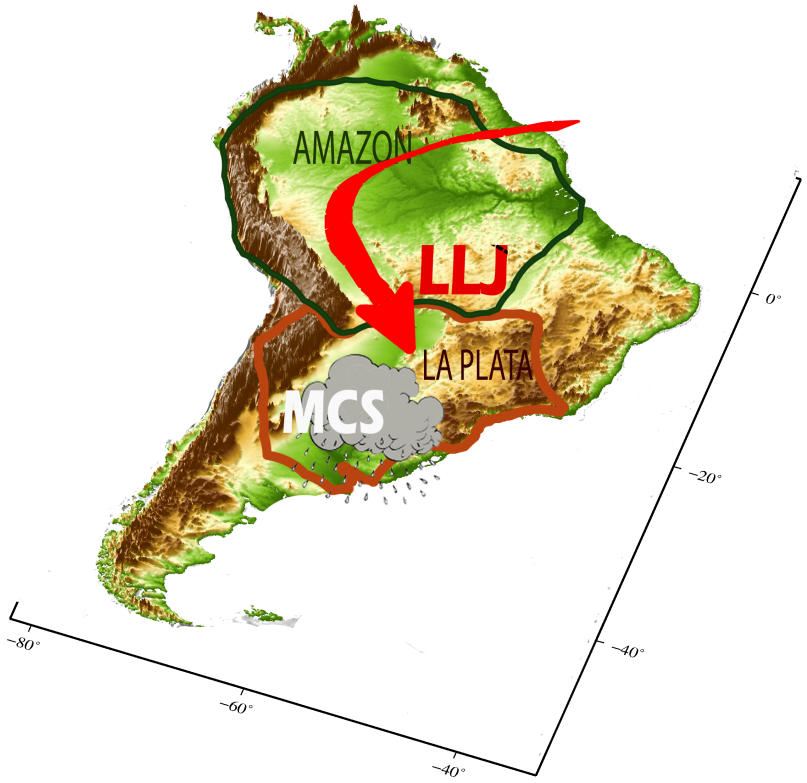

Figure 1.2: Schematic diagram of the role of the low-level jet (LLJ) in transporting moisture from the Amazons down to the La Plata Basin and in the development of mesoscale convective systems (MCSs). The LLJ is depicted as a ribbon-like flow of air with a wind maximum frequently detected at the pressure level of 850 hPa. The Amazon and La Plata Basins are delineated in green and brown lines, respectively. After Vera et al. (2006a).

1.2.1 SALLJEX (2002–2003)

The role of LLJs in the region's hydrological cycle and water exchanges between the Amazon Basin and the La Plata Basin was analyzed in the intensive campaign of SALLJEX during the austral summer of 2002–2003. The SALLJEX was the first World Climate Research Programme/Climate Variability and Predictability (WCRP/CLIVAR) study campaign in South America (Carson et al., 2004). Sci-

[2]http://www.eol.ucar.edu/projects/salljex
[3]http://www.claris-eu.org

entists, collaborators, students, government personnel, and local volunteers from Argentina, Brazil, Bolivia, Paraguay, Chile, Uruguay, Peru, and the USA participated in this coordinated effort to improve the understanding of the LLJ using the following strategies:

> *"i) obtain an improved description of the temporal and spatial structure of the SALLJ based on expanded monitoring activities and special field experiments; ii) evaluate the veracity of numerical representation (forecasts and analyses) of SALLJ against special observations; and iii) determine improvements to initial state representation and model parameterizations required to improve prediction"* (Vera et al., 2004).

In this dissertation, data from the SALLJEX campaign are used to evaluate short-term simulations.

1.2.2 CLARIS-LPB (2008-2012)

The CLARIS-LPB Project was a 4-year project of an integrated European–South American research network fostering collaborations on regional climate changes and their socio-economic impacts in the La Plata Basin. This project was the continuation of a previous European-commissioned project, the CLARIS Project (Boulanger et al., 2009), which aimed to perform climate studies and climate change impacts on the whole continent of South America.

The overarching goals of this project were "*improving predictions of the climatic and hydrologic system, and designing adaptation strategies for land-use, agriculture, rural development, hydropower production, river transportation, water resources and ecological systems in wetlands in the La Plata Basin*"(Berbery et al., 2011). Some of the specific goals of the project were to assess the regional climate change (Solman et al., 2011) and to evaluate the processes and future evolution of extreme climate events (Cavalcanti et al., 2011), particularly in the La Plata Basin. In order to assess the regional climate change over the basin, an ensemble of coordinated regional climate scenarios for dynamical downscaling was organized to characterize the uncertainties in reproducing the observed and future climate from the regional model simulations. Experiments were performed to analyze the present climate as well as climate change studies due to anthropogenic forcings.

The capability of a 7-member ensemble of RCMs to simulate the present climate were evaluated first to ascertain the uncertainties, strengths, and shortcomings of

the models. The design of the experiments followed the proposed setup of the COordinated Regional Downscaling EXperiment (CORDEX) Initiative (Giorgi et al., 2008, 2009). The seven regional climate simulations from state-of-the-art regional models (including the model used in this dissertation) and a stretched-grid global model are presented in Table C.1 in the Appendix C.

The participation in the CLARIS-LPB Project is of great importance for this dissertation especially in the evaluation of model performance for the analysis of mesoscale and regional scale atmospheric motions.

1.3 Motivation and research objectives

Based on the Integovernmental Panel on Climate Change (IPCC)[4] Fourth Assessment Report (AR4), the forecasts for the climate of South America, particularly in the La Plata Basin were: "*likely that there would be increases in droughts, intense tropical cyclones and extreme high sea level, very likely that warm spells and heavy precipitation events would increase and virtually certain that there would be more warm nights and fewer cold nights at the end of the twenty-first century compared to the end of the twentieth century*" (Christensen et al., 2007). Extreme precipitation events over the basin can cause severe damage in the region such as flooding and landslides, which pose detrimental effects to the densely populated area. In this regard, before addressing the effects of climate change in the basin, it is necessary to study the mechanisms that produce these extreme convective events.

Several case studies have already attempted to analyze the synergism of LLJs and MCSs. These detailed studies, which are further described in the individual chapters, emphasize the characteristics and variability of LLJs and MCSs but only in a short period or using a coarse resolution reanalysis. The contribution of this study is the long-term analysis of LLJs and MCSs characteristics using reanalysis and high resolution regional climate simulations. The results of this study could be used to set up an observational system for monitoring the LLJ and MCS in preparation for extreme events.

[4] http://www.ipcc.ch/

In the course of the dissertation study, the following questions are investigated:

- What is the role of the MCSs and LLJs in South America?
- How do LLJs modulate the climate of South America?
- How do the MCSs form and how frequently do they occur?
- How strong is the correlaton between the LLJs and MCSs during austral summer?

The structure of the thesis is the following:

- Chapter 2 describes the regional model used in this study along with the modifications to adapt the model to the region of interest;
- Chapter 3 analyzes the characteristics of LLJs using different definition criteria;
- Chapter 4 investigates the MCSs over the La Plata Basin;
- Chapter 5 quantifies the correlation between LLJs and MCSs; and finally
- Chapter 6 summarizes the major conclusions and open questions for further study.

2 The Regional Climate Model

2.1 Introduction

Regional Climate Models (RCMs) are state-of-the-art tools used for understanding the climates of the past, present and future at regional and local scales. With high spatial and vertical resolution, RCMs are able to resolve important atmospheric processes that affect the regional climate (Jacob et al., 2001; Giorgi et al., 2008, 2009). In a detailed assessment of the status of climate models by Bader et al. (2008), processes resolved by RCMs include the jet stream activity, tropical storms, and orographic effects. Currently, RCMs are widely used for regional climate studies especially in areas where observational datasets are sparse, for assessments of climate change, and applications for impact studies such as hydrological and agricultural modelling.

The regional climate model REMO (Jacob and Podzun, 1997; Jacob, 2001; Jacob et al., 2001) is a three-dimensional, hydrostatic, atmospheric circulation model, which solves the discretized primitive equations of atmospheric motion within a limited area. The dynamical core of REMO is based on the Europa-Modell (EM), the former numerical weather prediction model of the German Weather Service (Majewski, 1991). The physical parameterization package of the current REMO version is taken from the general circulation model ECHAM4/5 (Roeckner et al., 1996, 2003) with some modifications.

As a limited area model, REMO is forced with initial and lateral boundary conditions such as temperature, winds, moisture, and surface pressure. The boundary conditions of REMO are derived from global circulation models for climate change simulations or from reanalyses for hindcast simulations. A relaxation scheme (Davies, 1976) is used to adjust the prognostic variables towards the boundary forcing in a zone of eight lateral grid boxes. At the lower atmospheric boundary, REMO is driven by the land surface characteristics over land, and by the sea surface temperature and sea ice distribution over sea. The sea surface temperature is obtained either from the large-scale forcing, observational datasets, or calculated online by a

regional ocean model coupled to REMO (Aldrian et al., 2005; Elizalde, 2011). The model can be integrated in a forecast or climate mode. In the climate mode, the influence of the driving fields is weaker compared to the forecast mode.

The atmospheric prognostic variables of REMO are the zonal and meridional winds, surface pressure, temperature, specific humidity, cloud ice, and cloud liquid water. The discretization through time utilizes the leap-frog scheme with semi-implicit correction and time filtering to minimize numerical effects (Asselin, 1972). The momentum, temperature, and water content equations use a linear fourth-order horizontal diffusion scheme. The transfer coefficients of momentum, heat, moisture, and cloud water in the planetary boundary layer are calculated for the vertical diffusion and turbulent surface fluxes using the Monin-Obukhov similarity theory (Louis, 1979) with a higher order closure scheme. The eddy diffusion coefficients are calculated as functions of the turbulent kinetic energy.

The REMO modelling system integrates the input data from the native pressure levels to the model's vertical and horizontal coordinate system. The vertical grid of the model is a hybrid coordinate system (Simmons and Burridge, 1981). At the surface or the k-th model level, the pressure is equal to the surface pressure (p_s) and follows the terrain (Figure 2.1). The orography at the surface strongly influences the lowest vertical level ($n = k$) while at the upper levels, the orographic influence weakens and the pressure levels become more homogeneous. At the uppermost level ($n = 1$), the pressure is equivalent to the pressure at the top (p_T). The prognostic variables (φ) are simulated at full-levels in the center of each model layer while the vertical velocities (ω) are calculated at half-layers or at the layer interfaces.

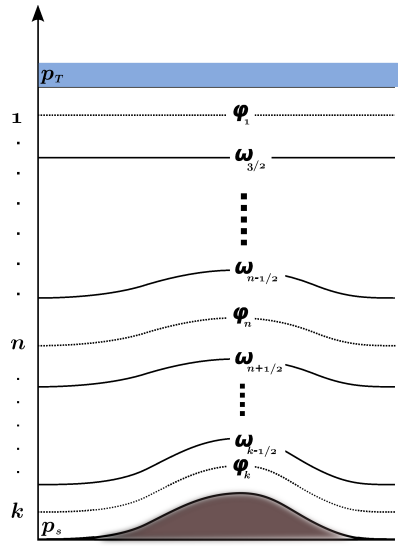

Figure 2.1: Schematic diagram of the vertical structure of the model. The hybrid coordinate system has vertical grids from the pressure at the top ($n = 1$) down to the pressure at the surface ($n = k$). Scalar values (φ) are calculated at the center of the layers ($n = 1, ..., k$, dotted lines). Vertical velocities (ω) are calculated at the layer boundaries ($n = 3/2, ..., k - 1/2, k + 1/2$, solid lines).

In terms of the horizontal coordinate system, REMO utilizes the Arakawa-C grid

(Arakawa, 1988), where the scalar variables except the winds are defined at the centers of each respective grid box (Figure 2.2). The map projection is a rotated latitude/longitude grid with grid spacing ranging from 0.5° to 0.088° in hydrostatic mode, and 0.088° or less in non-hydrostatic mode. This projection is a spherical coordinate system derived from the geographic coordinate system by certain rotations using the Eulerian angles. The rotations move the geographic North Pole to a new position relative to the domain of interest and the rotated equator coincides with the center of the model domain.

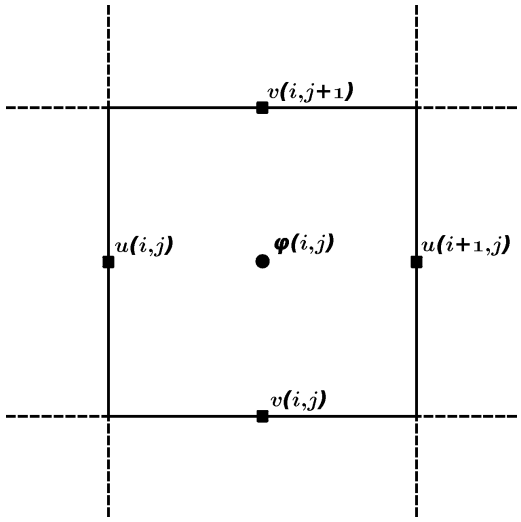

Figure 2.2: Schematic diagram of an Arakawa-C grid box (top-view). Scalar values (φ) are defined at the center of the grid boxes, while wind-vector components (u, v) are located at the borders of the grid boxes. The i, j indices correspond to the grid in the x- and y-direction, respectively.

The physical parameterizations of REMO, which are based on the Max Planck Institute for Meteorology global climate model ECHAM4 (Roeckner et al., 1996), have been modified in the recent years. A subgrid-scale tile approach for land, water and sea ice surfaces is implemented (Semmler, 2002). Cumulus convection is calculated using the mass flux convection scheme after Tiedtke (1989) with modifications after Nordeng (1994). The scheme has been extended to account for convection due to cold air outbreaks connected to extratropical cyclones (Pfeifer, 2006). The statiform cloud scheme is composed of prognostic equations for the vapor, liquid, and ice phase and a cloud microphysical scheme by Lohmann and Roeckner (1996). The radiation scheme is calculated after Morcrette et al. (1986) with modifications for additional greenhouse gases, the 14.6 μm band of ozone, and various types of aerosols. The land surface and atmosphere interactions include an improved surface runoff scheme (Hagemann and Dümenil, 2003), inland glaciers (Kotlarski, 2007), and vegetation phenology (Rechid and Jacob, 2006). The soil hydrology is represented by a bucket scheme, in which a bucket exists at each model grid point and the depth of the bucket is equivalent to the mean rooting depth of the grid box (Kotlarski, 2007; Haensler et al., 2011).

REMO has demonstrated reasonable skill in simulating the regional climatic characteristics in different regions of the globe including South America (Jacob et al.,

2012). Examples of these process studies include the simulations of the precipitation in water isotopes (Sturm et al., 2007), air pollution in megacities (Teichmann, 2010), and the mean climate state of the whole continent (Silvestri et al., 2008), particularly in the Colombian-Caribbean Catchment Basin (Hoyos et al., 2013). The aforementioned studies use an older version of REMO. With the recent version of REMO, simulations are performed to investigate the climate of South America particularly on the interactions between tropospheric circulations and large convective systems. The goals of this chapter are to introduce the latest model version, the model setup, and the modifications done in the land surface scheme to improve the representation of the South American climate. The skill of REMO in representing the different regions based on hydrological sub-basins and climate characteristics is also evaluated.

2.2 Experimental setup

2.2.1 Changes in the land surface scheme

Vegetation cover plays an important role in defining the surface energy budget and influences the near surface atmosphere. The main interactions between the atmosphere and the land surface are parameterized in five ways: evapotranspiration, momentum transfer, soil moisture availability, radiative fluxes, and insolation (Stensrud, 2007). In the current section, changes in the land surface scheme are applied to the parameterization of the soil moisture availability. Several studies showed a linear correlation between soil water content in the root-zone and the daily maximum values of sensible heat flux and latent heat flux such as the observational study of Basara and Crawford (2002). Vegetation type, density, and variability influence the release of latent heat fluxes since vegetation is able to tap into deep moisture sources.

The REMO land surface scheme has been briefly introduced in Section 2.1. After the preprocessing stage in REMO, the vegetation land cover within a grid box is described by the ratio of one-sided leaf area to ground area or leaf area index (LAI), fraction of green vegetation cover, background surface albedo, surface roughness length due to vegetation, fractional forest cover, and water holding capacity (ω_{cap}) depending on plant rooting depths. The monthly fields of LAI, fractional green vegetation cover, and background surface albedo provide the annual vegetation cycle

without interannual variability (Rechid and Jacob, 2006; Rechid, 2009).

In South America, the climate is strongly influenced by the Amazon rainforest, which is a main source of evapotranspiration. Li and Fu (2004) highlighted the importance of the surface evapotranspiration and large-scale moisture transport in determining the onset of the wet season over the Amazon Basin. Regional models as well as global models have difficulties in representing the land-atmosphere interaction within the Amazon basin. In Silvestri et al. (2008), a persistent overestimation of simulated temperature more than 5 $^{\circ}K$ over the Amazon region during spring was obtained. In that study, where they used an older version of REMO driven by the ERA-40 reanalysis within a 43-year period, a strong warm bias was calculated, although the simulated precipitation was comparable to observations.

In order to reduce the overestimation of surface temperature over the Amazon Basin, sensitivity studies are conducted by changing the permanent wilting point parameter. In the land surface scheme, the volumetric permanent wilting point (f_{pwp}) is defined as:

$$f_{pwp} = \frac{\omega_{cap} - \omega_{ava}}{\omega_{cap}} \tag{2.1}$$

where ω_{cap} is the maximum amount of water the soil can hold, f_{pwp} is the condition where plants can no longer extract water from the soil, and ω_{ava} is the difference of the two quantities. In REMO, as well as in the global model ECHAM, the f_{pwp} parameter is set to a constant value of 35%. Hagemann et al. (1999) suggested that the rooting depth can be extended by increasing the water holding capacity (ω_{cap}), which is parameterized in the ECHAM model using the available water capacity (ω_{ava}) and the permanent wilting point (f_{pwp}). Kleidon and Heimann (2000) emphasized the need to increase the rooting depth in the land surface scheme of the global model ECHAM to represent the deep roots especially in the Amazon Rainforest.

The hypothesis of the sensitivity study is that the surface warming during spring can be minimized by lowering the threshold of the permanent wilting point, hence, indirectly extending the rooting depth. Increasing the rooting depth especially in the Amazon Rainforest increases the access to stored water in the deep soil during dry periods and will lead via more transpiration to evaporative local cooling and moister air.

In order to indirectly extend the rooting depth in the model, the f_{pwp} is lowered from 35% to 10%. To verify the hypothesis, the f_{pwp} adjustments are first calculated over

the whole continent and last, on the forest-covered regions. Figure 2.3 shows the approximate location of the dense forest cover ($LAI \geq 8$), which is characterized in the model and depicted in green-shaded contours.

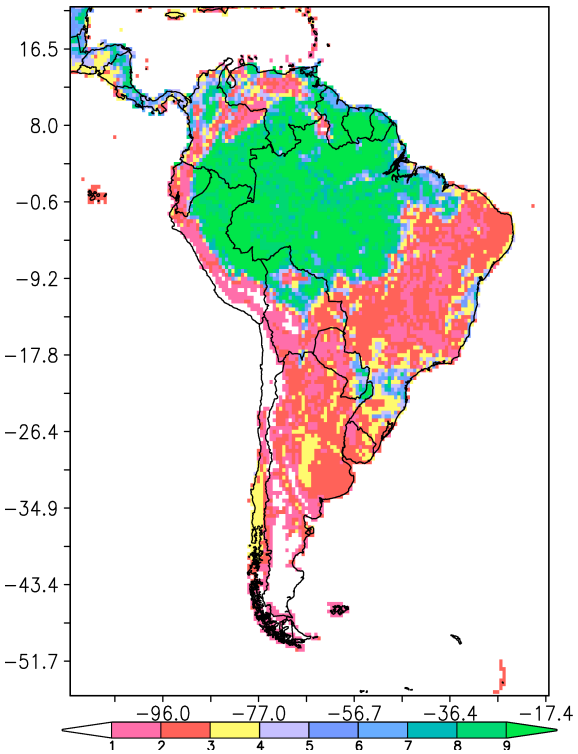

Figure 2.3: Leaf area index (LAI) parameter in the model in m^2/m^2. The geographical longitude and latitude are approximations in the rotated grid.

To calculate the f_{pwp} threshold value as a function of the LAI (Figure 2.3), the following conditional equations are added in the model:

$$f_{pwp} = \begin{Bmatrix} 0.35 \; \forall \; LAI < 8 \\ 0.10 \; \forall \; LAI \geq 8 \end{Bmatrix}. \tag{2.2}$$

2.2.2 Experiments

Short sensitivity studies listed in Table 2.1 are designed to test the hypothesis on how to reduce the warm bias over the Amazon region. The experiments modify the permanent wilting point parameter (f_{pwp}) from 35% (REMO_{CTRL}), 25% ($\text{REMO}_{0.25}$), and 10% ($\text{REMO}_{0.10}$). The last experiment ($\text{REMO}_{0.10forest}$) modifies the f_{pwp} at regions with high values of LAI (Equation 2.2). The f_{pwp} with the value of 10% means that 90% of the water holding capacity is potentially available for transpiration.

Table 2.1: Short sensivity experiments on the modification of the f_{pwp} parameter for a two-year period (1989-1990).

Experiment	f_{pwp}	Description
REMO_{CTRL}	35%	Control setup, Standard REMO
$\text{REMO}_{0.25}$	25%	f_{pwp} reduction over the whole domain
$\text{REMO}_{0.10}$	10%	f_{pwp} reduction over the whole domain
$\text{REMO}_{0.10forest}$	10%	f_{pwp} reduction over the forested region only and 35% for the rest

The model version used in the sensitivity study is **REMO2009** (Jacob et al., 2012). The horizontal grid resolution is 0.44×0.44 ° (approximately 50×50 $sq.\ km$) in the rotated coordinate system with the rotated North Pole located at 56.06 $°W$ and 70.6 $°N$. The size of the model domain, which covers the South American continent, contains 151×181 grid points and 31 vertical levels. The pressure at the top (p_T) is defined as 10 hPa. The model is integrated with a time step of 240 s. For the model to reach an equilibrium state, a spin-up period of 20 years is implemented.

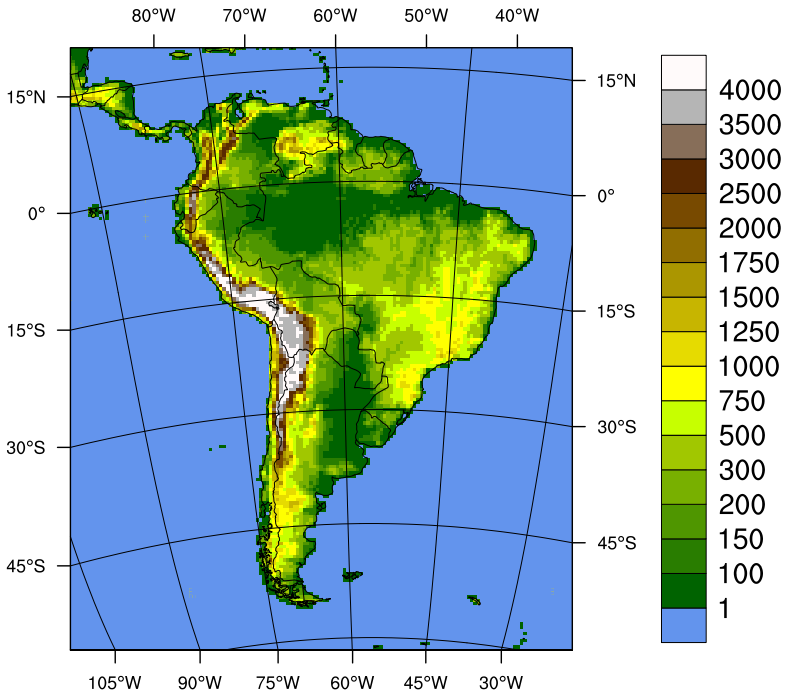

Figure 2.4: Model domain with orography in m.

Initial and lateral boundary conditions are driven by so-called "perfect" boundary conditions from the European Centre for Medium-Range Weather Forecasts (ECMWF) ERA-Interim Reanalysis (Dee et al., 2011), hereafter referred as **EITR**.

The simulation period for the sensitivity experiments is from 1989-1990. Figure 2.4 shows the model domain encompassing the South American continent and surrounding areas of Central America, and the Pacific and Atlantic Ocean. The Andes Mountain range flanks the western part of the continent with terrain heights reaching above 4,000 m.

2.2.3 Study regions

Within the CLARIS-LPB Project (cf. Chapter 1.2.2), the performance of REMO has been compared with other RCMs (cf. Table C.1). To compare regions with similar climate characteristics, several study regions are selected based on hydrological sub-basins and climate types (Figure 2.5). The regions have been used in providing a general overview of the the South American climate characteristics. The sub-basins of Paraguay, Uruguay, Upper and Lower Parana (Figure 2.5a) and the subtropical humid (Cr) climate type (Figure 2.5b) represent the La Plata Basin and these areas are used for further analysis in Chapter 4.

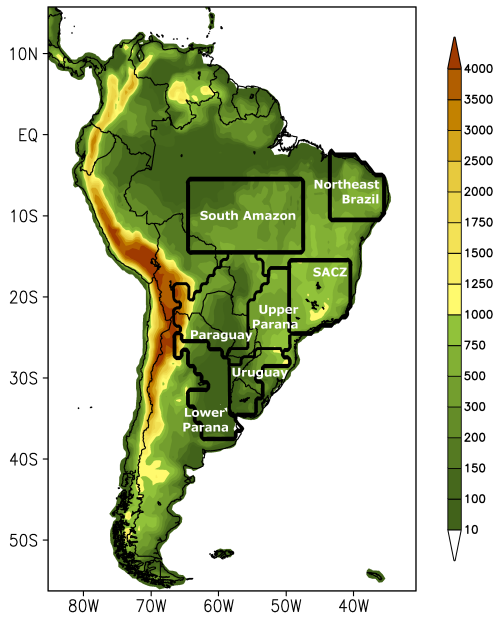

(a) Model domain with orography (m) and subregions. From Solman et al. (2013).

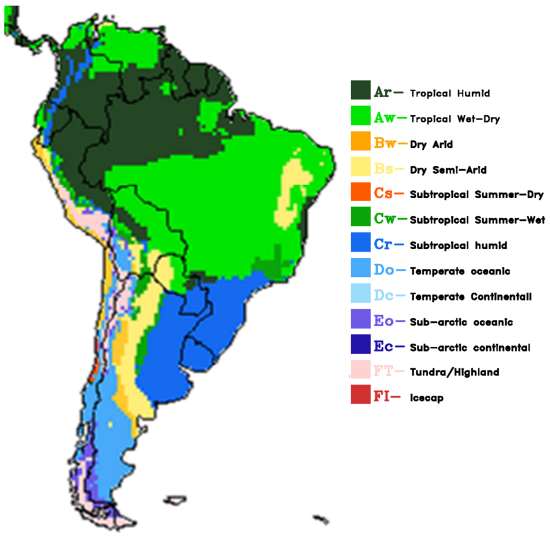

(b) South America climate classification according to Koeppen-Trewartha. From Jacob et al. (2012).

Figure 2.5: Model domain with study regions including hydrological sub-basins (a) and areas with similar climate types (b).

2.3 Results and discussions

The simulations are evaluated using various observational datasets. Appendix D compiles the complete list of these datasets used throughout the study.

2.3.1 Land surface experiments

The results of the sensitivity experiments in order to reduce the springtime warm bias over the Amazon are shown in this section. Figure 2.6 displays the temperature difference of the control run (REMO_{CTRL}) against the observational dataset from the University of East Anglia Climate Research Unit (CRU) version TS3.0 (Mitchell and Jones, 2005). The warm bias over the Amazon Basin ranges from 2 to 8 K.

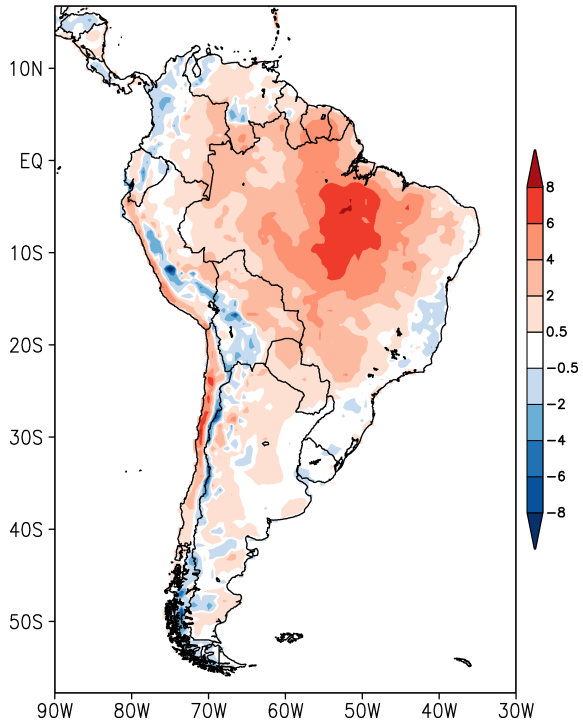

Figure 2.6: Austral spring (SON) temperature bias of a two-year experiment using the new model version REMO2009 compared to the CRU observational dataset. The units are in K.

Due to the the lack of soil moisture during spring, the soil tends to become dry, which can be attributed to more sensible heat fluxes compared to the latent heat fluxes. The lack of evaporative cooling leads to a too high surface temperature. The springtime warm bias of surface temperature is related to the roots that are not

deep enough to reach the available water in deeper layers. They are parameterized in the model indirectly through the amount of soil water available for plants. In order to extend the rooting depths, the plant available water in the soil is increased by reducing the f_{pwp}. This reduction increases the amount of water available for plants in the bucket scheme model.

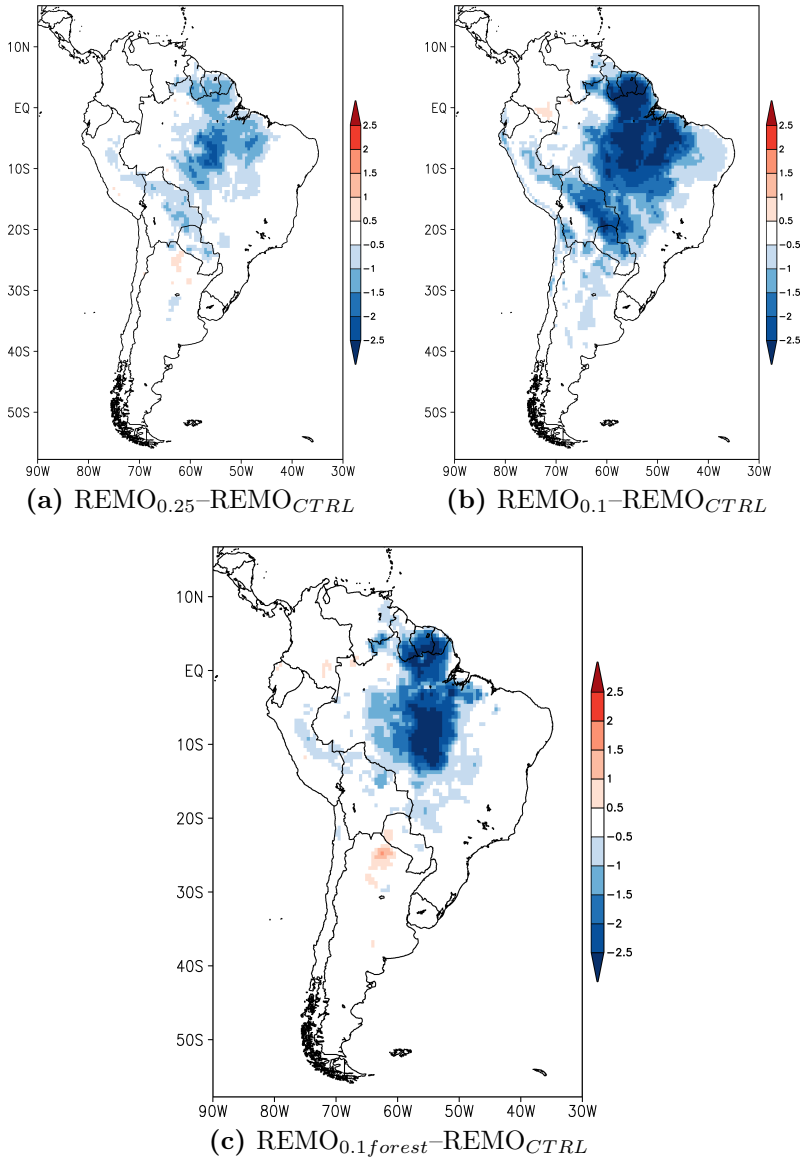

(a) $\text{REMO}_{0.25}$–REMO_{CTRL} **(b)** $\text{REMO}_{0.1}$–REMO_{CTRL}

(c) $\text{REMO}_{0.1forest}$–REMO_{CTRL}

Figure 2.7: Temperature biases (K) of the different experiments listed in Table 2.1 from the control run (REMO_{CTRL}) during austral spring 1989-1990.

Figure 2.7 shows the comparison of the sensitivity test results with the standard REMO (REMO_{CTRL}). The change in f_{pwp} from 35% to 10% results in overall

cooling over the Amazon Basin. The cooling in the $\text{REMO}_{0.10}$ experiment (Figure 2.7b) is more than 2 K, which is the highest in terms of magnitude and spatial extent compared to the other experiments. The surface cooling in the realistic $\text{REMO}_{0.10forest}$ experiment (Figure 2.7c) appears mostly over the Amazon Basin compared to the wider coverage in the $\text{REMO}_{0.10}$ simulation.

The surface fluxes are also investigated. The latent heat fluxes exhibit higher rates in both $\text{REMO}_{0.10}$ and $\text{REMO}_{0.10forest}$ compared to the REMO_{CTRL} setup while the sensible heat fluxes remain almost constant (figure not shown). As a consequence of the increase in available water supply in the soil, the latent heat flux also increases. As a response, the near surface temperature is lower compared to the control run (REMO_{CTRL}).

The mechanism of indirectly altering the root depths in the Amazon rainforest reduces the warm bias by up to 3 K during spring. This model configuration of $REMO_{0.10forest}$ experiment partially resolves the surface warm bias. Therefore, the $REMO_{0.10forest}$ setup is used further for longer simulation and this modified version will be referred hereafter as **REMO**. REMO is the tool used for the analysis of the low level jets and the mesoscale convective sytems in South America.

The complete simulations performed using this new modified version of REMO including the sensitivity experiments are listed in Appendix B. In addition, within the CLARIS-LPB Project Framework (cf. Section 1.2.2), climate projections using the CMIP3 A1B[1] and CMIP5 RCPs[2] scenarios have been simulated. Results for the downscaling of climate simulations using A1B and RCPs are not included here but they are presented in Samuelsson et al. (2013) and Teichmann et al. (2013), respectively.

2.3.2 Temperature and precipitation

The new model version with the modified soil water parameterization in the Amazon Rainforest reduces the springtime temperature bias over the Amazon as shown in Figure 2.7c. To simulate the climate of South America, the experiment is extended from two to twenty years. The simulation period is from 1989 to 2008. The derived climate variables of temperature, precipitation, and winds are evaluated using observational datasets and reanalysis.

[1] http://esg.llnl.gov:8080/home/publicHomePage.do
[2] http://cmip-pcmdi.llnl.gov/cmip5/forcing.html

Detailed analyses of the model performance in simulating the monthly temperature and precipitation are written in two papers (cf. Appendix E and F). The findings are briefly summarized here.

The uncertainties in simulating temperature and precipitation using seven regional models including REMO are listed in the coauthored paper of Solman et al. (2013). The abstract of the manuscript and contributions of the author are written as Appendix E. In this work together with scientists from South America, the variability of the models in simulating the climate at seven subregions including hydrological sub-basins (cf. Figure 2.5a) are shown. REMO simulates the annual cycle of precipitation and temperature reasonably well compared to the other models in six out of the seven subregions. In the South Amazon region, most models including REMO show a warm bias as shown in Figure 2.8. The possible reasons for the large spread of surface temperature among the models during spring are due to the different treatment of land surface processes and insufficient observations over the region. However, the simulated precipitation annual cycle in South Amazon from the different models approximates the observed annual cycle, which peaks during November to March.

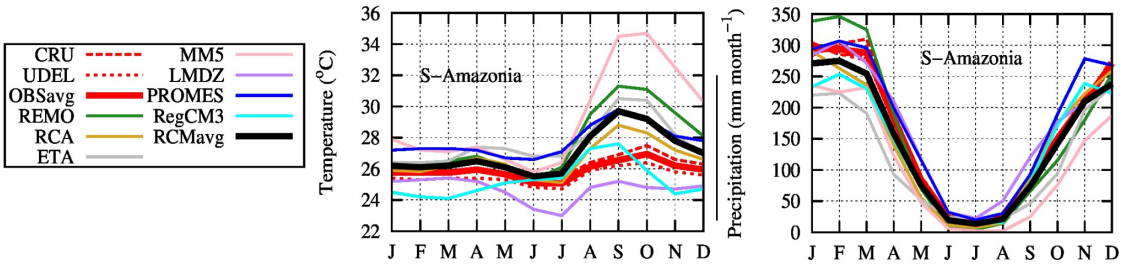

Figure 2.8: Annual cycle of mean monthly temperature (K) and precipitation ($mm/month$) spatially averaged over sub-basins defined in Figure 2.5a. Solid lines indicate individual RCM (e.g. REMO, green) and thick black line indicates the ensemble mean of the RCMs. Dashed red lines are individual observational datasets and thick red line is the ensemble mean of the observations. The period considered is from 1990 to 2008. Adapted from Figure 6 and 7 of Solman et al. (2013).

Jacob et al. (2012), another coauthored paper, highlights the transferability of the regional model REMO to different CORDEX regions namely Africa, Europe, Mediterranean, West Asia, North and South America. The goal of that study was to assess the capability of REMO to reproduce the observed climate over regions apart from Europe, the model testbed. The skill of REMO in simulating precipitation and surface temperature in regions with similar climate characteristics based on the Koeppen-Trewartha classification (Trewartha, 1954) are quantified using probabili-

tistic functions. In South America, the major climate types are tropical humid (Ar), tropical wet-dry (Aw), dry semi-arid (Bs), subtropical humid (Cr), subtropical summer-dry (Cs), and temperate oceanic (Do) climates. Table 2.2 shows the overall temperature and precipitation skill scores at different climatic regions[3]. The scores are relative to the reference dataset, CRU. REMO has relatively high (relatively low) skill scores for regions with subtropical (tropical) climate types. Further details about the abstract of the manuscript and contributions of the author are attached as Appendix F.

Table 2.2: Skill score summary for REMO based on probability density functions (PDF) for temperature (T) and precipitation (P) for each sub-regions based on climate types defined in Figure 2.5b. The last column shows the weighted mean of PDF skill scores (W_mean_CT) across different domains for every climate type. The period considered is from 1989 to 2006. Taken from Figure 6 in Jacob et al. (2012).

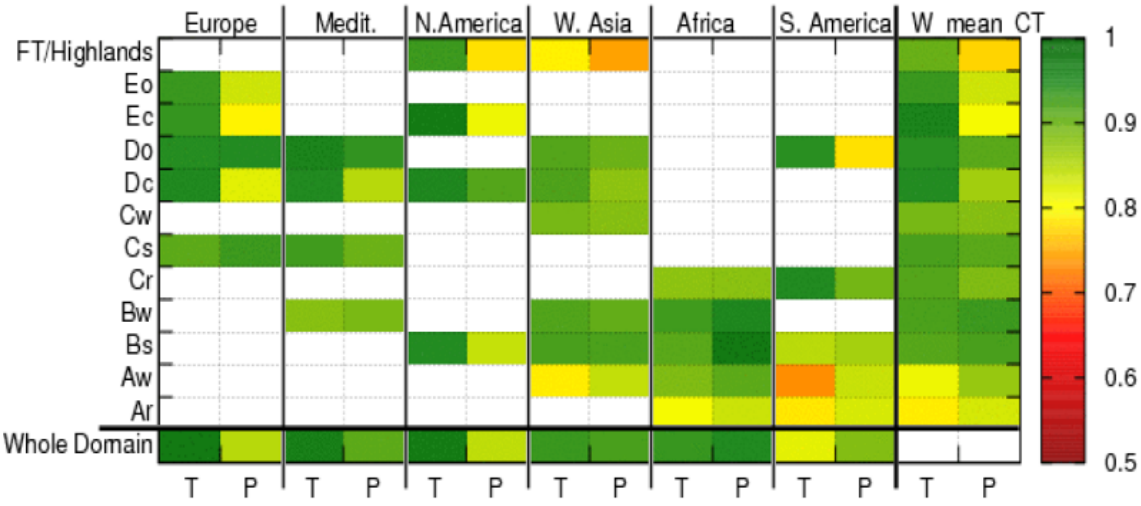

2.3.3 Upper air circulation

In this section, the results of the 20-year model simulations (REMO) are compared with the reanalysis (EITR). Note that the observed circulations in South America have been discussed in the first chapter (cf. Chapter 1.1).

[3]Other climate types not mentioned in the text but included in the skill score table: dry arid (Bw), subtropical summer-wet (Cw), temperate continental (Dc), sub-arctic oceanic (Eo) and continental (Ec), and tundra or highland (FT).

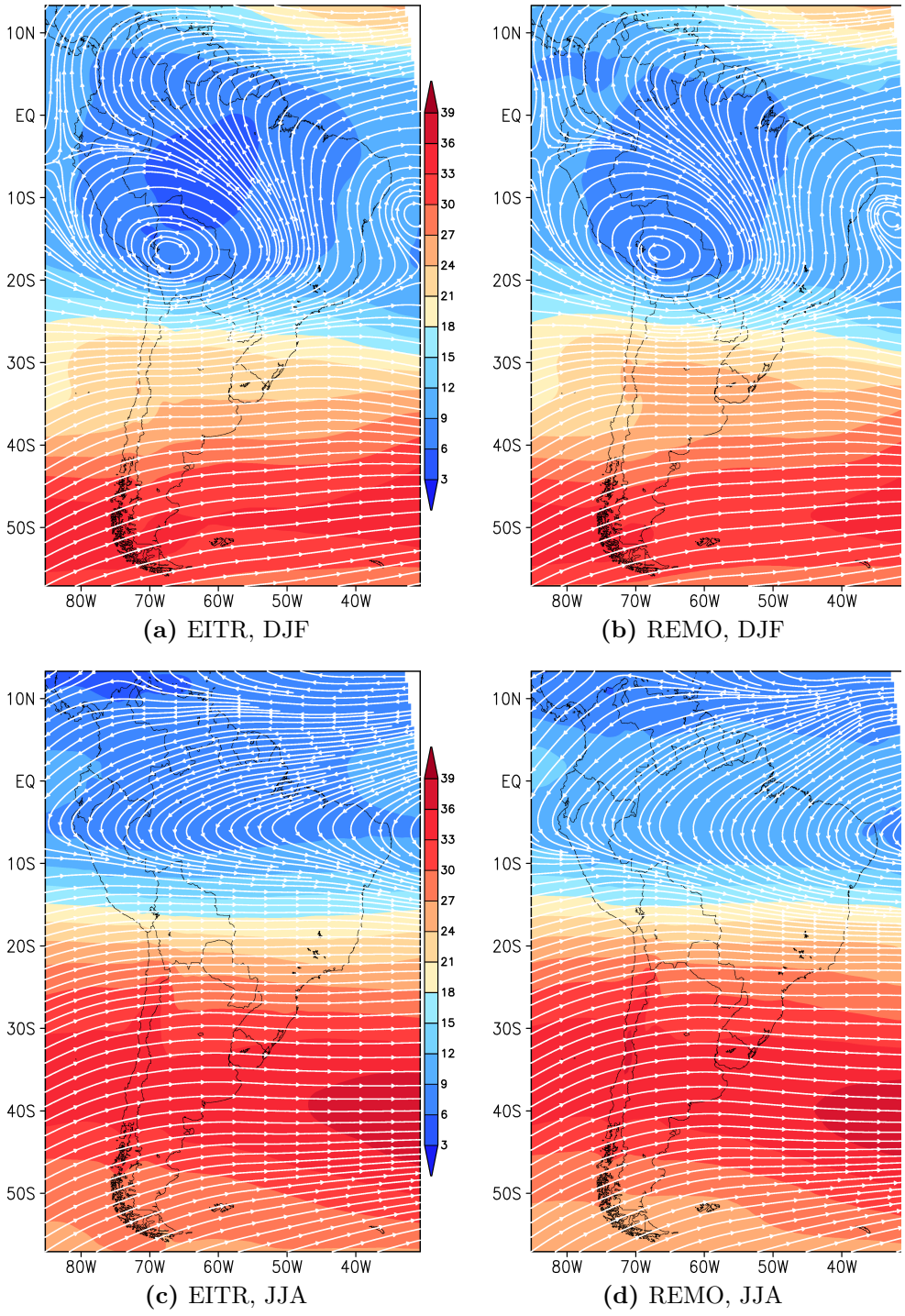

(a) EITR, DJF **(b)** REMO, DJF

(c) EITR, JJA **(d)** REMO, JJA

Figure 2.9: Mean wind at 300 hPa during austral summer (DJF, top panels) and winter (JJA, bottom panels) from ERA-Interim reanalysis (left panels) and REMO (right panels) for the 1989 to 2008 period. Wind speed is in coloured contours and streamlines indicate the wind direction. Units are m/s.

Figure 2.9 shows the seasonal means of observed and simulated upper air circulation at 300 hPa for 1989 to 2008. During austral summer (Figure 2.9a & 2.9b), the anticyclonic circulation over Bolivia (Bolivian High) is clearly defined in both EITR and REMO. The cyclonic circulation or the Nordeste Trough over the Northeastern coast of Brazil is also depicted during the warm season. These two circulations are associated with the release of diabatic heating in the Amazon Region (Lenters and Cook, 1997). At higher latitudes, strong westerlies extend from 40 $^{\circ}S$ towards the pole.

During austral winter (Figure 2.9c & 2.9d), the Bolivian High disappears and, instead, the incursion of easterlies occurs over the northern part of the continent due to the shift of the ITCZ during this season. Another possible reason for the absence of the Bolivian High is due to the absence of deep convective systems. During the cold season, the upper air is more stable compared to the warm season. The westerlies at higher latitudes also migrate equatorward strenghtening the subtropical jetstream, which brings cold air from the South.

2.3.4 Lower troposphere circulation

The winds and mean sea level pressure at 850 hPa show the circulations near the top of the planetary boundary layer. Figure 2.10 describes the 20-year mean climatology of the observed and simulated regional circulations during austral summer and winter. The observed low level jet east of the Andes is present in both seasons but more intense during winter than during summer. The semi-permanent anticyclonic circulation over the Pacific and Atlantic oceans as well as the strong westerlies near Antarctica are depicted in EITR during both seasons (Figure 2.10a & 2.10c).

The high wind speeds over the northeast coast of Brazil are more intense and penetrate further inland in REMO than in EITR for both seasons. The simulated low level jets near the Andes appear to have higher wind speeds (Figure 2.10b & 2.10d) compared to the reanalysis. The difference in the magnitude is approximately 1–2 m/s especially during austral summer. In a previous study, which simulated the climate of South America using an older REMO version and was driven by a coarser resolution reanalysis, the simulated low level jets were weaker than the ERA-40 driving fields (Silvestri et al., 2008). The comparison implies that the new version of REMO driven by a high resolution analysis is able to simulate the magnitude and spatial extent of the low-level circulations.

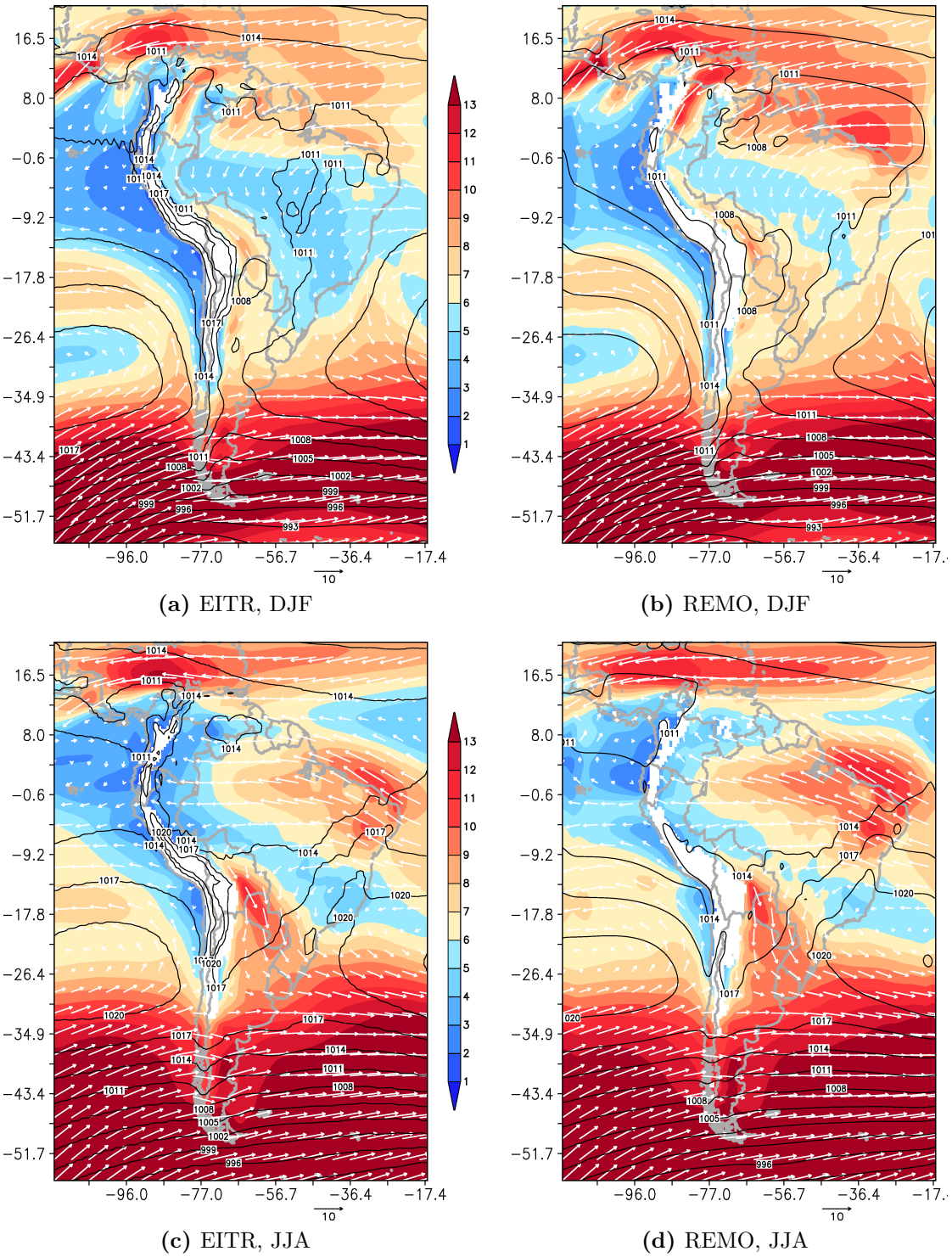

(a) EITR, DJF

(b) REMO, DJF

(c) EITR, JJA

(d) REMO, JJA

Figure 2.10: Mean winds (m/s) at 850 hPa and mean sea level pressure during austral summer (DJF) and winter (JJA) from ERA-Interim *(left panels)* and REMO *(right panels)* for the 1989 to 2008 period. Contours or isobars are the mean sea level pressure (hPa), vectors and shaded contours indicate wind direction and speed, respectively.

2.4 Summary and conclusions

Regional climate models are state-of-the-art tools that are widely used for process studies especially in regions where observations are sparse. In the analysis of the regional scale interactions of low level jets and mesoscale convective systems in South America, the regional climate model REMO is used. The aim of this chapter is to assess the suitability of REMO as a tool for the current study. The chapter is summarized as follows:

- The default model version of REMO during the course of the dissertation is REMO2009. The dynamical and physical parameterization schemes of the model as well as the model setup covering the South American continent have been described. The horizontal grid resolution is $0.44°\times0.44°$ (about 50 $km\times$ 50 km). The number of grid points in the x– and y–direction is 151×181 with 31 vertical levels. The model uses a rotated coordinated system and the location of the rotated North Pole is at 56.06 $°W$ and 70.6 $°N$.

- RCMs are not able to represent well the surface temperature over the Amazon Basin especially during austral spring, when the moisture level is low due to the preceding winter. The common problem is due to insufficient representation of the land surface and atmosphere interaction over the region. The warm bias also appears in REMO2009, the default model setup of REMO. Short sensitivity studies with a simulation period of two years after a spinup period of 20 years, are designed to represent the land surface characteristics over the Amazon Rainforest. Four tests are performed using the REMO2009 version driven by the ERA-Interim reanalysis with varying values and coverage of the permanent wilting point parameter, which influences the water holding capacity of the vegetation in the affected region. The setup in which the permanent wilting point parameter is set to 10% over regions with high leaf area index ($\geq 8\ m^2/m^2$) exhibits the most realistic decrease of surface temperature in terms of affected regions. The modifications lead to the increase of latent heat fluxes while allowing the sensible heat to be almost constant, thereby, reducing the surface temperature over the Amazon basin by approximately 3 K during spring. This setup is further used in the analysis and herein referred to as REMO.

- The simulations of REMO driven by the ERA-Interim reanalysis are extended covering the 1989 to 2008 period. The simulated climate in terms of tem-

perature and precipitation values are compared against various observational datasets. The regions used for comparison are classified either according to hydrological subbasins or based on the Koeppen-Trewartha climate types. Two collaborative papers are written and are summarized below:

In the framework of the CLARIS-LPB Project, the uncertainties in simulating monthly temperature and precipitation using seven regional models including REMO are evaluated in several regions based on its hydrological and climate characteristics. In six out of the seven subregions, REMO is able to simulate the mean annual cycle of precipitation and temperature reasonably well compared to the other models. Over the South Amazon region, most models including REMO still exhibit the spring time warming. Possible reasons are the different land surface scheme of each model and an insufficient density of observations in the region.

In the framework of the CORDEX initiative, the transferability of REMO to six CORDEX regions including South America are assessed for regions defined by the Koeppen-Trewartha climate classification types. Major climate types of South America are the tropical humid, tropical wet-dry, dry semi-arid, subtropical humid, subtropical summer-dry, and temperate oceanic climates. The skill of the model in simulating the observed precipitation and temperature within the 13 regions based on climate types is measured using probability density functions. Based on the skill scores relative to the CRU observations, relatively high scores are calculated over subtropical climate types including the La Plata Basin while relatively low scores are found in tropical climate types including the Amazon Basin.

- The simulated atmospheric circulations at 300 hPa and 200 hPa are evaluated using the EITR reanalysis. The main circulations such as the Bolivian High and Nordeste Trough during summer, the low level jets, and the semi-permanent anticyclonic circulations over the Pacific and Atlantic oceans during summer and winter are generally represented in REMO.

The ability of REMO to simulate the mean climatic features in South America is substantiated based on the results indicated above. This chapter illustrates that the modified version of the regional model REMO can be used as a reasonable tool for the analysis of the regional climate in South America.

3 Low-level jets over South America

3.1 Introduction

The classical definition of a low-level jet (LLJ) is a wind maximum found in the vertical profile of horizontal winds within the atmospheric boundary layer. The formation of LLJs occurs under favorable synoptic conditions such as diurnal changes in the vertical temperature structure near the ground, due either to sloping terrain or by heat exchanges at the surface. One theory from Blackadar (1957) is that the daily cycle of jets as a response to inertial oscillation. During daytime, the subgeostrophic speed of lower tropospheric air is decelerated due to vertical, turbulent mixing with the heated surface. During nighttime without surface heating, the layer of air in contact with the ground undergoes radiative cooling. This layer becomes statically stable, decouples from the layer of air above, which becomes nearly frictionless and turbulence-free, and accelerates due to the synoptic pressure gradient. The effect of the Coriolis force on this accelerating, nearly frictionless air stream is to cause an inertial oscillation with supergeostrophic speeds being reached after several hours.

Several other theories of LLJ formation are due to terrain sloping and the possible coupling with a return circulation in the jet streak or with other synoptic circulations. The LLJ mechanism as a response to the diurnal heating and cooling of sloping terrain results in a periodic variation of thermal wind and a subsequent surface geostrophic wind oscillation (Holton, 1967). In addition, a combination of several mechanisms such as favorable large-scale conditions contributes to the LLJ formation (Stensrud, 1996).

According to the pioneering study of Bonner (1968), LLJs can be detected from observational datasets using three selection criteria based on varying wind speeds at the level of the wind maximum. Identifying LLJs is essential because these jets transport moisture at the jet level, increase the low-level convergence at the nose of the jet, and are responsible for sustaining convection at night. LLJs are partly responsible for nighttime thunderstorms and the development of mesoscale convective systems at the exit region of the jet.

The importance of detecting the low-level jets over different regions are highlighted in several studies. Stensrud (1996), in his comprehensive review on LLJ studies, identified favourable regions where LLJs tend to develop. Some of the locations include the Great Plains of the United States (Whiteman et al., 1997), parts of North Africa (Fiedler et al., 2012) and the region east of the Andes in South America. The latter is analyzed mainly because of its impact on heavy precipitation and severe weather conditions.

Strong low-level jets in South America are detected near the foothills east of the Andes mountains (Figure 3.1). The LLJs in these regions are important especially in their impact on the poleward transport of moisture and advection of heat, which is associated with the development of severe convective events. The following possible mechanisms of the development of LLJ, which were proposed after the extensive short-term SALLJEX observational study by Vera et al. (2006a), were:

> *"a) the deflection of the trade wind circulation that crosses the Amazon basin; b) purely local, topographically generated feature, driven by dry dynamics, but possibly modified by moist convection on the Andean slopes; c) an externally forced feature, produced by variations in the pressure field in northern Argentina associated with transient perturbations in the westerlies; and d) propagation of low-level wind bursts from the North Atlantic toward the La Plata basin through the Amazon basin".*

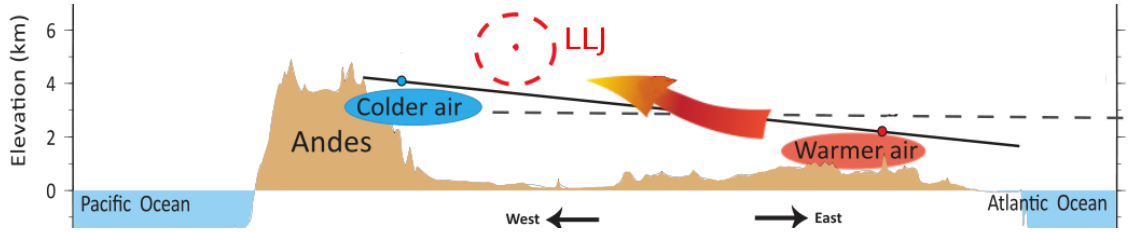

Figure 3.1: Schematic diagram for a possible LLJ mechanism in South America. The trade winds are deflected polewards due to the mountain barrier and the Coriolis force. The LLJ is actually like a ribbon of air parcels coming out of the page. The tilted isoline is exaggerated to emphasize the warmer air in the east compared to the cooler air near the Andes.

In South America, a climatology of the low-level jet east of the Andes mountain range was documented by Marengo et al. (2004) using the United States National Center for Environmental Prediction – National Center for Atmospheric Research reanalysis (**NCEP**, hereafter) with a horizontal resolution of 2.5°×2.5° resolution (Kanamitsu et al., 2002) and available upper-air observations from 1950 to 2000. In order to

ascertain the characteristics of the low-level jets, they applied the first Bonner criterion (Bonner, 1968) using the coarse-resolution NCEP reanalysis and selected eight upper-air observations from the Pan American Climate Studies–Sounding Network (PACS-SONET)[1] and other existing upper-air stations. The annual cycle of the number of LLJ events at grid points nearest to selected stations were investigated and results indicated that LLJs tend to occur all year long. Among the eight stations, five of them indicated a high frequency of LLJ occurrence throughout the years. Mariscal Estigarribia, Asuncion, and Foz do Iguassu Stations detected LLJs that peaked during winter while Santa Cruz and Robore Stations detected high LLJ activity during the austral summer in the region. The maximum LLJ events were detected in Mariscal Estigarribia Station with more than 500 cases in June during the 50-year time period. The stations Cobija, Trinidad, and Curitiba detected less than 200 cases as they were situated at the entrance and exit regions of the LLJ.

During the intensive campaign of SALLJEX (cf. Chapter 1.2.1), the northerly LLJs were analyzed as they were important drivers for the development of deep convective systems. Vera et al. (2006a) identified the Santa Cruz Station as the region with the highest frequency of LLJ episodes. Nicolini et al. (2006) characterized the spatial variability and the diurnal cycle of the low-level flow under different large-scale environments during the campaign. They found that the LLJ profile tends to have maximum strength at 12:00 UTC (8 am local time) in tropical stations (e.g. in Bolivia). In subtropical stations (e.g. in Argentina), the time of local maxima occurs earlier at 9:00 UTC (5 am local time).

Regional climate models have been used to analyze the characteristics of the LLJs in South America. Saulo et al. (2000) used the regional model ETA (Pesquero et al., 2009) driven by the NCEP reanalysis to simulate the LLJs during the austral summer of 1997–1998. The model with $0.4^\circ \times 0.4^\circ$ grid resolution was able to identify the LLJs and it detected more LLJs compared to the pilot balloon observations at the Santa Cruz Station. The large number of LLJ events in the model were due to the low and intermittent frequency of available observations. In contrast, da Silva et al. (2010) detected a lower frequency of LLJ during the same time period. They used the RegCM3 model (Pal et al., 2007) driven by the NCEP reanalysis during the SALLJEX Period to analyze the sensitivity of detecting LLJs using different cumulus parameterization schemes. Investigating a different time period over the same region, Vernekar et al. (2003) characterized the LLJs and their impacts on the austral summer climate using the ETA model driven by NCEP reanalysis during

[1] http://www.nssl.noaa.gov/projects/pacs/

normal years (no El Niño/La Niña Oscillations). They detected LLJs east of the Andes Mountains, west of northern Cordillera Occidental, and additionally, three distinct LLJ region over Columbia, Venezuela and Guiana. Silvestri et al. (2008) simulated the climate of the region using an older version of REMO driven by the ERA40 reanalysis for 43 years from 1958–2000. In a mean summer month, the intensity and spatial extent of the winds in the LLJ region was weaker and smaller compared to the driving reanalysis.

In this chapter, the spatial and temporal characteristics of LLJs are discussed. The following research questions are investigated: (1) how are LLJs detected? (2) what are the characteristics of LLJs? and (3) are the temporal and spatial variability of LLJ occurrences dependent on resolution? Using REMO, the spatial and temporal characteristics of the poleward flow in the lower troposphere in South America are identified and described. Note that low level jets from the south also occur in the region but only the low level jets from the north are considered due to their importance in transporting moisture during the warm season. Hence, hereafter, only the northerly low-level jets are discussed as LLJ.

3.2 Data and methods

In this study, the spatial and temporal characteristics of LLJs are described using a high resolution simulation of $0.44°\times\ 0.44°$ with **REMO** driven by the reanalysis of T255 spectral resolution (about 0.75°) from ERA-Interim (**EITR**). The 6-hourly EITR reanalysis are also used as the initial and boundary conditions for the REMO simulation. ERA-Interim has 60 model levels in hybrid pressure-sigma coordinates. During the study, REMO has 31 model levels due to computational costs and time consumption. The number of vertical levels can be increased, however, the model evaluation in Chapter 2.3 already substantiated the ability of REMO to simulate the observed climate of the region. The model levels are interpolated to 9 varying pressure levels at 1000-, 900-, 850-, 700-, 500-, 400-, 300-, 200-, and 100 hPa. The reanalysis and the SALLJEX data are used to compare the results obtained from REMO.

LLJs are originally identified using the first Bonner criterion (**BC**), which is based on long-term wind speed observations from North America. According to this classical definition, an LLJ event is detected when the wind speed at the level of maximum wind (V_{max}) is equal to or higher than 12 m/s. In addition, the wind speed should

decrease (ΔV) by at least 6 m/s either to the next higher minimum or up to the 3 km height level, whichever is lower (Bonner, 1968). Based on observational studies in South America (Marengo et al., 2004; Vera et al., 2006a), the level of maximum wind is considered to be at the 850 hPa pressure level. The vertical wind shear is calculated between the 850 hPa and 700 hPa pressure levels.

In the modified Bonner criterion (**MB1**), the **BC** criterion was adapted based on short-term observations focusing on meridional winds (ν). The wind speed threshold is lowered to 8 m/s to include LLJ events detected in other radiosonde stations (Sugahara et al., 1994; da Silva et al., 2010). The third criterion for detecting LLJs is **MB2**, which is similar to **BC** but using the meridional component only (Rozante and Cavalcanti, 2008). All three criteria are used in detecting LLJs at grid points closest to station observations. In addition, only northerly winds are considered and the meridional wind speed is higher than the zonal wind speed.

Table 3.1 summarizes the three criteria, which differs in wind speed components at 850 hPa, and vertical wind shear between 850 hPa and 700 hPa. The simulated number of LLJ events detected over the whole domain is compared to the events detected in the EITR reanalysis, which is also the driving field. The detected LLJs are compared at grid points nearest to the eight station locations (Figure 3.2) corresponding to the stations in the previous study of Marengo et al. (2004) on the LLJ climatology.

Table 3.1: Different low level jet selection criteria. V_{max} is defined as the wind speed at the 850 hPa level. ν is the meridional component of V_{max}. ΔV is the vertical wind shear between the 850 hPa and 700 hPa pressure levels. Criteria references are also shown.

Criterion	850 hPa winds	Wind shear	References
BC	$V_{max} \geq 12\ m/s$	$\Delta V \geq 6\ m/s$	Bonner (1968)
MB1	$\nu \leq$ -8 m/s	$\Delta V \geq 2\ m/s$	Sugahara et al. (1994)
MB2	$\nu \leq$ -12 m/s	$\Delta V \geq 6\ m/s$	Rozante and Cavalcanti (2008)

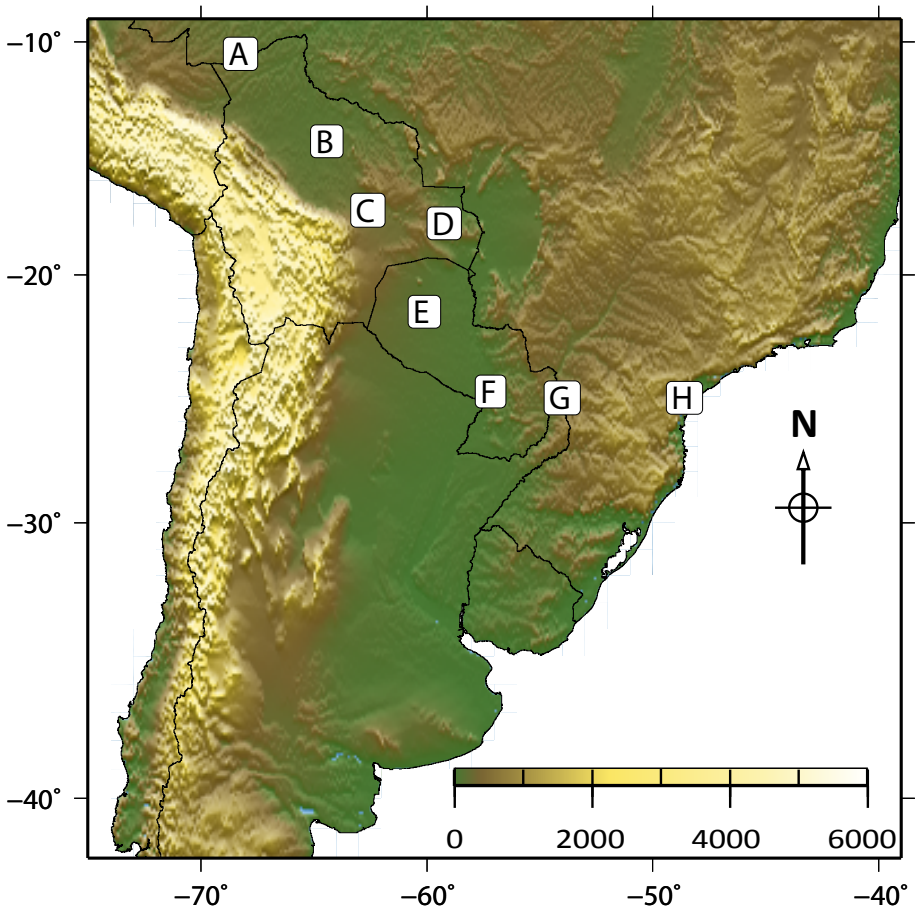

Station	Country	Longitude (°)	Latitude (°)	Elevation (m)
(A) Cobija	Bolivia	-68.78	-11.04	271
(B) Trinidad	Bolivia	-64.92	-14.82	156
(C) Santa Cruz	Bolivia	-63.15	-17.76	373
(D) Robore	Bolivia	-59.76	-18.33	277
(E) Mariscal Estigarribia	Paraguay	-60.60	-22.02	155
(F) Asuncion	Paraguay	-57.63	-25.27	83
(G) Foz do Iguassu	Brazil	-54.58	-25.52	180
(H) Curitiba	Brazil	-49.17	-25.52	908

Figure 3.2: Upper air station locations used for sampling LLJ events and orography (m). The station locations and elevation are indicated in the table inside the figure. Source of station locations at http://www.nco.ncep.noaa.gov.

3.3 Results and discussions

3.3.1 Model evaluation during SALLJEX

Before assessing the LLJs in the 20-year simulation, a subset of the reanalysis (EITR) data and simulation (REMO) are validated using the SALLJEX observations. Note that one of the aims of this campaign was to be a platform for validating simulations performed during the austral summer of 2002–03 (Vera et al., 2006a). The simulated LLJs during this period are identified and compared with the observations in Santa Cruz Station (cf. point C in Figure 3.2).

In addition, the NCEP reanalysis data is shown for comparison. The NCEP reanalysis has a horizontal resolution of $2.5° \times 2.5°$ and 17 vertical levels from the surface up to 10 hPa. The temporal resolution is 6-hourly at 00:00, 06:00, 12:00 and 18:00 UTC. The NCEP reanalysis dataset has been widely used in SALLJEX as well as several other LLJ studies in the region.

Figure 3.3 depicts the LLJ episodes using the vertical profile of the meridional winds at a grid point close to the Santa Cruz Station during SALLJEX. In the NCEP reanalysis (Figure 3.3a), four LLJ episodes are detected using the **BC** criteria (Vera et al., 2006a). Note that within a given period, an LLJ event is detected every six hours while an LLJ episode comprises of a series of connecting events. The duration of this LLJ episodes could last up to a few days. The breaks in between the episodes are partially due to incursions of southerly meridional winds. The relevance of the southerly meridional winds are not fully explored in this comparison since the sample period is short.

The Bolivian High, which is a semi-permanent subtropical high pressure system present at upper levels during summer, is also depicted in Figure 3.3 and perturbs the low-level flow structure or vice versa. However, the short time period is not sufficient in the analysis of synoptic conditions at upper levels. In comparison, the meridional wind data of EITR and REMO have stronger northerly meridional wind components (Figure 3.3b & 3.3c, darker shades of blue) than the NCEP reanalysis data especially at the 850 hPa pressure level. This result may be due to differences in spatial resolution. The difference in horizontal resolution from 300 km down to 50 km leads to different grid point location close to the actual longitude-latitude coordinates of the station, in this case, Santa Cruz. The sensitivity of detecting LLJs at different grid points is further investigated and discussed in the next section

(3.3.2). In addition, the REMO model is used in the climate mode wherein the influence of the driving reanalysis is weaker than in the forecast mode. In the climate mode, REMO develops its own climate, which could be different from the driving fields.

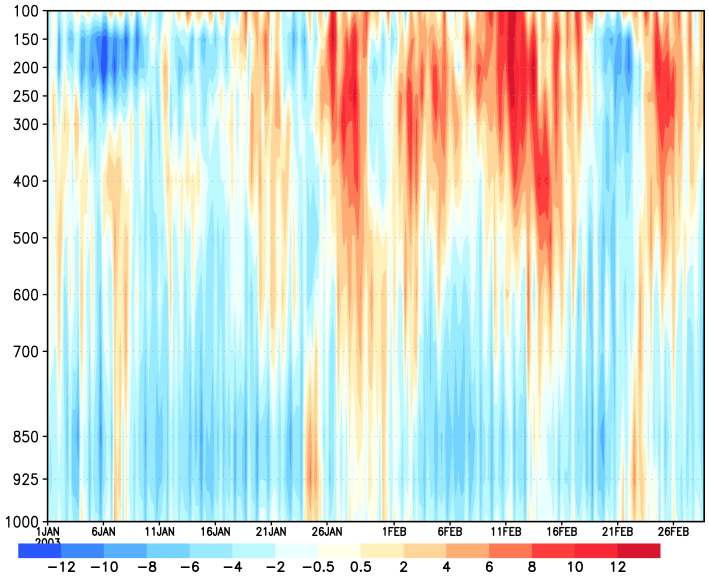

(a) NCEP, 2.5×2.5°

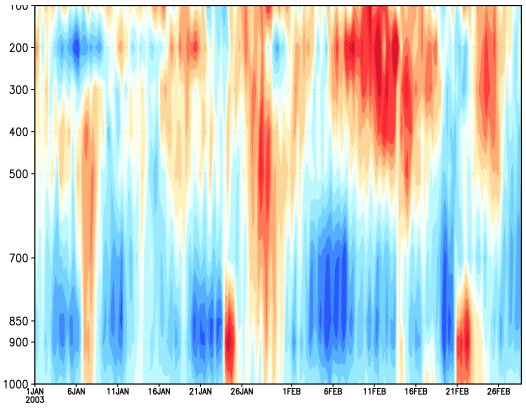

(b) EITR, T255 (∼0.75°)

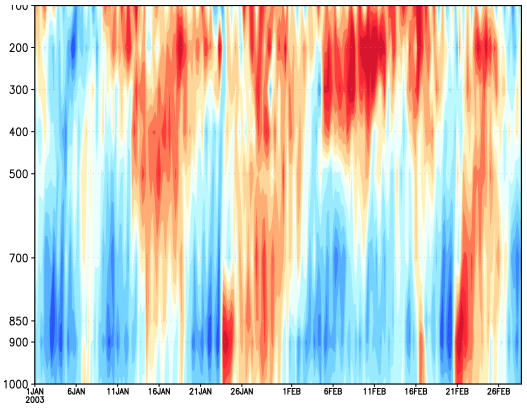

(c) REMO, 0.44×0.44°

Figure 3.3: Evolution of the meridional wind component (ν) at different pressure-height levels in hPa during the January-February 2003 period for the grid point closest to the Santa Cruz Station using reanalyses and REMO simulations. ν in the Hovmoeller diagram is in m/s. Blue (red) shades indicate northerly (southerly) wind direction. Horizontal resolutions are indicated in the subcaptions.

The mean vertical profiles of the wind speed at the Santa Cruz Station during the LLJ events are shown in Figure 3.4. The observations (Figure 3.4a) are from pilot balloon (PIBAL) measurements obtained only during 12:00 and 21:00 UTC (08:00

and 17:00 Local Time). In the reanalyses and REMO, the horizontal winds at different model levels are available every six hours. Thus, the direct comparison in this figure is only at 12:00 UTC, in which REMO and the reanalyses coincide with the time of the PIBAL observations.

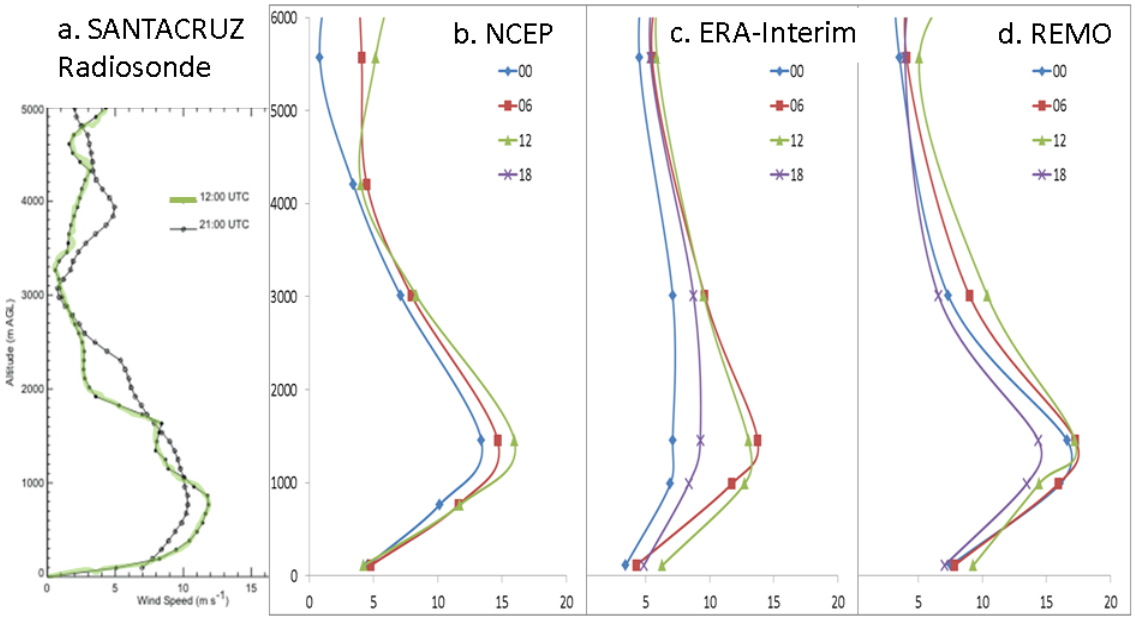

Figure 3.4: Profiles of mean wind speed vs height from a composite of detected LLJs following the first Bonner criterion (**BC**) during SALLJEX. Observations (a) released at Santa Cruz (adopted from `http://www.nssl.noaa.gov/projects/pacs/salljex/ppbb/LLJ_Crit1_SCZ.speed.jpg`) and $y-$axis indicates the altitude above ground level in (m). Winds from NCEP (b) and EITR (c) reanalyses, and REMO (d) simulation are obtained from the nearest grid point location. The station elevation is 373 m (Figure 3.2).

At 12:00 UTC (green line in Figure 3.4), the vertical profiles of the two reanalyses and REMO follow the behavior of the observations, in which the mean wind speeds increase from the ground up to around 1,200 m followed by a decrease with height up to 3,000 m. At the level of the wind maximum, which is near 1,000 m above ground level, the observed mean value in Santa Cruz, Bolivia during LLJ events is 12 m/s (Figure 3.4a). Comparing REMO with the reanalyses (Figure 3.4b–d), REMO has the highest wind speed of about 18 m/s, followed by NCEP (15 m/s), and EITR (14 m/s). The height level of the maxima or the LLJ core are located at about the same height and the wind speed decreases above the core, which satisfies the detection criteria.

The diurnal variation of the mean vertical profile during LLJ events can be inferred from the two reanalyses and REMO data. However, due to sparsity in the obser-

vational dataset (Figure 3.4a), the diurnal variation is difficult to infer from twice-a-day measurements. In the NCEP reanalysis (Figure 3.4b), no LLJ is detected at 18:00 UTC. At the LLJ core, the minimum is at 00:00 UTC in both NCEP and EITR reanalysis and the maximum occurs earlier in EITR data (06:00 UTC) than in NCEP data (12:00 UTC). However, the wind speed for NCEP at 06:00 UTC is almost equal to the one at 12:00 UTC. In REMO, the preferred wind maximum at 850 hPa (about 1.5 km) is both at 06:00 and 12:00 UTC and the preferred wind minimum in the same vertical level is at 18:00 UTC.

The spatial variations of the mean horizontal wind speed and their magnitudes at 850 hPa over South America during LLJ events detected in Santa Cruz are shown in Figure 3.5. The mean flow begins from the northeast due to the trade winds. As the flow passes the equator, and encounters the Andes, the winds are deflected and turns southwards. Upon entering the northern tip of Bolivia, the winds have intensified gaining its maximum value at about 16 m/s. As it exits down to the La Plata Basin, the flow decelerates as other circulation features interfere such as the strong westerlies in the south.

In the coarse horizontal resolution of NCEP (Figure 3.5a), the spatial extent (red area) of the LLJ is larger compared to EITR (Figure 3.5b) and REMO (Figure 3.5c). In a high resolution, the LLJs tend to be more concentrated region and the intensity is higher than the 15 m/s of NCEP, as shown in EITR and REMO. The number of events detected using the **BC** has also increased with resolution from 7, 12, and 17 events in NCEP, EITR, and REMO, respectively.

During the short SALLJEX Period, the REMO simulation data represent the spatial and vertical characteristics of LLJ. Evidently, a higher horizontal resolution detects more frequent LLJs than a lower one and enhances the spatial variability and vertical structure of LLJs. In the next section, the study of LLJs extends further through twenty years and the driving reanalysis (EITR) is used to evaluate the long-term simulation (REMO).

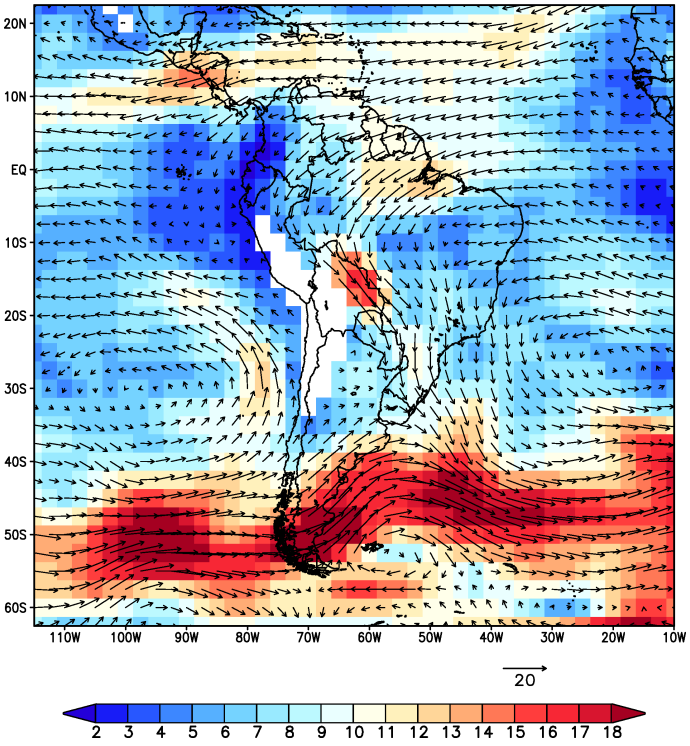

(a) NCEP, 7 events

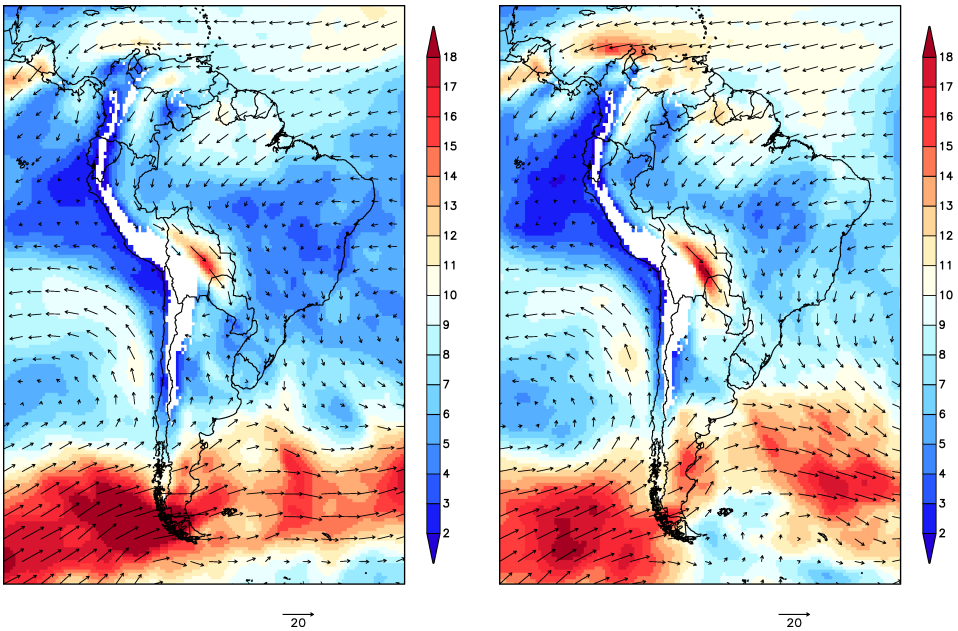

(b) EITR, 12 events **(c)** REMO, 17 events

Figure 3.5: Mean horizontal winds at 850 hPa over South America for situations when LLJs have been detected using the Bonner criterion in Santa Cruz during the SALLJEX period (January to February 2003). Elevations above 1.5 km are masked out. The number of events detected is given in each subcaptions. Wind speed (m/s) is in shaded contour and wind vectors are plotted at each grid point in (a) and every 7th grid point in (b) and (c).

3.3.2 LLJ climatology

A climatology of LLJ in South America is constructed using a high resolution reanalysis and dynamical downscaling results. The spatial variability, frequency, and intensity of LLJs are presented using the sampling statistics for 1989 to 2008 listed in Table 3.2.

Table 3.2: Sampling statistics at 6-hourly for each season from 1989 to 2008.

Seasons in the Southern Hemisphere	Samples	Days
Summer (DJF)	7,220	1,820
Autumn (MAM)	7,360	1,855
Winter (JJA)	7,360	1,855
Spring (SON)	7,280	1,835

Based on **BC**, the LLJs are present throughout the year in the reanalysis (Figure 3.6). The region with the LLJ maximum is located east of the central Andes. The LLJs occur about 21% (1,533) in wintertime (Figure 3.6a). During austral summer (Figure 3.6c), local LLJ maxima exist in the following locations: east of the central Andes, and east of the northern Andes in Columbia and in Costa Rica. The tropospheric circulation responsible for the summertime maxima in the central Andes has been discussed in Chapter 2.3. The maxima in the northern regions are influenced by the northeast trades as well as the location of the ITCZ during summer (Garreaud et al., 2009).

During the other seasons, the regions with LLJ maxima are located also east of the central Andes. In addition, another local maximum can be found in Costa Rica during austral autumn (Figure 3.6b) and just over the Atlantic ocean near to the coasts connecting Uruguay and Brazil (Figure 3.6d) during austral spring (SON). As discussed in the validation of the simulated upper and lower tropospheric circulations (Chapter 2.3), the semi-permanent high pressure system over the Atlantic then migrates from east to west. During winter, this system approaches the coasts of Brazil and Uruguay bringing moisture from the Atlantic as well as strong winds further inland.

The LLJs in the northern regions of South America have been observed by Vernekar et al. (2003). They are strongly influenced by the northeasterly trade winds over Columbia, Venezuela and Guiana. These LLJs have their exit region in the northern part of the Amazon Basin. The LLJs detected over the coasts of Brazil and Uruguay

may be due to the South Atlantic Convergence Zone (Marengo et al., 2004) but their frequency of occurrence is low (about 1%).

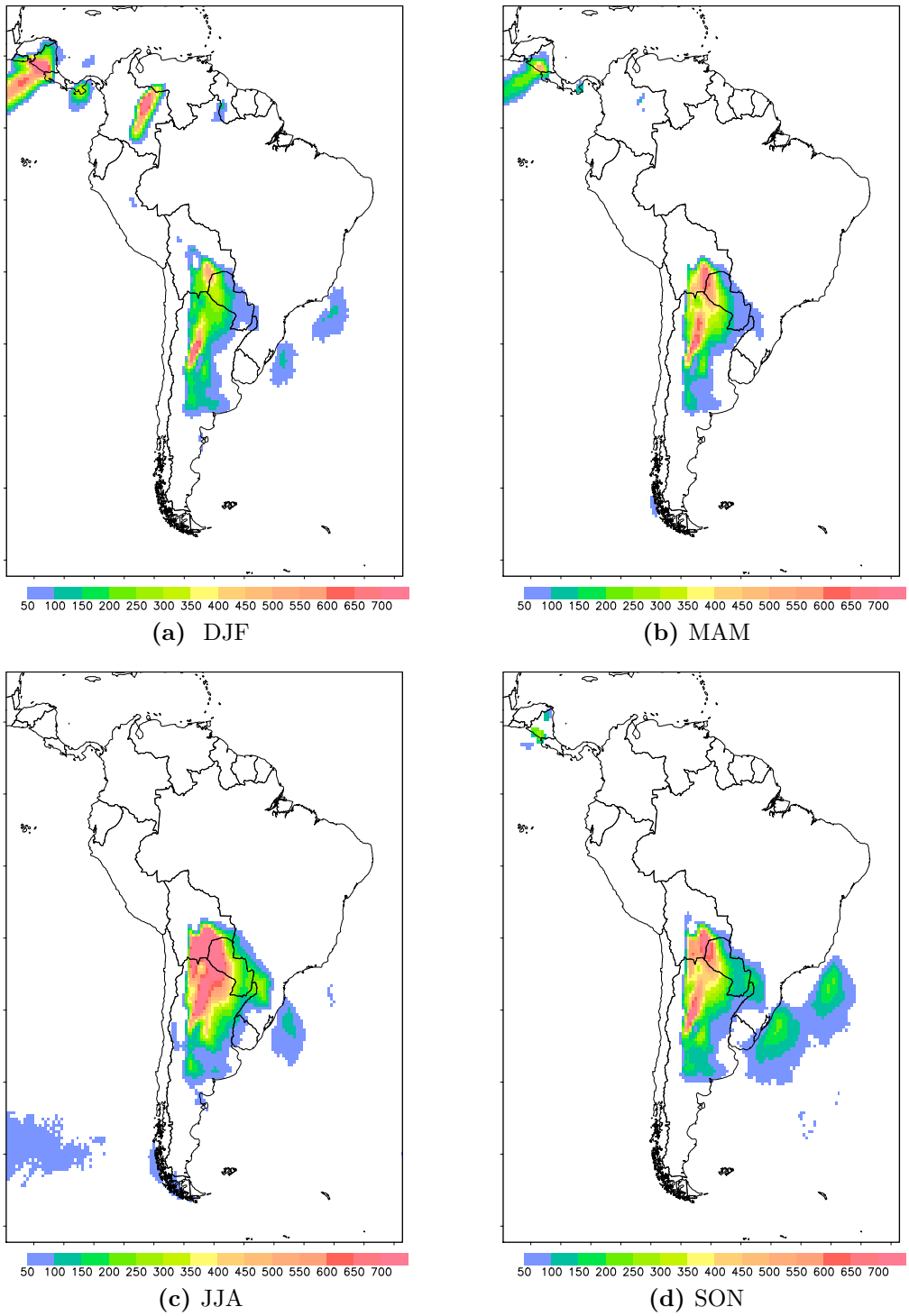

(a) DJF **(b)** MAM

(c) JJA **(d)** SON

Figure 3.6: The seasonal frequency of LLJ events detected at 6-hourly intervals in the EITR reanalysis for the period 1989 to 2008.

The spatial characteristics of the REMO simulation results (not shown) portrays similar features as the EITR reanalysis in Figure 3.6. The differences due to different selection criteria indicated in Table 3.1 and due to selection of grid points closest to station locations shown in Figure 3.2 are highlighted in the next subsections.

Sensitivity to different detection criteria

As discussed in Section 3.2, three criteria in detecting LLJs are used. The figures for the LLJs detected using the **BC** and **MB2** criteria for both EITR and REMO are not shown since the spatial characteristics are similar to Figure 3.6. The **MB2** criterion detects about 10% more than the other two, especially in winter (Figure 3.7). In this criterion, the threshold of ν is low to include observed LLJ events detected in Asuncion Station, Paraguay (da Silva et al., 2010). Due to this low threshold, more LLJ events are detected.

Comparing reanalysis and simulation data, the intensity and the extent of the LLJ maxima are almost the same in austral summer and winter. It is interesting to note that during winter, regardless of the criterion used, the LLJ maximum is centered between Bolivia, Paraguay and northern Argentina. The LLJs occur more frequently in winter than in summer.

In order to quantify the difference among the LLJ criteria, the LLJ events are compared at the nearest model grid point for the stations listed in Figure 3.2. The annual LLJ cycle near each station (Figure 3.8) generally tends to peak during austral winter. As observed previously, the primary reason for the winter maxima is the anticyclonic circulation over the Atlantic, which allows a stronger poleward flow. For most stations, except Cobija, which is located at the northern edge of Bolivia, the reanalysis and the simulation have a high LLJ activity during winter. In general, the numbers of simulated events across different stations and criteria tend to be higher or equal to the reanalysis throughout the year.

The **MB1** criterion detects more low level jet episodes compared to **BC** and **MB2** due to a low threshold of meridional wind speed (Table 3.1). Evaluating the low level jet events in a grid point close to the radiosonde station in Santa Cruz, Bolivia, REMO and EITR have similar counts of monthly LLJ events. The number of events detected in the EITR and REMO data have peaks during the austral winter (e.g. Figure 3.8c), which is dissimilar in comparison to the previous study of Marengo et al. (2004) wherein the **BC** criterion indicated a peak activity during the austral

summer. This shift in the annual cycle could be attributed to the fact that Marengo et al. (2004) have used the NCEP reanalysis, which has a coarser resolution of about 300 km and a different time period (1950-2000). The sensitivity to the choice of grid point locations is discussed further in the next subsection.

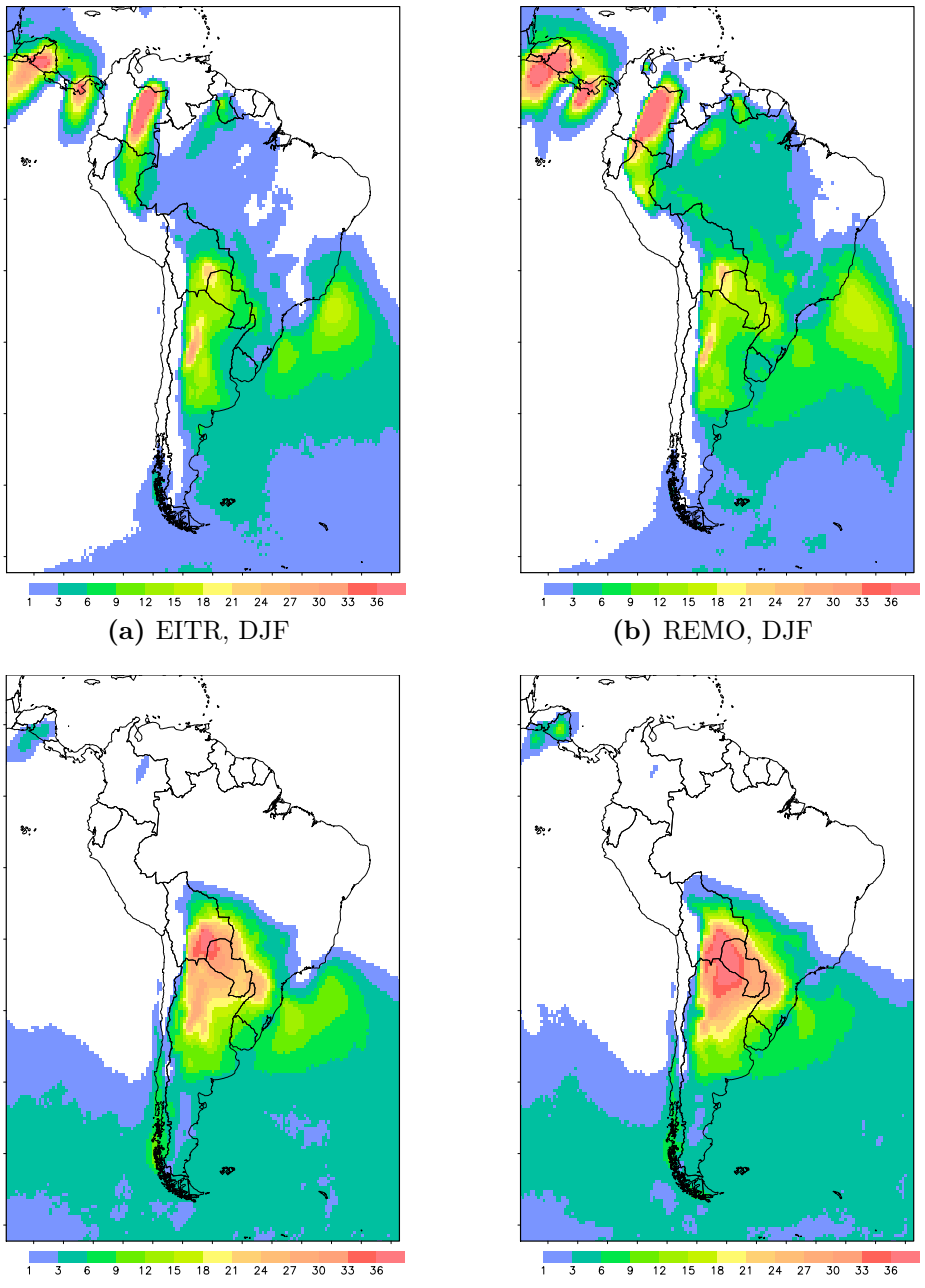

(a) EITR, DJF **(b)** REMO, DJF

(c) EITR, JJA **(d)** REMO, JJA

Figure 3.7: The percentage of LLJ events detected using the **MB1** criterion in the reanalysis (left panel) and simulation (right panel) during austral (a, b) summer (DJF) and (c, d) winter (JJA) during the 1989 to 2008 period.

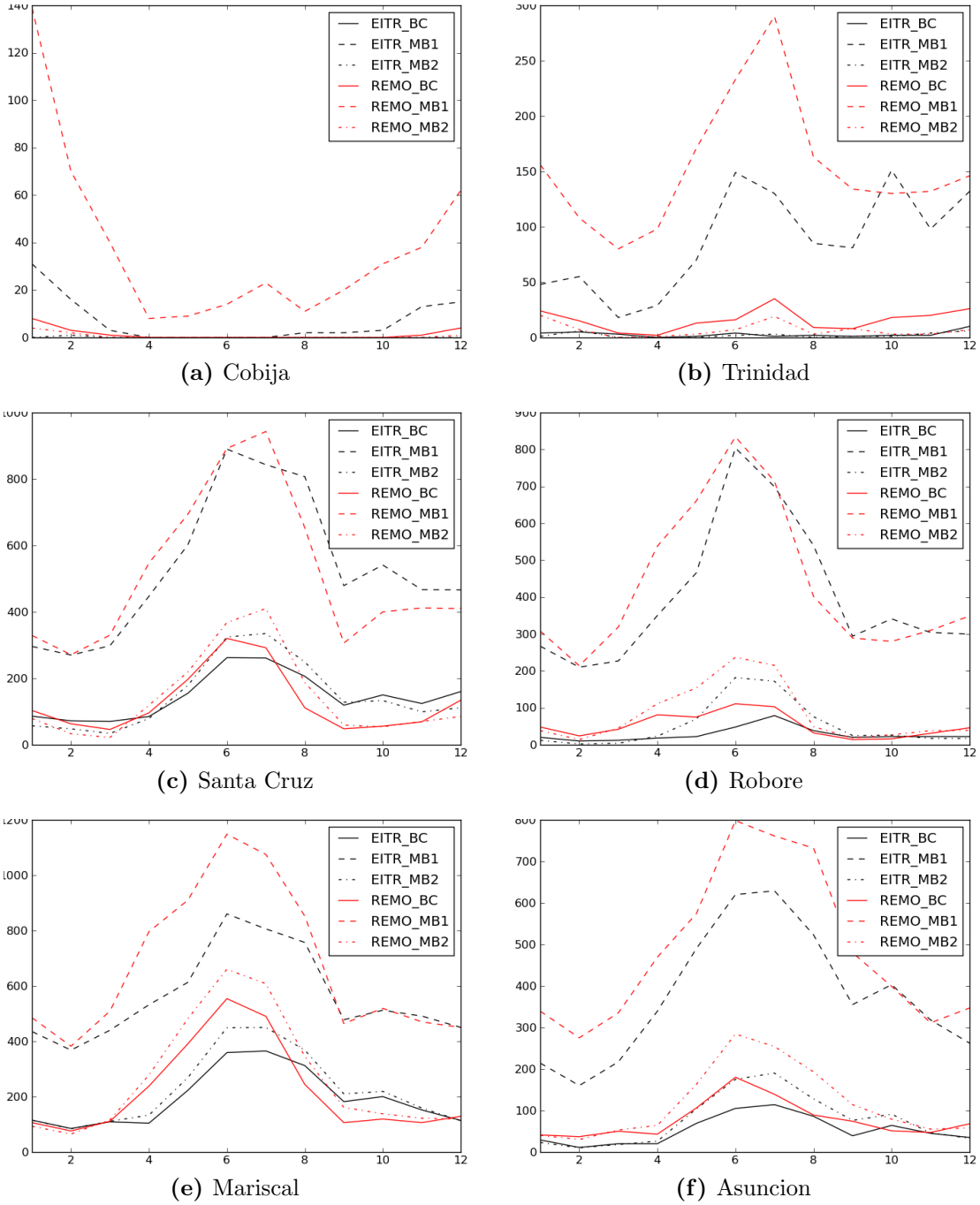

(a) Cobija **(b)** Trinidad

(c) Santa Cruz **(d)** Robore

(e) Mariscal **(f)** Asuncion

Figure 3.8: Annual cycle of LLJ frequency using different LLJ criteria at grid points nearest to each station shown in Figure 3.2. Solid for **BC**, dashed for **MB1**, and dashed-dotted for **MB2**. Black indicates the reanalysis while red stands for the simulation. Model data were used at 00:00, 06:00, 12:00, and 18:00 UTC.

Based on Figure 3.8, regardless of which criterion is used for detection of LLJ, the annual cycles are very similar with the tendency to detect more LLJs in the high

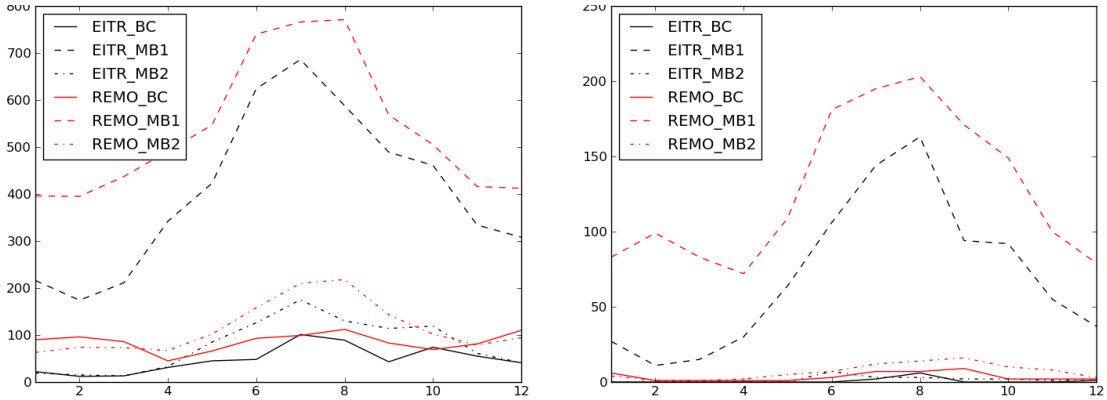

(g) Foz do Iguassu **(h)** Curitiba

Figure 3.8: *cont.*

resolution REMO simulation than the EITR reanalysis. The Santa Cruz, Robore, Mariscal de Estigarribia, Asuncion, and Foz do Iguassu Stations (Figure 3.8 c–g) have detected the highest frequency of LLJ occurrences. These five stations are considered the core regions for LLJ activity in the succeeding sections.

Detection sensitivity at different locations

Previous studies using short-term observations have identified that the region with the highest number of northerly LLJs is the Santa Cruz Station in Bolivia. In Marengo et al. (2004), the annual cycle of the LLJ peaks with about 200 events during austral summer and with less than 100 events during winter using the NCEP reanalysis for a duration of 50 years. In Figure 3.8c, the pronounced peak occurs during winter in both the EITR reanalysis and REMO simulation. The discrepancy between the previous study and the current study becomes clear in Figure 3.9, which shows the different grid points closest to the station location in the two reanalyses (NCEP and EITR) and in the simulation (REMO). The distance between the NCEP grid point and the Santa Cruz station is approximately 80 km while the grid point locations in EITR and REMO are closer to the station by approximately less than 10 km.

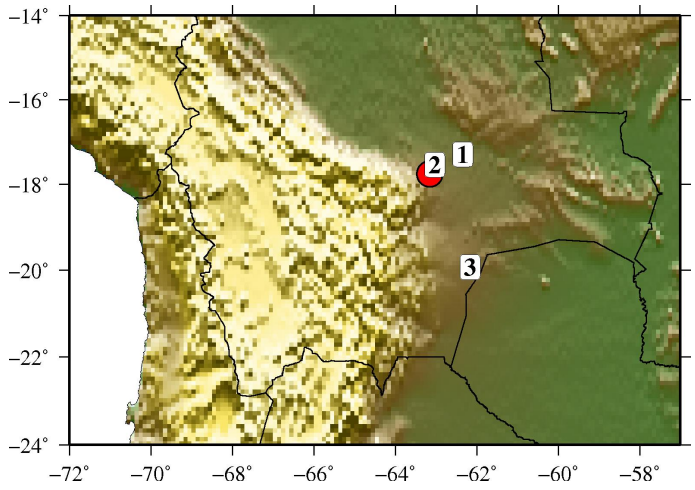

Grid point	Santa Cruz at different resolutions	Longitude (°)	Latitude (°)
(1) **NCEP**	2.5° resolution	-62.50	-17.50
(2) **EITR**	0.7° resolution	-63.18	-17.75
(3) **MAX**	0.44° resolution and location with maximum LLJ events	-62.32	-20.13

Figure 3.9: Test locations for sensitivity of LLJ events to different grid point locations close to the Santa Cruz Station (63.15 °W, 17.76 °S) indicated by a red dot.

The region with the maximum number of events is also identified in the reanalysis and the simulation. Incidentally, the grid point with the maximum number of events (POINT MAX) are the same in both EITR and REMO, with 12% and 15% LLJ events detected, respectively. The grid point is situated in the Gran Chaco, a region in the southeastern corner of Bolivia bordering with Argentina and Paraguay. The Gran Chaco region has a subtropical semi-arid climate, which indicates a harsh environment such as "impenetrable flat land of thick brush, cactus and grassy expanses with some forested areas" (http://www.explorebolivia.com/our-country/map-of-bolivia). Other studies refer to the strong meridional winds in this region as the Chaco Jet Events Salio et al. (2002).

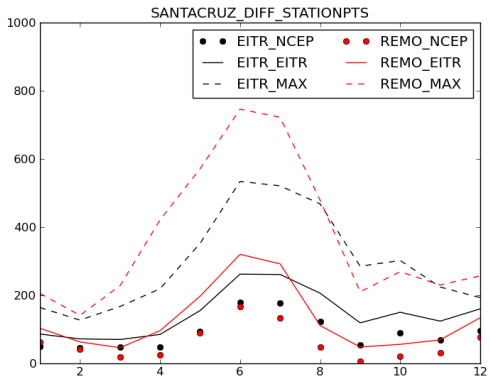

Figure 3.10: The annual cycle of the frequency of LLJ events at the grid points close to the station Santa Cruz, black for reanalysis and red for the model simulation. Circles indicate Point NCEP, solid line Point EITR and dashed lines Point MAX, as shown in Figure 3.9.

The annual cycles of the low level jet occurrences from the three grid points (Figure 3.9) are displayed in Figure 3.10. The winter maximum is still prominent albeit the values in the POINT NCEP are significantly lower (less than 200 events). The tendency in POINT NCEP is to have a maximum during summer too, which agrees with the previous study of Marengo et al. (2004). The number of LLJs detected at the NCEP grid point is the lowest among all locations. REMO shows the highest counts of LLJs but only during austral winter. During spring, the number of LLJ events in REMO are lower than the EITR, which could be a result of the model bias indicated in Chapter 2.3.

The percentage of LLJ occurrence is presented for the points close to the Santa Cruz Station in Figure 3.11. A day with LLJ is defined as a day with an LLJ between 06:00 and 00:00 UTC, corresponding to 04:00 to 20:00 local time. In general, at the NCEP and EITR gridpoints, the percentage of days with an LLJ is higher in the EITR reanalysis than in the REMO simulation for all seasons. However, at the highest activity point (POINT MAX), REMO simulates more LLJ events than EITR, especially during winter and summer, but REMO is slightly lower than EITR during spring.

Based on Figure 3.10 and 3.11, detecting LLJ events is sensitive to the grid point selected. The differences may be attributed to different elevation of the three grid points. The NCEP grid point has an elevation of 264 m, the EITR grid point 276 m and the grid point MAX has the highest elevation of about 386 m. Orographic influences are obvious factors for the generation of strong winds, but a main factor is the strength of the prevailing winds, which will be shown in the spatial characteristics subsection. There the region with the highest LLJ count is identified, which is the same for both the reanalysis and the model simulation (POINT MAX in Figure 3.9).

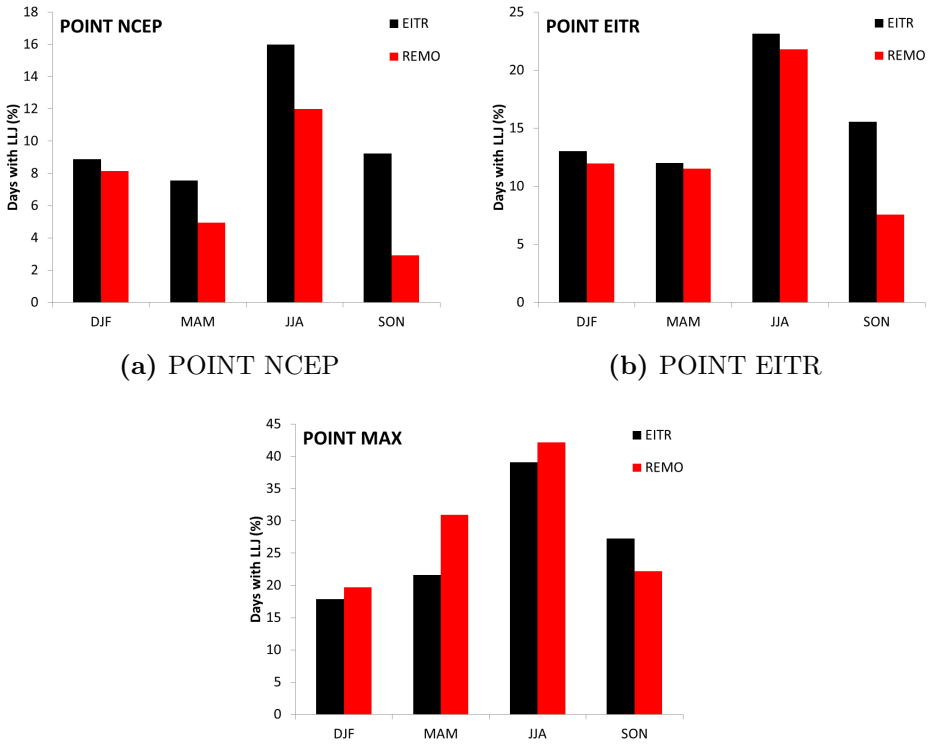

(a) POINT NCEP

(b) POINT EITR

(c) POINT MAX

Figure 3.11: Percentage of days with an LLJ for each season during 1989 to 2008 at different test locations shown in Figure 3.9.

Spatial characteristics

From Figure 3.8, five stations (Santa Cruz, Robore, Mariscal Estigarribia, Asuncion, and Foz do Iguassu) are identified to be the core LLJ region. The intensity, spatial extent and frequency of LLJ events detected in 5 stations are depicted in Figure 3.12 and 3.13. Figure 3.12 depicts the LLJ region during winter, which extends further southward to the coasts near the La Plata Basin than during summer. The mean wind speed of LLJs during winter is higher than 18 m/s, which is faster than the mean intensity (13–16 m/s) during summer (cf. Figure 2.10). The REMO simulation results show lower mean wind speeds compared to the reanalysis data because the frequency of events is higher (about 2–3% higher than the EITR reanalysis). The differences in the percentage of LLJ days between EITR and REMO are shown in Figure 3.13

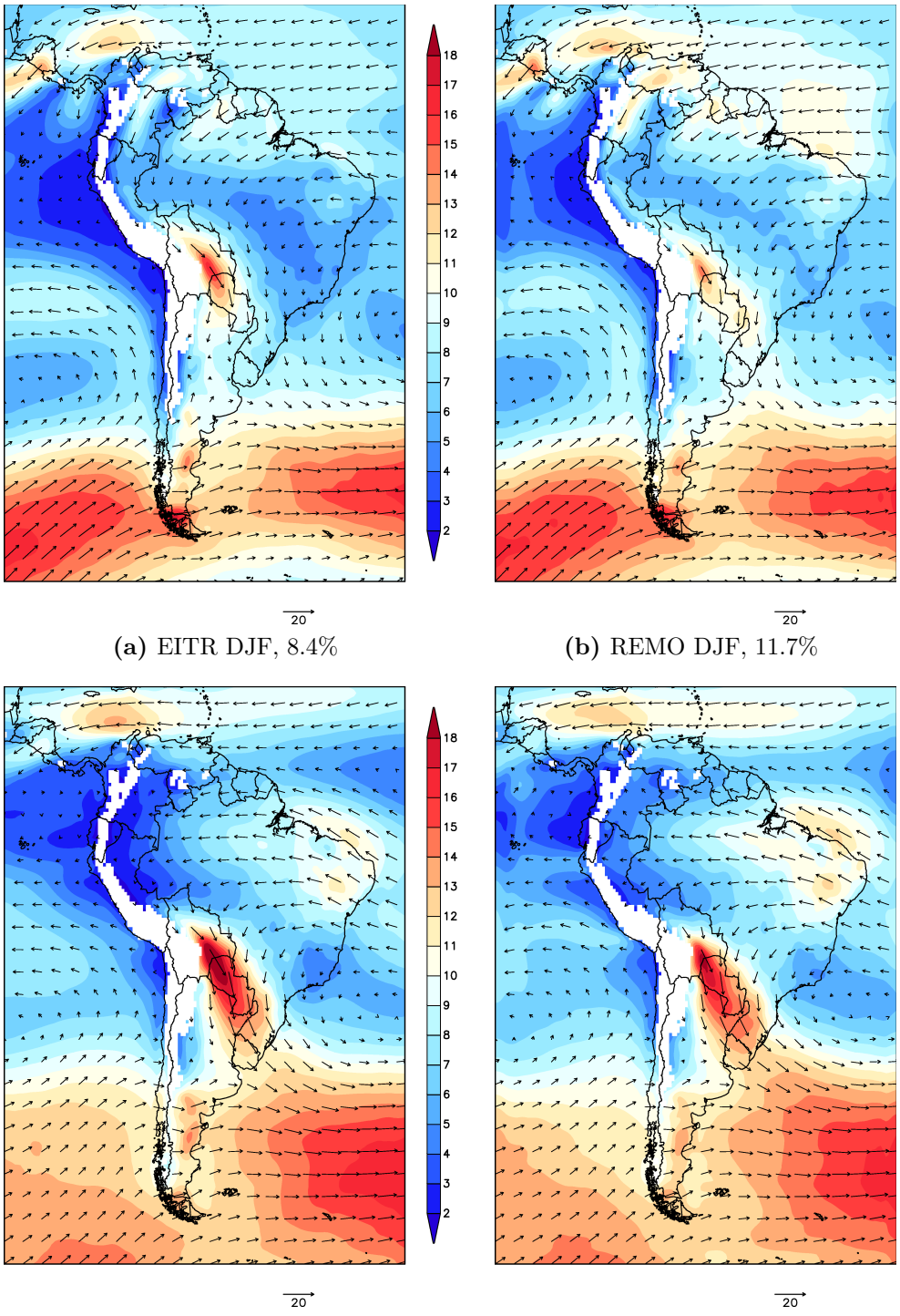

(a) EITR DJF, 8.4%

(b) REMO DJF, 11.7%

(c) EITR JJA,19.2%

(d) REMO JJA,22.7%

Figure 3.12: Mean wind (vector) and wind speed (contoured every 1 m/s) composite at 850 hPa for LLJs detected at the 5 core stations indicated in subsection 3.3.2. EITR Reanalysis (left panel) and REMO simulation (right panel) for austral (a, b) summer (DJF) and (c, d) winter (JJA). The percentages of LLJ events are also indicated at each sub-caption. The period is 1989 to 2008.

The warm bias during spring in REMO (cf. Chapter 2.3) contributes to the lower frequency of LLJ events compared to EITR in Figure 3.13. The spatial extent of the LLJ maximum during each season characterizes the spatial and temporal variability of LLJ. During summer, the region of LLJ maximum is concentrated within the Gran Chaco region. During winter, the exit region of the LLJs extends further south towards the coasts of southern Brazil and Uruguay.

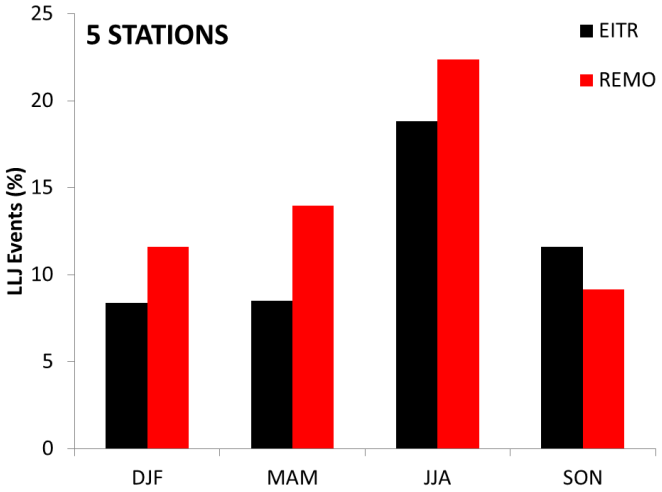

Figure 3.13: Percentage of days with LLJ detected at the five core stations (Santa Cruz, Robore, Mariscal Estigarribia, Asuncion, and Foz do Iguassu) for each season during the period of 1989 to 2008.

Diurnal variation at the Gran Chaco

The diurnal variation of the LLJs detected in POINT MAX or the Gran Chaco region with the **BC** criterion in the EITR reanalysis and REMO simulation is discussed in this subsection. The diurnal variation at each season is shown in Figure 3.14. The tendency of the EITR reanalysis is to have a preferred maximum at 00:00 and 06:00 UTC especially during the warm season. REMO has the same tendency with additional events detected at 18:00 UTC. This behavior is persistent regardless of the detection criterion used (figure not shown). Note that the analysis during the SALLJEX period at stations near the LLJ core, the observed summertime LLJs tend to have their peak intensity during the morning (12:00 UTC) and not in the late afternoon (21:00 UTC). Also note that from the LLJ climatology derived by NCEP (Marengo et al., 2004), three stations along the main axis of the low-level flow exhibited more cases earlier at 06:00 UTC followed by a peak intensity six hours later (12:00 UTC).

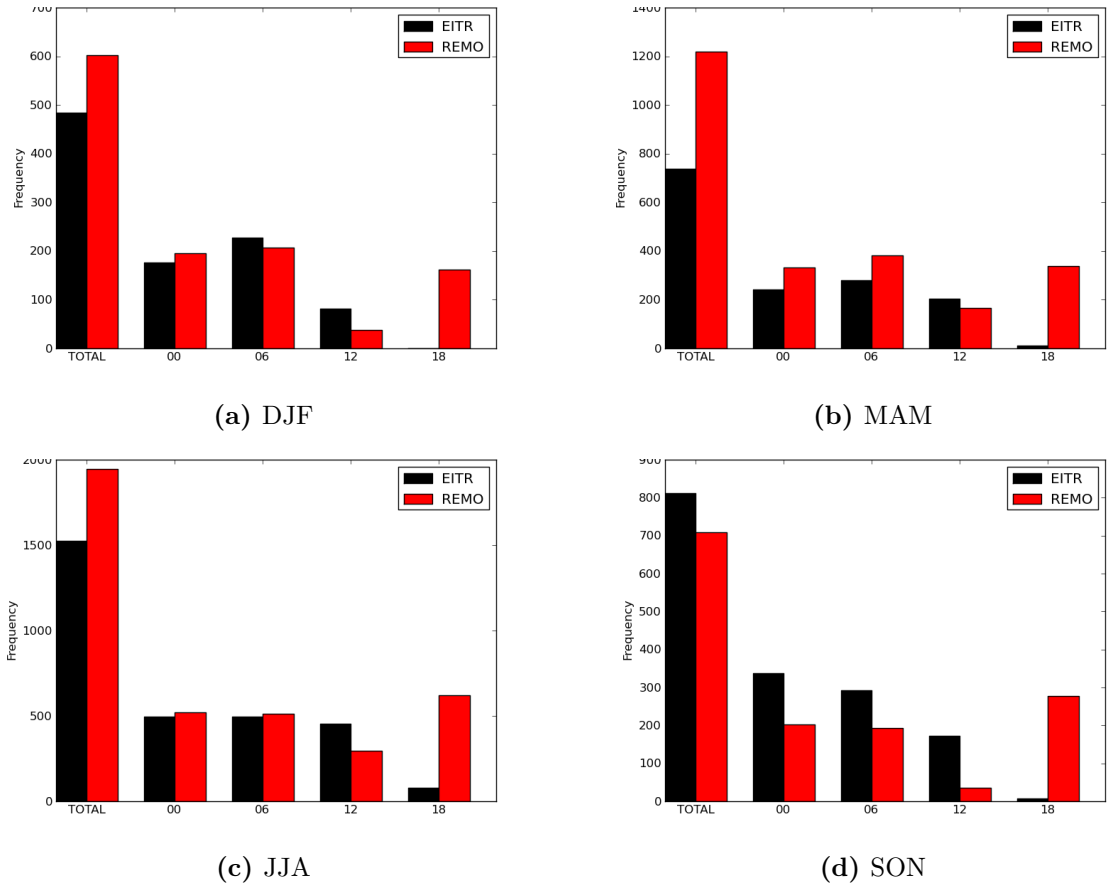

(a) DJF **(b)** MAM

(c) JJA **(d)** SON

Figure 3.14: Diurnal variation for 00:00, 06:00, 12:00, and 18:00 UTC (20:00, 02:00, 08:00, and 14:00 local time, respectively) of seasonal LLJ events at the POINT MAX in Figure 3.9. Black bars for the EITR reanalysis, and red bars for the REMO simulation. The period is 1989 to 2008.

Based on Figure 3.14, REMO tends to overestimate the frequency of LLJ occurrences at 18:00 UTC (14:00 local time) during all seasons. This tendency of a late afternoon maximum (18:00 UTC) in REMO is investigated using the mean wind speeds, temperature, specific humidity, and meridional winds (Figure 3.15–3.16). These figures show the variables' vertical profile of the mean and the LLJ composite during austral summer season.

The vertical profile of the mean winds and temperature at the latitude of POINT MAX during summer and the LLJ composite are shown in Figure 3.15. During the mean summer, the mean intensity of winds at the LLJ region (near 56.5 $°W$) is higher by about 2 m/s in REMO compared to EITR. The temperature at 850 hPa is also higher in REMO than in EITR. The magnitudes of both winds and temperature are intensified during the LLJ composite, with REMO still having higher wind speeds

and higher temperature than EITR.

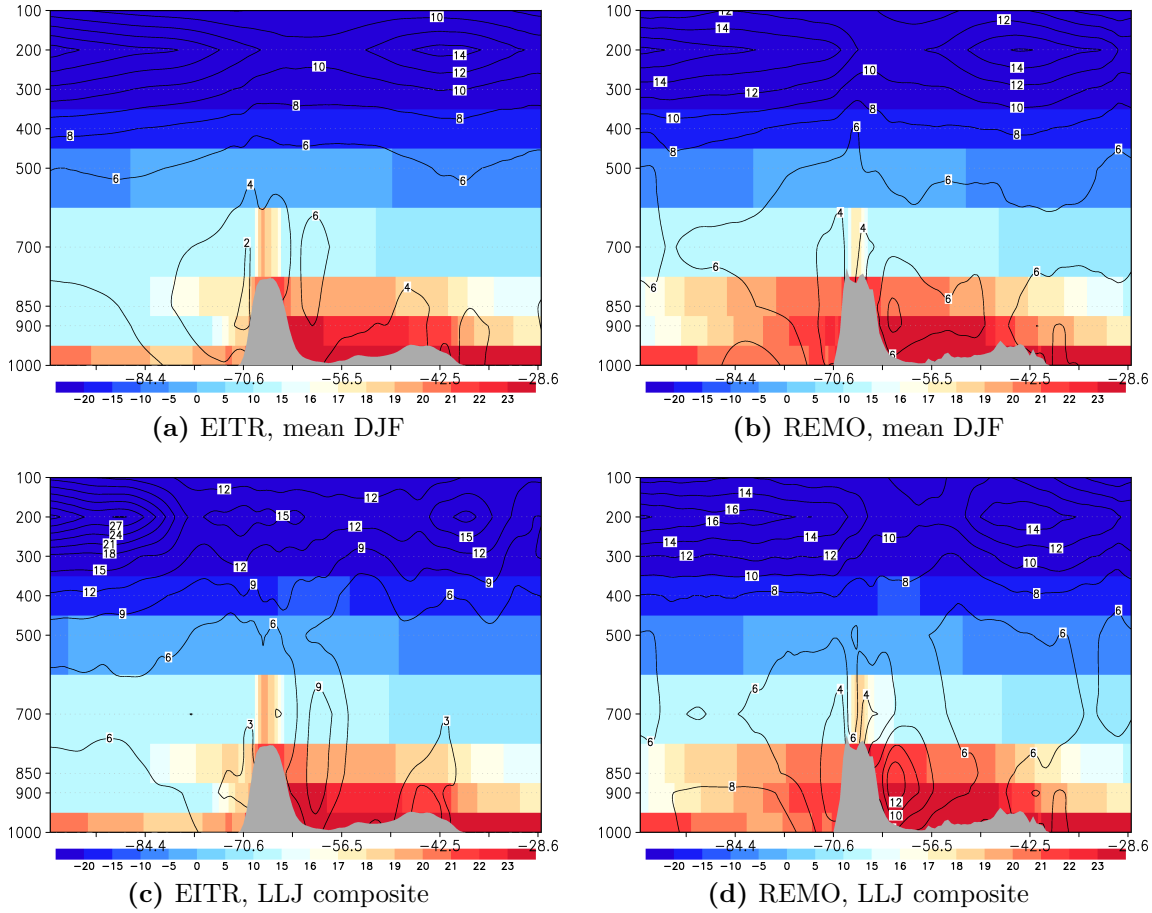

(a) EITR, mean DJF

(b) REMO, mean DJF

(c) EITR, LLJ composite

(d) REMO, LLJ composite

Figure 3.15: Vertical profile of mean wind and temperature at the latitude of maximum LLJ (20.13 $°S$) during the austral summer of 1989 to 2008. Temperature (t) in shaded contours, $°C$. Wind speed (V) with contours in m/s. Orography, overlayed in gray contour.

Figure 3.16 shows the meridional wind speed and specific humidity at the latitude of POINT MAX during summer and the composite of LLJ events. During summer, EITR has a higher mean meridional wind speed than REMO, but REMO has slightly higher mean moisture content than EITR at the LLJ region (near 56.5 $°W$). In the composite of LLJ events, the magnitudes of both meridional wind speed and specific humidity are intensified with REMO having the higher values compared to EITR.

The high values of wind speed, temperature and moisture in REMO result in a high number of LLJ events detected at 18:00 UTC. The implications of the large number of LLJ events in the transport of moisture are discussed further in Chapter 5.

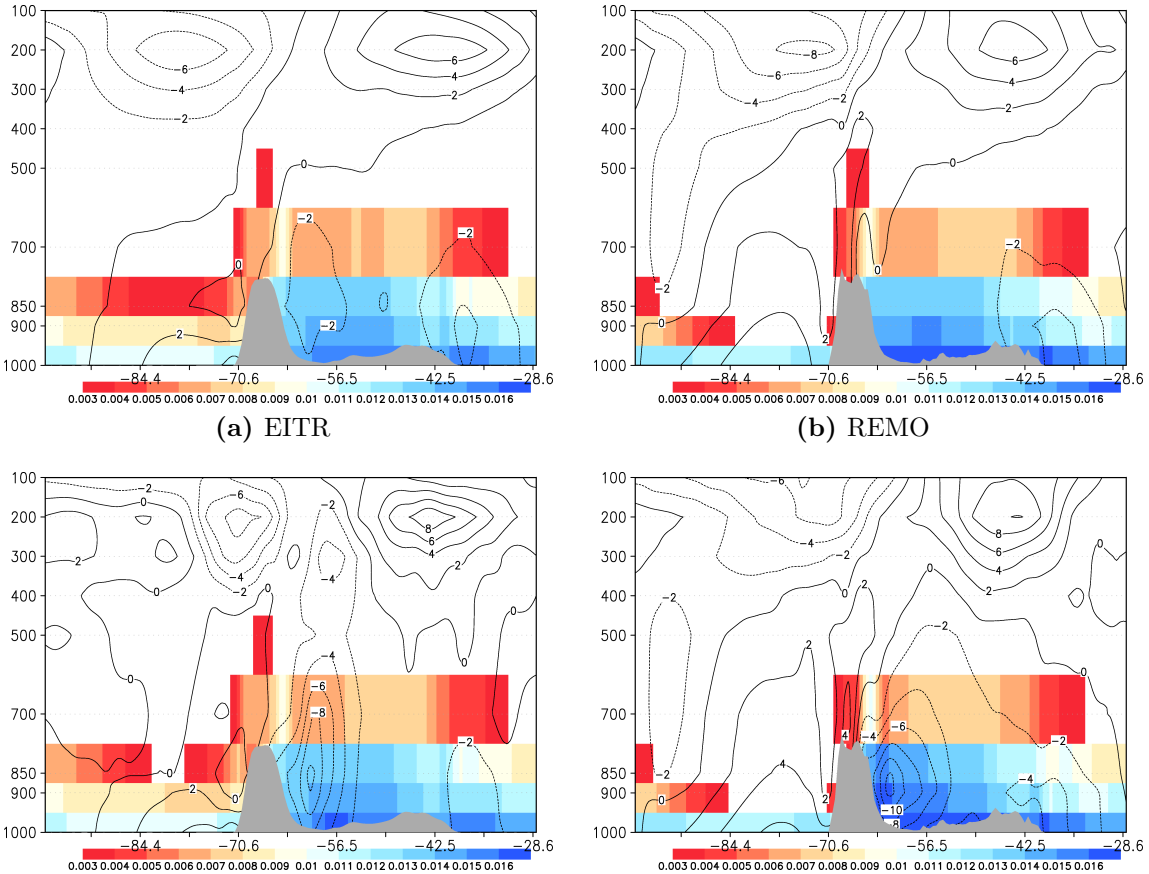

(a) EITR **(b)** REMO

(c) EITR, LLJ composite **(d)** REMO, LLJ composite

Figure 3.16: Vertical profile of mean meridional wind and specific humidity at the latitude of maximum LLJ (20.13 °S) during the austral summer of 1989 to 2008. Specific humidity (q_d) in shaded contours, kg/kg. Meridional winds (ν) in contours with intervals of 2 m/s. Orography overlayed in gray contour.

3.4 Summary and conclusions

A significant climatic feature in South America is the low-level wind maximum detected near the foothills east of the Andes mountains. The low level jets (LLJs) transport moisture and heat from the Amazon Basin towards the La Plata Basin. During austral summer, LLJs are often associated with the development of mesoscale convective systems (MCSs) at the exit region of the LLJs. The formation of LLJs is strongly influenced by the orographic characteristic of the region. This chapter aimed to investigate the criteria for detecting LLJs, its spatial and temporal characteristics, and dependence on horizontal resolution. Using station observa-

tions, reanalyses, and REMO simulation, the spatial and temporal characteristics of the poleward flow in the lower troposphere in South America are identified and described. The results are summarized as follows:

- During the short SALLJEX campaign period, the spatial and temporal characteristics of LLJs are described using station observations, NCEP and EITR reanalyses, and REMO. The spatial characteristics of 850 hPa winds in NCEP, EITR, and REMO delineate the LLJ region. Due mainly to high resolution, the detected LLJs using the **BC** have a spatial extent concentrated east of the central Andes and the meridional wind speed is higher in EITR and REMO than in NCEP. Comparing the winds at the level of the wind maximum, the preferred maximum in the observational datasets and REMO is around 12:00 UTC (8:00 am local time) while the preferred minimun varies.

- Using EITR and REMO, the climatology of the LLJs in South America are analyzed during the period of 1989 to 2008. The LLJs are detected throughout the year with a maximum number of occurrences during austral winter (JJA). The LLJs are detected using three criteria varying on thresholds of wind components and wind shear. Comparing the criteria at the grid points of 8 station points, REMO shows a tendency of higher occurrences than EITR. Five stations (Santa Cruz, Robore, Mariscal Estigarribia, Asuncion, and Foz do Iguassu) represent the LLJ core region. The region with the highest number of LLJ occurrences in EITR and in REMO is located in the Gran Chaco (62.3 $°W$, 20.1 $°S$), near the border between Bolivia and Paraguay.

- Detecting LLJ events is sensitive to the selection of grid point locations. Because of high resolution, the LLJs in REMO are more numerous than in EITR at POINT MAX averaged over all seasons. However, REMO simulates less LLJ events than EITR during spring, which may be partially due to the springtime warm bias over the Amazon basin in REMO.

- The spatial and temporal variability of the days with LLJ events are characterized by maximum occurrence and large spatial extent during austral winter (JJA).

- For the diurnal variations of LLJ occurrences at POINT MAX, REMO simulates a higher number of LLJ events compared to EITR from summer to winter. During spring, however, EITR shows a higher number of LLJ events than REMO. REMO also has a tendency to have more LLJ events at 18:00

UTC than EITR. During the LLJ events, the mean wind, temperature and specific humidity are generally higher in REMO than in EITR at 18:00 UTC.

Based on the results discussed above, the high resolution regional model REMO driven by a high resolution EITR reanalysis is able to simulate the spatial and temporal characteristics of LLJs in South America. An updated LLJ climatology for 20 years using EITR and REMO data shows the presence of the low level flow throughout the year. In this new climatology, the areas frequented by the strong low level flow are identified as the LLJ core region and the annual cycles at selected station locations are described. The composite of LLJ events have higher wind speeds (about 30–50%) than the seasonal mean wind speed at the 850 hPa level.

The LLJs are an important feature in South America especially during the warm seasons, because they play a critical role in defining the precipitation regimes of the region. The LLJ variability in location and intensity has a large impact on the development of mesoscale convective systems, which are further discussed in the remaining chapters.

4 Mesoscale convective systems over La Plata Basin

4.1 Introduction

Mesoscale convective systems (MCSs) are responsible for a large proportion of rainfall in the tropical and warm mid-latitude regions. The precipitation regions of these systems cover at least 100 km in diameter and they last from hours to several days. These systems often produce severe convective weather events such as strong winds, hail, tornadoes, lightning, and flooding. A textbook definition by Cotton et al. (2011) describes MCS as "*a deep convective system that is considerably larger than an individual thunderstorm and that is often marked by an extensive middle to upper tropospheric stratiform-anvil cloud of several hundred kilometers in the horizontal dimension.*" The typical lifecycles of these cloud systems are between six to twelve hours and the stratiform-anvil structure of the system can exist for several days. Figure 4.1 illustrates the typical structure of a mature MCS.

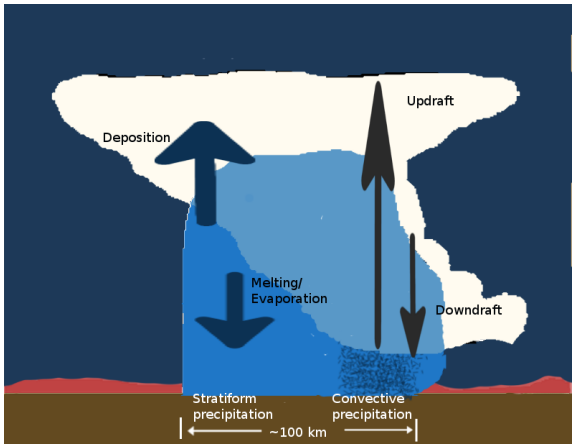

Figure 4.1: Schematic diagram of a typical MCS structure in a mature stage adapted from Houze (2004). Convective (stratiform) precipitation covers approximately ≈30% (≈70%) of the precipitation region. Black arrows indicate updraft and downdraft. Thick blue arrows indicate precipitation processes such as vapor deposition, melting, and evaporation.

The classical definition of mesoscale disturbances is a system between the synoptic scale and the microscale. The atmospheric motions in the synoptic scale are quasi-geostrophic and hydrostatic while in the microscale, they are non-geostrophic, non-hydrostatic and turbulent. After the original definition of Orlanski (1975), Thunis and Bornstein (1996) have proposed new atmospheric scales based on a more rigorous approach using several approximations of the governing equations, including temporal, horizontal, and vertical spatial scales. Mesocale systems are generally

considered as the overlapping scales ranging from a horizontal length of 2 km to 200 km with a duration of an hour to several days, which are large enough in horizontal scale to be considered hydrostatic but not quasi-geostrophic conserving motions. These mesoscale disturbances have been considered as an important link from the large-scale to the small-scale atmospheric motions and vice versa.

Several classifications of MCSs have been identified. In Lin (2007), an MCS can be categorized from squall lines and rain bands, mesoscale convective complexes, to tropical cyclones. Squall lines are narrow bands of convective clouds usually not wider than approximately 5 km. They form in the warm sector of a midlatitude cyclone, ahead of the cold front. The lifetime of a squall line lasts between a few hours to 3–4 days. Squall lines are also common in South America due to the presence of warm, humid air from the North Atlantic meeting cooler, drier air from the southwest winds coming from Antarctica and the Andes. Wind shear is essential for the formation of thunderstorms into a squall line. A supercell storm, another type of MCSs, creates hail, damaging winds, and can generate tornadoes. This storm is generally a single, violent storm cell of intense rotation and wind shear, which lasts for about 2–4 $hours$.

The largest subclasses and relatively significant systems in this study are the mesoscale convective complexes (MCCs). These systems comprise quasi-circular formations of many thunderstorms. They exhibit large oval or nearly circular cloud shields with an area of about 50,000 km^2 or larger and the systems persist for 6 $hours$ or longer. Because the system is rather large, the conditions permit formation of other storms to develop, thus MCCs tend to self-propagate.

MCCs need warm moist air sources such as from the Gulf of Mexico for North America or from the Atlantic and Amazon Rainforest for South America. The MCCs developing over South America gain moisture by crossing a large moisture source due to evapotranspiration, the Amazon Basin. The system also needs dry air in the troposphere coming from a different direction such as winds from the Andes to generate instability and wind shear. Aside from the Americas, regions with high frequency of MCCs occurrences can be found in various parts of Africa, India, China, Australia, and Europe (Zipser et al., 2006).

MCSs are intensively analyzed for its positive and negative impacts to the climate of the region. As previously mentioned, the systems are main contributors to rainfall that provide water resources for agriculture, human consumption and energy production (Cotton et al., 2011). MCSs provide the necessary sources of moisture due

to the large spatial coverage from a few to hundred kilometers with duration from a few hours to days. The negative aspect of these systems occurs in extreme cases. Long-lasting and slow moving MCSs can bring severe weather events such as hail, tornadoes, thunderstorms and heavy downpour leading to floods over large areas. Inversely, the absence of these systems dries up the soil and causes severe drought leading to scarcity of agriculture products.

Predicting the lifecycles of mesoscale convective systems started in North America using satellite imagery in combination with surface and radar data. Several conceptual models were put forward in the late 20^{th} century and further developed with better instrumentation techniques. Maddox (1980) provided a conceptual model to define a mesoscale convective complex (MCC) based on the analyses of enhanced infrared satellite imageries (Table 4.1). The definition was later on modified by Velasco and Fritsch (1987) using different satellite images available for a two year study to document the structure and dynamics of MCCs over the midlatitude regions of South America and in the tropical region between North and South America. Durkee and Mote (2009) used this definition in studying the climatology of MCCs in the subtropical regions of South America.

Table 4.1: MCC Definition originally developed by Maddox (1980).

	Physical characteristics
Size	Interior ice cloud shield with temperature $\leq -52\ ^{\circ}C$ must have an area $\geq$ 50,000 km^2
Initiation	Size definition first satisfied
Duration	Size definition must be met for a period $\geq 6h$
Maximum extent	Contiguous cold-cloud shield (Infrared temperature $\leq -52\ ^{\circ}C$) reaches maximum size
Shape	Eccentricity (minor axis/major axis) ≥ 0.7 at time of maximum extent
Termination	Size definition is no longer satisfied

Numerous studies in analyzing the structure and life cycles of MCCs exist because of drastic implications for the economy of the region. Laing and Fritsch (1997) identified regions including South America, which were favourable for MCC development based on two years of enhanced infrared satellite imagery. Zipser et al. (2006) indicated that the La Plata Basin had one of the highest frequencies of thunderstorms based on seven years of data from TRMM or the Tropical Rainfall Measuring Mission (Huffman et al., 2007). From the above-mentioned observational studies, the

MCSs have largely contributed to the global hydrological cycle.

In South America, the subtropical regions particularly within the La Plata Basin, have been identified as conducive for the development of MCSs (Laing and Fritsch, 1997; Durkee and Mote, 2009). The observed characteristics of MCSs over the La Plata Basin included a high density of lightning flashes, convective systems with extensive ice-scattering, and heavy precipitation events that persisted for several hours to few days (Nesbitt et al., 2000; Schumacher and Houze, 2003). In a 2-year study of Velasco and Fritsch (1987), an average of 29 events were documented in the subtropical region of South America during the warm season of 1981-1983. In a similar region, a longer study of 9 summers by Durkee and Mote (2009) characterized the life cycles of the MCCs using satellite estimates from TRMM. They documented 330 events with an average of 37 MCCs per warm season. The largest MCCs that they have recorded, reached a maximum cloud-shield size of 256,500 km^2 for a duration of about 14 hours. During the SALLJEX campaign (Vera et al., 2006a), MCSs cases were identified and simulated using regional climate models. They found that the models tend to underestimate the heavy precipitation during an MCS event.

Studies on MCSs were complemented with studies on precipitation especially focusing on extreme cases. Studies from South America such as Menéndez et al. (2009, 2010) have analyzed months with anomalous conditions such as droughts or extreme precipitation events using an ensemble of regional climate simulations using dynamical models and a statistical method. Their results indicated that the ensemble mean of the models produce better statistics than the individual members of the ensemble. The study was later on continued in order to analyze the climate over Southeastern South America including the La Plata Basin (Carril et al., 2012). In that study, four regional climate models were integrated to reproduce the climate over the La Plata Basin during the decade from 1991 to 2000. Precipitation, mean sea level pressure, maximum and minimum temperature fields were evaluated using seasonal means and indices for extremes based on percentile approach. They have concluded that although the seasonal means were comparable with observations, the models underestimated heavy precipitation events due to different convection schemes and the averaging of daily precipitation values over a 50×50 km^2 grid box compared to the point data of stations. For further reference, the abstract of the coauthored paper is attached in Appendix G.

Mesoscale convective systems are the main drivers for the summertime precipitation over the La Plata Basin. The water resources in the basin are crucial to five sur-

rounding countries (Berbery and Barros, 2002). One of its main tributaries is the Parana River, which feeds the Itaipu Dam, the world's largest hydroelectric power plant. Determing both the spatial and temporal variability of MCSs is crucial in characterizing the climate of the La Plata Basin. Over the basin, these systems tend to occur frequently, which can saturate the soil and cause severe flooding. The potential for flooding over the region depends on the precipitation regime and river discharge conditions (Berbery and Barros, 2002). On the other hand, absence of MCSs leads to scarcity of water and causes severe drought. Precipitation anomalies over the La Plata Basin are also correlated to the large scale conditions such as the El-Niño Southern Oscillations or ENSO (Chen et al., 2010).

Due to the hydrological as well as economic impacts over the La Plata Basin, the characteristics and predictability of MCSs have been investigated strongly. Studies using observations, satellite techniques and climate simulations have multiplied through time due to the importance of having a better understanding of MCSs in its horizontal and temporal scales. In this study, the aims are to identify the regions frequented by heavy precipitation events associated with MCSs and quantify their contributions with respect to the total summertime precipitation using observational datasets and high resolution simulation from REMO for a longer period of time compared to previous short-term studies. The research objectives of this chapter are to:

- ascertain the spatial and temporal variability of MCSs including the environment favourable for development;
- explore several test cases during the intensive SALLJEX period;
- evaluate the observed and simulated characteristics of MCS for longer periods using satellite estimates of outgoing longwave radiation, cloud cover and heavy precipitation thresholds;
- measure the skill of regional climate models in simulating the distribution of daily precipitation at certain regions through model intercomparison
- establish criteria for selecting precipitation associated with the MCSs

In preparation for the analysis of the link between LLJs (c.f. Chapter 3) and MCSs, the spatial and temporal variabilility of the characteristics of MCSs are analyzed first in this chapter followed by the long-term analysis.

4.2 Data and methods

The characteristics of MCSs during the austral summer are analyzed using the outgoing longwave radiation (OLR), cloud cover, and precipitation fields. Low values of OLR indicate regions with deep convection and they correlate to the state of cloudiness. The rainfall regions of MCSs have both the stratiform and convective structures and are contiguous at least 100 km with a duration from hours to several days. The impact of MCSs on the precipitation regimes are first analyzed over the La Plata Basin using different rainfall thresholds. Then the rainfall events associated with MCSs are analyzed to identify regions frequently visited by MCSs during the decade of 1999 to 2008, when observations are robust.

The National Oceanic and Atmospheric Administration (NOAA) OLR (Liebmann, 1996) and the International Satellite Cloud Climatology or ISCCP (Rossow and Schiffer, 1999) cloud cover dataset covers different time periods and sampling frequencies (c.f. Table D.1). The mean climatologies for the 20-year period are primarily established for both datasets. Variations of the OLR during the decade from 1999 to 2008 are used as indicators for deep convection. The climatological OLR is substantiated by the total cloud cover from ISCCP.

Precipitation datasets from the NOAA Climate Prediction Center for Unified Precipitation or CPCUNI (Chen et al., 2008), TRMM, and MERGE (Rozante et al., 2010), which are based on a merged dataset using the TRMM and observations, are used to analyze the different rainfall regimes over South America. The three datasets are also utilized to assess the spread among the simulations and observations.

For the evaluation of daily precipitation distribution, several methods are used. The skill of the simulations is computed using the scoring method devised by Perkins et al. (2007). First, regions are defined based on hydrological basins and climate types defined in Figure 2.5. Later in this chapter, the focus is shifted to the La Plata Basin. Second, at each region, the daily precipitation values are aggregated over time for calculating the normalized empirical probability distribution functions (PDFs). As an example, the region with subtropical humid climate type (Cr) contains 805 grid boxes in REMO. Thus, the rainfall distribution during summer has a sample size (N) of 850 $\times$ number of days with rain. Note that the threshold for rain days is at least 1 mm/day to remove the discrepancies of drizzle between observations and models (Kjellström et al., 2010). In addition, the contribution of precipitation with low intensity is not significant (Dai, 2001). Last, the skill score SS is computed using

the cumulative minimum probability between two distributions (with N samples). The SS measures the common area between the reference distribution (REF) and the distribution for comparison (M) e.g. REMO or TRMM. The formula for SS is

$$SS = \sum_{1}^{N} min(Z_M, Z_{REF}). \tag{4.1}$$

The score serves as a good quantitative measure of the similarity of two distributions in predefined regions with similar characteristics. A score of 1 would mean that the distributions are exactly the same. The skill score is sensitive to the bin width. Similar to Kjellström et al. (2010), the scores tend to decrease when the bin width deviates from 1 mm/day, the standard value for climate impact-related studies. Thus for this study, the bin width of 1 mm/day is selected.

In addition to the predefined regions, the MCS region is identified based on the occurrences of the MCS centroids defined by Durkee and Mote (2009). The region extends from 67.5−55 °W and from 40−20 °S. Note that this region contains the estimated centers of the MCSs during nine warm seasons.

Furthermore, the analysis of daily precipitation includes a model intercomparison within the framework of the CLARIS-LPB Project. As mentioned in Chapter 2, REMO and six other regional climate simulations have been used to simulate the climate over South America. This short model intercomparison provides a robust description on how models simulate the daily precipitation. The list of regional models used in the project including the setup and basic references of each model is given as Appendix C.

The method of isolating the rains due to MCSs is applied mostly to satellite data. Past studies performed area averaging of precipitation at defined regions due to the limit of predictability in models (Vera et al., 2006a). In the current research, an attempt has been made to calculate the rains due to the MCSs. The segregation method involves two steps. The first step is to select the heavy rain days with deep convection. The thresholds of OLR daily values that indicate deep convection is determined. Several studies have shown that the model derived OLR is dependent on the radiation scheme of the model. To avoid this model bias, the OLR thresholds are calculated based on the daily anomalies from the seasonal mean. The threshold is then based on days with negative anomalies at least one standard deviation apart. Deep convection is assumed if the anomaly of OLR is lower than one standard deviation. The second step is to select the days with heavy precipitation. Two

different thresholds are investigated. The first threshold is based on Velasco and Fritsch (1987), wherein heavy precipitation measures at least 25 mm/day. The second threshold is based on climatological studies of daily precipitation studies in South America such as by Carril et al. (2012) and references therein. They have considered the 75^{th} percentile of the daily rainfall distribution as the threshold for heavy precipitation.

The lifecycles of MCSs, particularly MCCs, generally start during the late afternoon, reach maximum size at midnight, and dissipate during the morning. However, due to the limited frequency of observations, the method currently selects rainfall associated with systems that have similar characteristics as MCSs (quasi-MCSs). Also, note that the 25 mm/day threshold is a strict criterion for a rainfall averaged over a 50×50 km region.

4.3 Results and discussions

4.3.1 Model evaluation during SALLJEX

During the four-month SALLJEX campaign, more than a hundred MCSs have been detected over the La Plata Basin. The observed total rainfall amount is greater than 900 mm based on the CPCUNI dataset (Figure 4.2). Note that the climatological mean monthly rainfall over the basin is about 100–250 $mm/month$ (Solman et al., 2013). During this time period, the MCS region and parts of Brazil have precipitation greater than 500 mm. Less precipitation are expected in the lee side of the Andes.

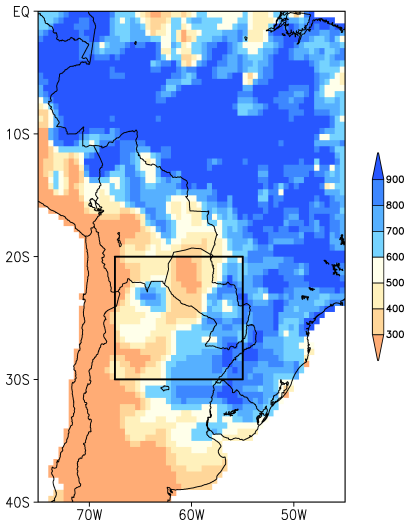

Figure 4.2: Total precipitation from CPCUNI during the SALLJEX campaign. MCS region indicated by the black box.

Table 4.2 shows the statistics of the area-averaged observed and simulated daily precipitation over the MCS region. The variation among the three observational datasets is low. Considering the spatial average, the 75^{th} percentile (75p)

threshold values are considerably smaller than the perceived heavy rainfall events of 25 mm/day by Velasco and Fritsch (1987).

Table 4.2: Daily precipitation statistics area averaged over the MCS region (67.5–55 $°W$ and from 30–20 $°S$) during the SALLJEX Period. The total number of days within the austral summer season of 2002–2003 is 120. Rainy days are days with values ≥ 1 mm/day. The percentage of the accumulated rainfall during days $\geq$ 75p is relative to the total rainfall amount.

Dataset	Rainy days (%)	Total rain mm	Mean mm/day	Max mm/day	75p mm/day	Days $\geq$ 75p (%)	Total 75p (%)
CPCUNI	71	527	4.5	20.2	7.3	35	66
TRMM	64	531	4.6	22.5	7.3	39	70
MERGE	68	529	4.5	21.6	6.5	37	70
REMO	79	627	5.3	25.8	8.1	31	60

From Table 4.2, daily precipitation statistics from REMO tend to be higher than the three observational datasets except for the number of days and the total rainfall amount that are equal or greater than the 75^{th} percentile threshold. These low values of REMO illustrate that REMO tends to simulate lighter rains than the 75^{th} percentile threshold more often during the SALLJEX Period.

Figure 4.3 displays the anomaly of daily precipitation from the austral summer mean value of 2002–2003. The anomaly values are normalized to the mean and approximately range from -1 to 4 mm/day. The rainfall evolution from observations and satellite estimates are similar with a slight tendency for TRMM to estimate higher values compared to CPCUNI and MERGE. Rozante and Cavalcanti (2008) observed similar tendencies of TRMM overestimation, which they associated with the method used to estimate precipitation. This figure also shows the OLR anomalies from the seasonal mean. During this period, observed low OLR anomalies correspond to high rainfall anomalies especially on two episodes with MCSs on January 16 to 19 and 22 to 24, 2003 (Vera et al., 2006a; Rozante and Cavalcanti, 2008). REMO OLR and precipitation anomalies are comparable to the observational datasets with some differences.

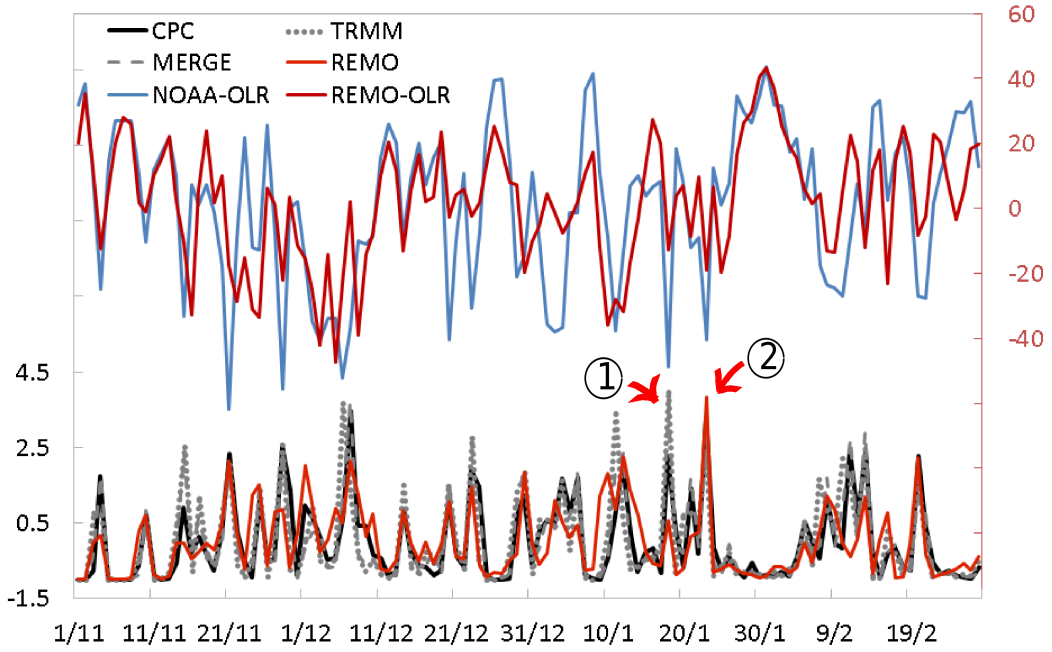

Figure 4.3: Spatial average of the OLR anomalies (right axis) and daily precipitation normalized anomalies (left axis) from the mean during the SALLJEX period from November 2002 to February 2003. The subregion extends from 67.5−55 °W and from 30−20 °S. Two test cases for MCSs events: (1) January 16 to 19, and (2) January 22 to 24. Black, gray, and blue (red) lines are based on observations or satellite estimates (simulation).

Several MCSs have been documented during the SALLJEX Period. According to Zipser et al. (2004), 42% of the 112 MCS cases occurred in the subregion between 45–55 °W and 20–30 °S. As can be seen from Figure 4.3, REMO simulates well the latter case but not the former case. The possible reasons could be the location of the MCS during the event and the inherent limitations of the convective parameterization scheme of the model. Also, the REMO model version used is run in the climate mode, for which the model produces its own internal variability (Laprise et al., 2012).

In retrospect with Section 3.3.1, the results indicate that REMO is able to represent the daily precipitation statistics over the La Plata Basin. Although the timing is not exact for some cases and few of the wet anomaly values are lower than the observed, the mean statistics of REMO are comparable with the observations over the MCS region during the short-term SALLJEX Period. The MCSs spatial variability for a longer period will be discussed in the next sections.

4.3.2 MCS climatology

The heavy precipitation events associated with the characteristics of MCSs are derived based on the daily OLR and daily precipitation values. The period considered is the warm season from the 1999–2008 decade. The period of analysis is limited to the ten overlapping years due to the coverage among the observational datasets, i.e. TRMM has available precipitation data starting from 1997 only. The OLR values are analyzed first followed by the analysis of daily precipitation values.

Outgoing longwave radiation

The MCSs, particularly the MCCs, are identified as large regions with cold cloud tops and deep convection. Using estimates of outgoing longwave radiation (OLR), the regions with high MCSs activity are identified. The monthy and daily means of interpolated OLR data from NOAA (Liebmann, 1996) are used for this purpose.

Figure 4.4 shows the daily mean negative OLR anomalies from the seasonal mean during the austral summer of 1989 to 2008 period. The negative anomalies ranges from 0 to -40 W/m^2 and the standard deviation ranges from 15 to 42 W/m^2. Note that the observed low values over the La Plata Basin and over the South Atlantic Convergence Zone where large numbers of upper troposphere cold clouds (e.g. deep convection anvils) are expected. The highest OLR anomalies are located over the Pacific Ocean, which is close to the cold upwelling regions due to the Humboldt/Peru current. Near the coast of Chile, the Atacama Desert can be identified as a region with high OLR anomalies. The lack of water vapour and clouds in the desert allow the effective infrared temperature to radiate back to space therefore OLR values are high in these regions. The contours in the figure indicate the standard deviation of the daily anomalies from the seasonal mean. High values of standard deviation are observed over the La Plata Basin and the Amazon Basin.

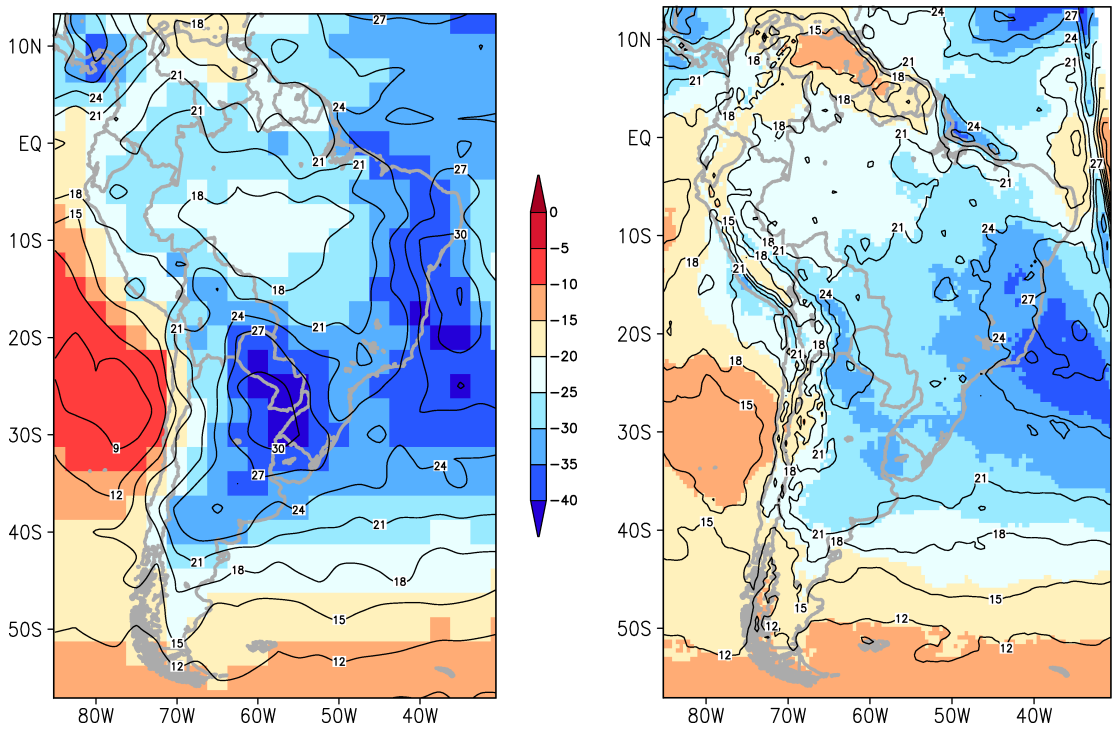

(a) NOAA **(b)** REMO

Figure 4.4: Austral summer mean (filled contour) and standard deviation (contour lines) of the negative OLR daily anomalies from the seasonal mean over the period 1989 to 2008. From (a) NOAA and (b) REMO. Units are in W/m^2.

Also in Figure 4.4, the regions with negative OLR anomalies and high variance e.g. blue regions and contour values can be identified. The anomalous regions with one standard deviation away from the mean serve as a criterion in selecting rains associated with MCSs. The spatial patterns of REMO-derived negative OLR anomalies are similar to the NOAA OLR. The regions of deep convection over the La Plata Basin, Amazon Basin and the South Atlantic Convergence Zone are indicated with values ranging from -20 to -40 W/m^2. Over the La Plata Basin, REMO signal is weaker compared to NOAA OLR.

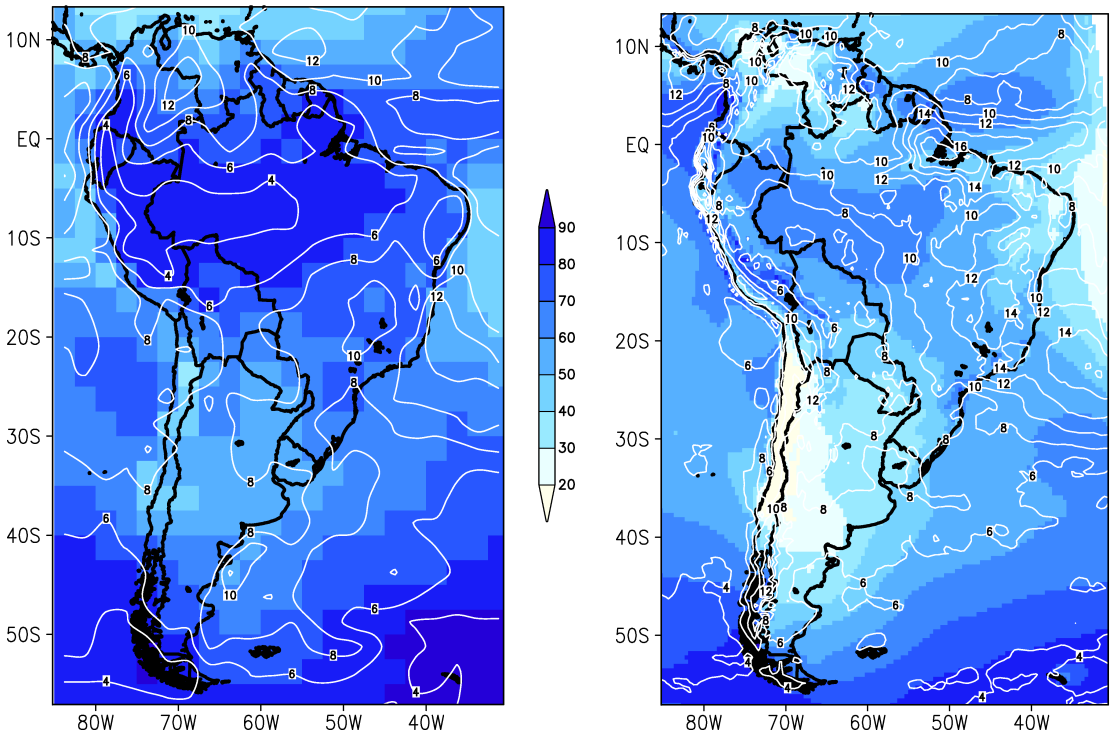

(a) ISCCP ($\sim$ 280 km) **(b)** REMO ($\sim$ 50 km)

Figure 4.5: Austral summer mean total cloud cover (filled contours, %) and standard deviation (contour lines) of the cloud cover monthly anomalies from the seasonal mean over the period 1989 to 2007. The standard deviation is normalized to the summer mean values. Note that white shades indicate clear skies, blue for clouds.

Using the available monthly values of total cloud cover from ISCCP and REMO, the cloudiness of the continent and surrounding areas can be determined in Figure 4.5. The regions with high values of cloud cover ($\geq$ 80%) are over the Amazon Basin due to deep convective clouds (Marengo, 1995) and the South Pole (Town et al., 2007). In REMO, the spatial pattern looks similar but the values are underestimated, which is about 10–20% lower compared to ISCCP. The derivation of cloud cover in REMO as well as the caveats in its derivation are thorougly discussed in Pfeifer (2006). The lifecycles of convective clouds in REMO are calculated in one timestep with no memory of the previous timestep is included. The low values of cloud cover in REMO correspond to higher values of OLR, e.g. in some parts of the Amazon and La Plata basins.

Daily precipitation

The uncertainty in simulating the daily precipitation distribution, mean and extreme thresholds are characterized following Carril et al. (2012). Within the CLARIS-LPB Project (cf. Chapter 1.2.2), an ensemble of six regional models and one global model with a stretched grid are compared on a common grid with 0.5°×0.5° resolution based on the reference dataset (CPCUNI). For comparison, the TRMM data are also upscaled from a high resolution of 0.25°×0.25° to the common grid. The different model configurations are listed in Appendix C.

Using the Perkins et al. (2007) method in evaluating the skill of the seven models in representing the warm season precipitation distribution, the PDFs are derived at different regions for the overlapping period of 1999 to 2008. One of the advantages in using regions with similar climate characteristics is the coherent approach in representing the precipitation regimes. Moreover, the regions of interest cater for different needs of impact studies such as hydrological or ecological models.

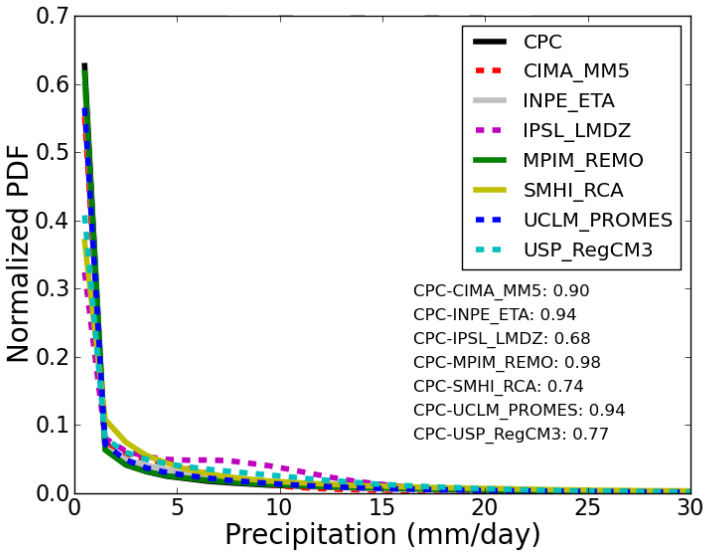

Figure 4.6: The normalized PDF and skill score for the subtropical humid (Cr) climate type. Bin width is 1 mm/day. REMO is indicated in green line. Daily precipitation values are truncated to highlight bin values less than or equal to 30 mm/day.

As an example, Figure 4.6 shows the normalized PDF of the rainfall distribution over the subtropical humid climate type, Cr. The PDF curves illustrate the disparity of the different model distributions. Some models tend to simulate rainfall more frequently in the 5–15 mm/day range. The figure also indicate the individual skill score (SS) for this climate type. Scores are simple indications of how similar the other distributions differ from the distribution of the reference dataset, in this case the CPCUNI.

The skill of the models in simulating the austral summer daily precipitation is summarized in Table 4.3. The simulated rainfall distribution from the seven models and rainfall estimates derived from TRMM are compared with CPCUNI. The skill score of TRMM is relatively high indicating that the daily precipitation distribution of the two observational datasets are very similar. The ensemble (ENS) distribution is calculated by aggregating all the rainfall values of the simulations.

Table 4.3: Daily precipitation skill score summary based on probability density functions (PDFs) at 12 regions (climate types and subregions including hydrological subbasins c.f. Figure 2.5). The period considered is austral summer of 1999 to 2008.

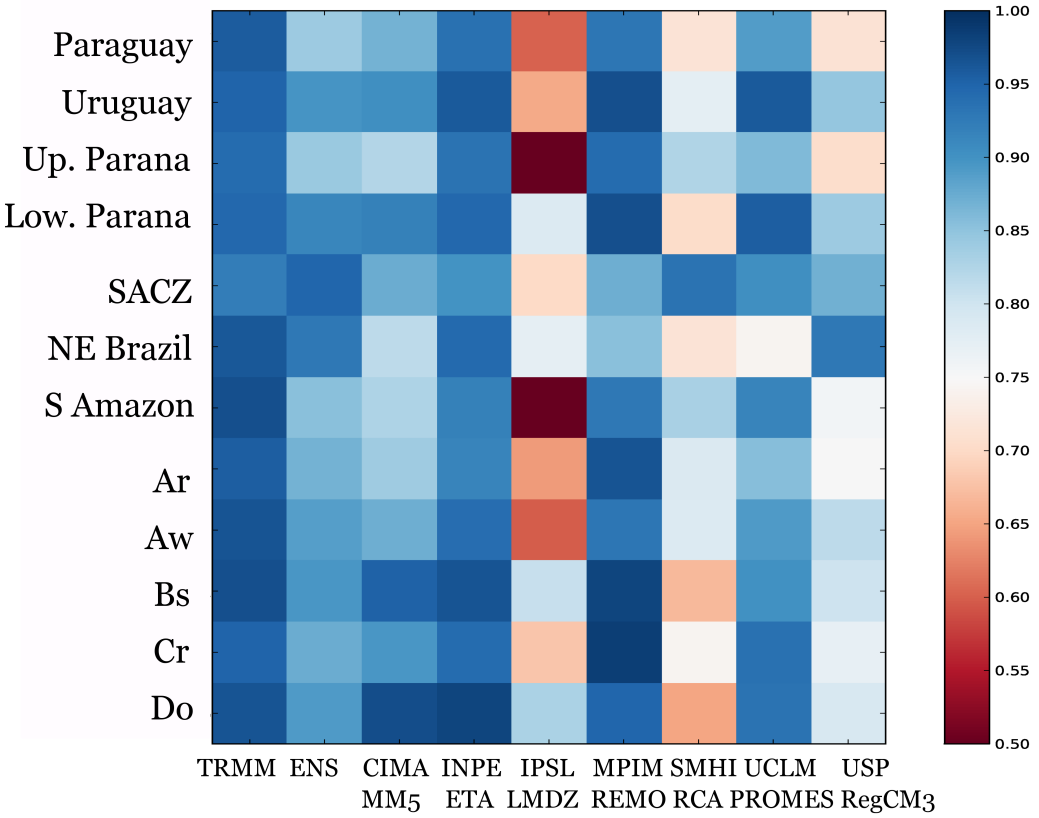

In simulating the daily rainfall distribution at twelve different subregions, REMO has a relatively high skill compared to CPCUNI. REMO represents well the distribution of the daily precipitation particularly over the La Plata Basin (Paraguay, Uruguay, Upper- and Lower Parana) and region with the Cr climate type. Some models have a tendency to have relatively low skill in simulating the daily rainfall distribution. In the case of the global stretched-grid model LMDZ, the simulated distribution tend to have too frequent rainfall events between 5-15 mm/day (e.g. Figure 4.6) in certain subregions, e.g the tropical climate regions (Ar, Aw) including the South Amazon and Upper Parana subregions. As in Carril et al. (2012), although the ensemble represents the general climate regime for precipitation (relatively high skill scores of ENS), the performance of individual members must be closely examined.

After evaluating the skill of the models in simulating the daily precipitation distribution, the performance of simulating heavy precipitation events is investigated using the box-and-whisker statistics. The threshold used for the heavy precipitation events is the 75^{th} percentile at different regions in the La Plata Basin (Figure 4.7).

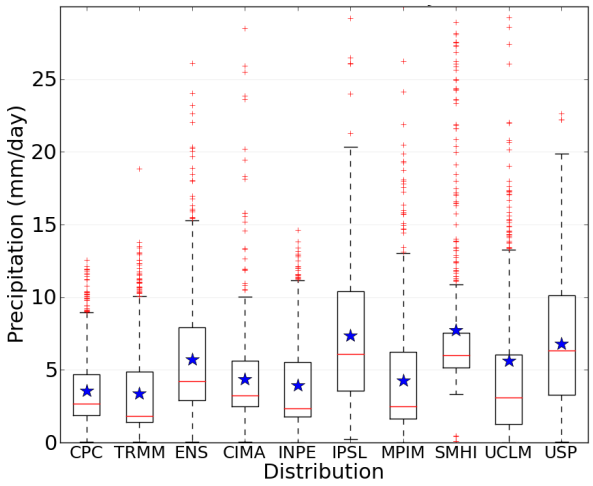

(a) Subtropical humid (Cr) climate type

Figure 4.7: Box-and-whisker plots showing the spatial variability of seasonal heavy precipitation using the 75%-ile threshold within subregions based on climate type **(a)** and hydrological basins **(b–e)** in the La Plata Basin for the period of 1999-2008. Each box represents the distribution of the reference dataset (CPCUNI), TRMM, the 7-member ensemble mean (ENS) and each member of the ensemble. The box plot shows the interquartile distance (IQD, 25-75^{th} percentiles), the median (red line), and the mean (blue stars). Values farther from the median more than 1.5 times the IQD (horizontal bars outside boxes) are considered outliers (red crosses).

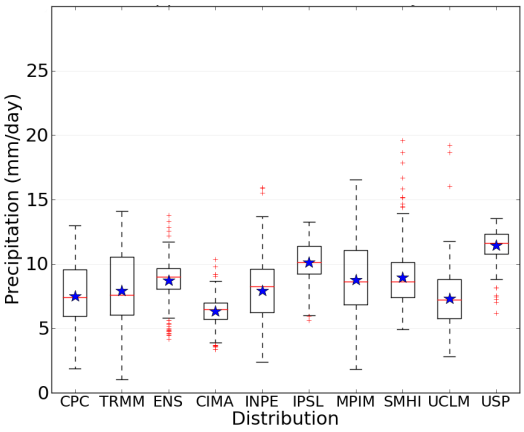

(b) Upper Parana

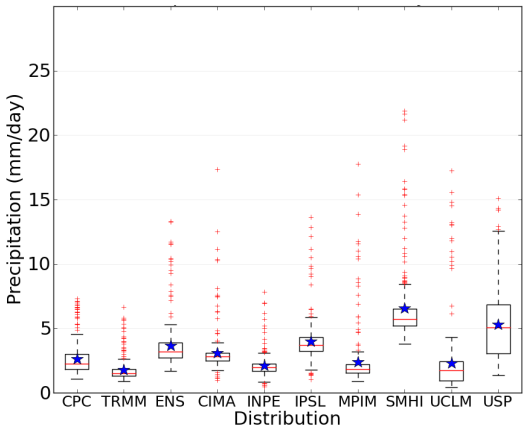

(c) Lower Parana

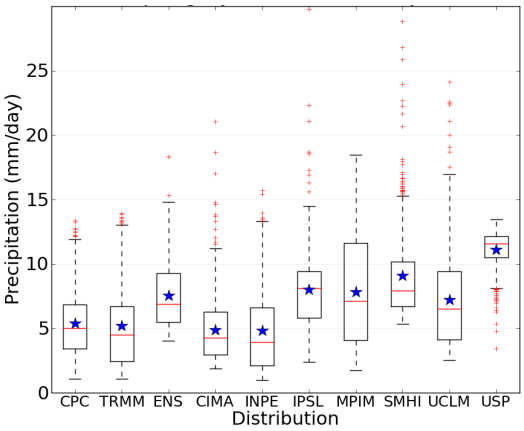

(d) Paraguay

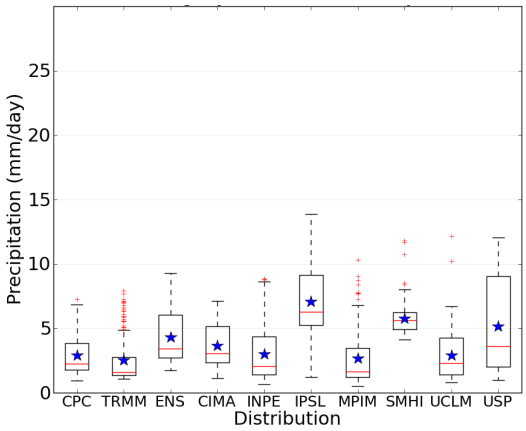

(e) Uruguay

Figure 4.7: *cont.*

The subregions included are four subbasins (Paraguay, Uruguay, Upper and Lower Parana) and the Cr climate type, which include some grid boxes outside the La Plata Basin (cf. Figure 2.5). The box plots show the quantitative comparison of distributions by exploring the range or spread, mean, median, and identifying the outliers. The boxplots indicate the sensitivity of selecting the regions and area-averaging statistics. For example, the distribution for Cr and Lower Parana subbregions are skewed towards the high values, which indicates higher occurrences of extremes (outliers). The other three regions have a centered distribution with less outliers. Area-averaging these regions indicates a good representation of the precipitation regime.

The 75^{th} percentile threshold in most regions are lower than the 25 mm/day threshold. Thus, in order to represent rainfall due to MCSs, the latter threshold is used for further analysis.

MCS Rain

After evaluating the spatial and temporal variability of the OLR anomalies and the daily precipitation distribution, the rainfall associated with MCSs is derived. Two conditions are used to select precipitation events associated with the MCSs:

- Condition 1: Daily OLR negative anomalies that deviate more than one standard deviation from the seasonal mean
- Condition 2: Daily rainfall values of at least 25 mm/day

The succeeding figures are going to show only the MCS region defined in Figure 4.2 and some surrounding areas.

Figure 4.8 shows the number of days relative to the length of austral summer days that satisfy the first condition during the period of 1999 to 2008. For both the coarse grid NOAA and the high resolution REMO, 30–60% of the ten summers show low daily OLR values. High frequency of negative OLR anomaly occurrences is also visible over the Gran Chaco Region at about 67 $°W$ and 27 $°S$. This figure also shows that the observed spatial characteristic of the occurrences are represented in REMO with additional regions of maxima over the southeastern Bolivia.

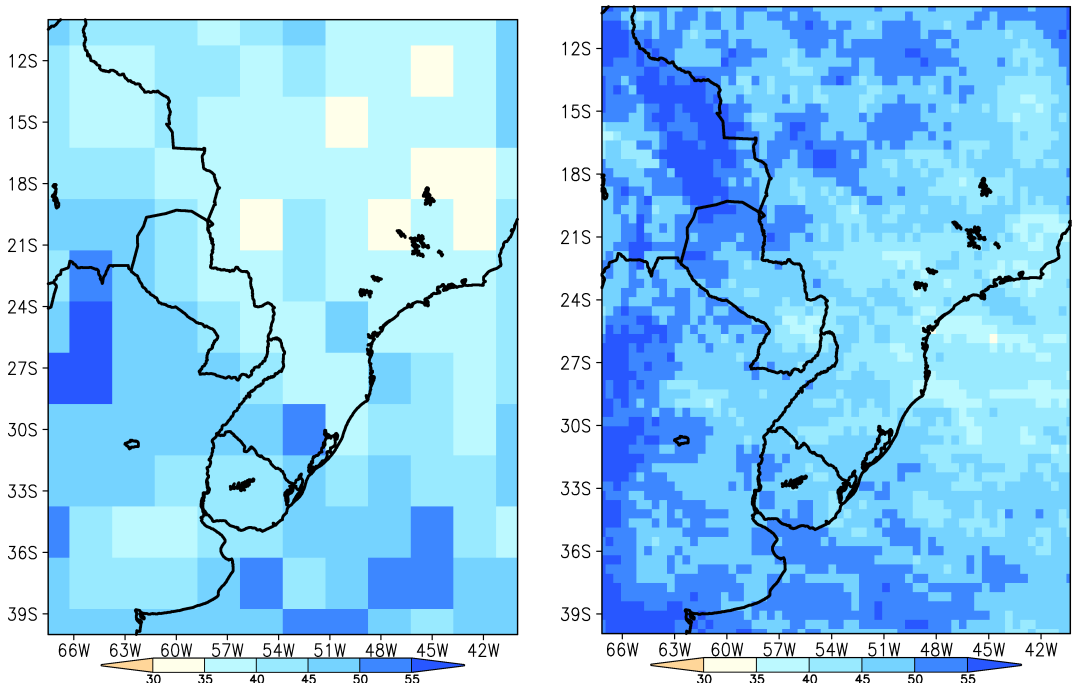

(a) NCEP, 2.5°×2.5° **(b)** REMO 0.44°×0.44°

Figure 4.8: Number of days (%) with negative OLR anomalies one standard deviation apart relative to the total number of austral summer days over the MCSs region during the 1999-2008 period. The resolution of each dataset is indicated in the subcaptions.

The mean negative OLR anomalies are shown in Figure 4.9 with values ranging from -16 to -2 W/m^2. The anomaly signal over the La Plata Basin is well-defined in the NOAA dataset while in REMO, the signal is spread towards the eastern and western part of the MCS region, closer to the Andes mountains and over the SACZ. The values in REMO are slightly higher compared to the NOAA dataset, however, the spatial distribution of the model is similar to the satellite estimates. The location of the OLR minimum is important in identifying the regions with MCSs structures for the second condition.

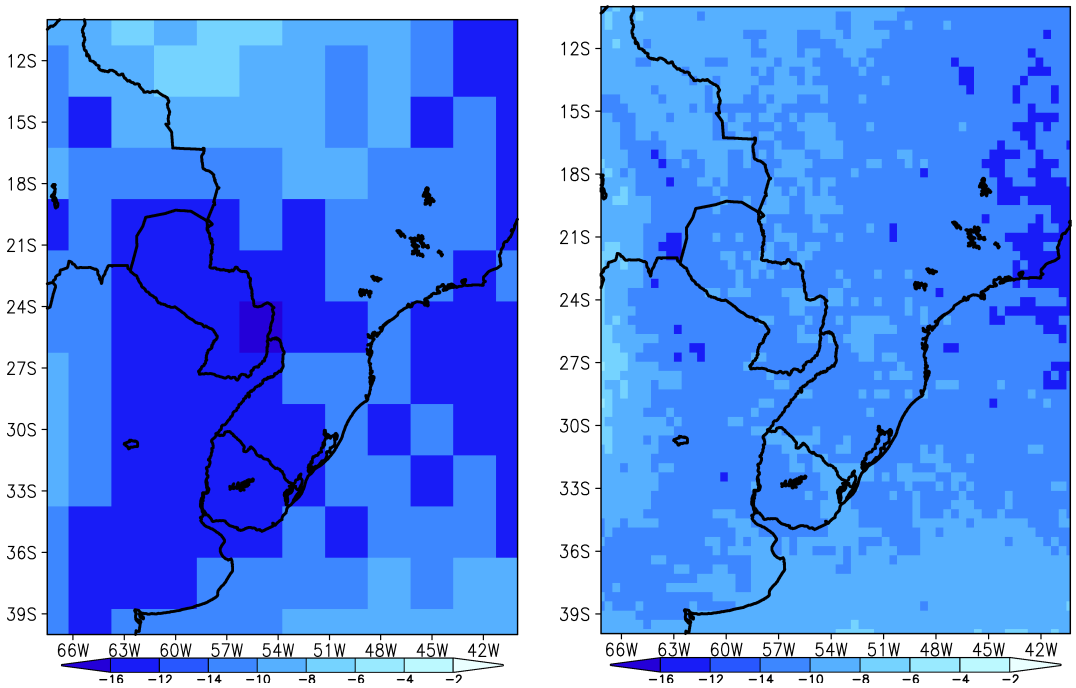

(a) NCEP, 2.5°×2.5° **(b)** REMO 0.44°×0.44°

Figure 4.9: Average negative OLR anomalies beyond one standard deviation over the MCS region during the austral summer of 1999–2008. The horizontal resolution of each dataset is indicated in the subcaptions.

For Condition 2, the days with rainfall of at least 25 mm/day are counted in the CPCUNI, TRMM, MERGE, and REMO datasets. Figure 4.10 shows the percentage of days over the MCS region that satisfies this criterion during the austral summers from 1999 to 2008. The heavy precipitation events have a tendency to occur over the SACZ and the La Plata Basin. The frequency of heavy precipitation events ranges from 3–30% during the ten summers. Over the La Plata Basin, the frequency of occurrence increases as the resolution increases in the observational datasets (Figure 4.10a–c). In REMO, the occurrence of heavy rain events is less compared to TRMM and MERGE, but the range is comparable to the CPCUNI with a similar resolution.

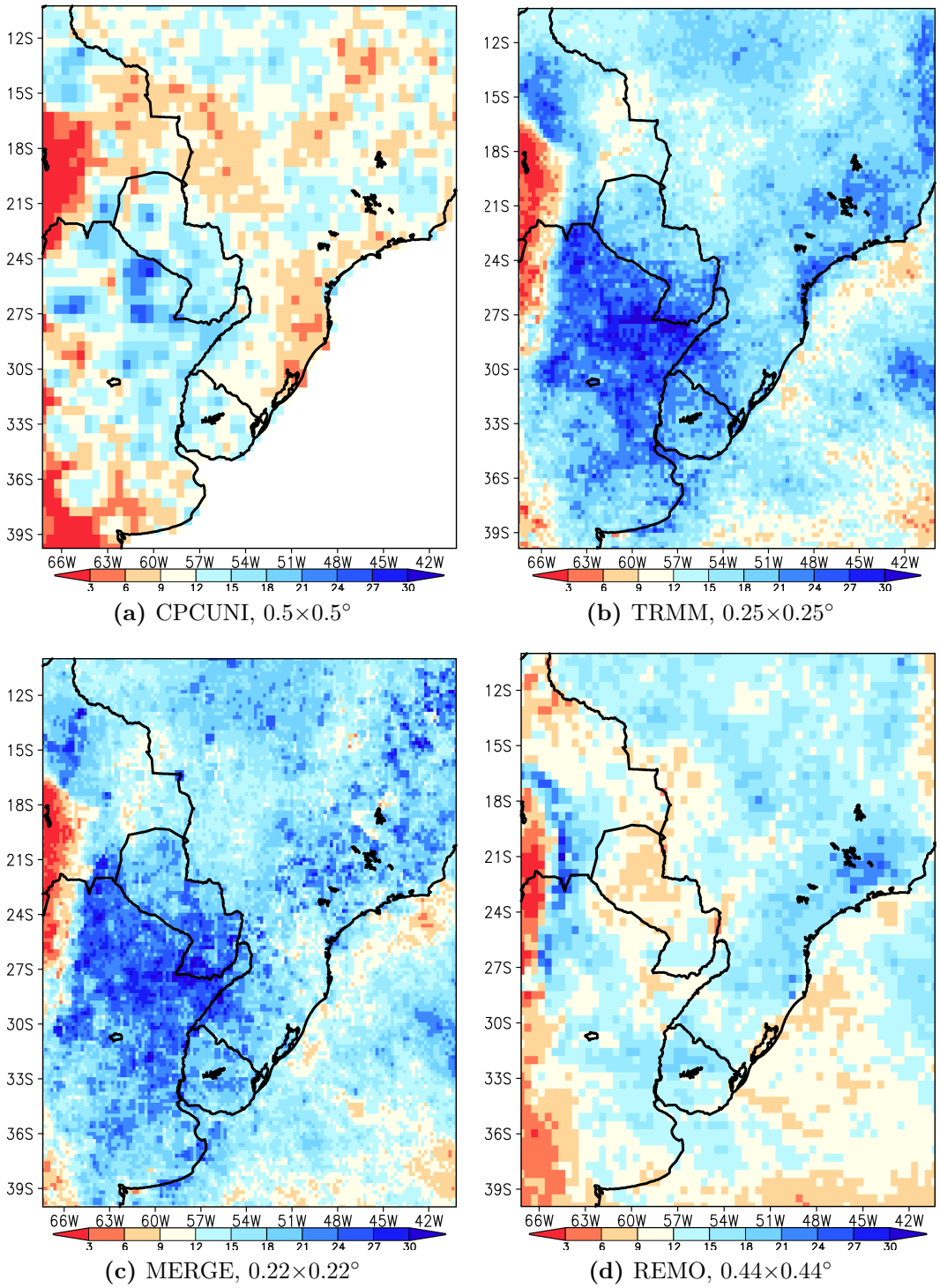

(a) CPCUNI, 0.5×0.5°

(b) TRMM, 0.25×0.25°

(c) MERGE, 0.22×0.22°

(d) REMO, 0.44×0.44°

Figure 4.10: Percentage of heavy precipitation events (rainfall $\geq$ 25 mm/day) relative to the total number of austral summer days in the MCS region during the period of 1999–2008. The resolution of each dataset is indicated in the subcaptions.

Figure 4.11 depicts the average heavy rainfall with values ranging from 25 to 65 mm/day. The mean heavy precipitation fields of REMO are relatively higher than the observations especially close to the mountains. Large areas with mean rainfall intensity above 45 mm/day exist. The observational datasets generally have a local maximum over the La Plata Basin. For TRMM and MERGE, an additional local maximum occurs over the Atlantic Ocean. Both local maxima are present in REMO.

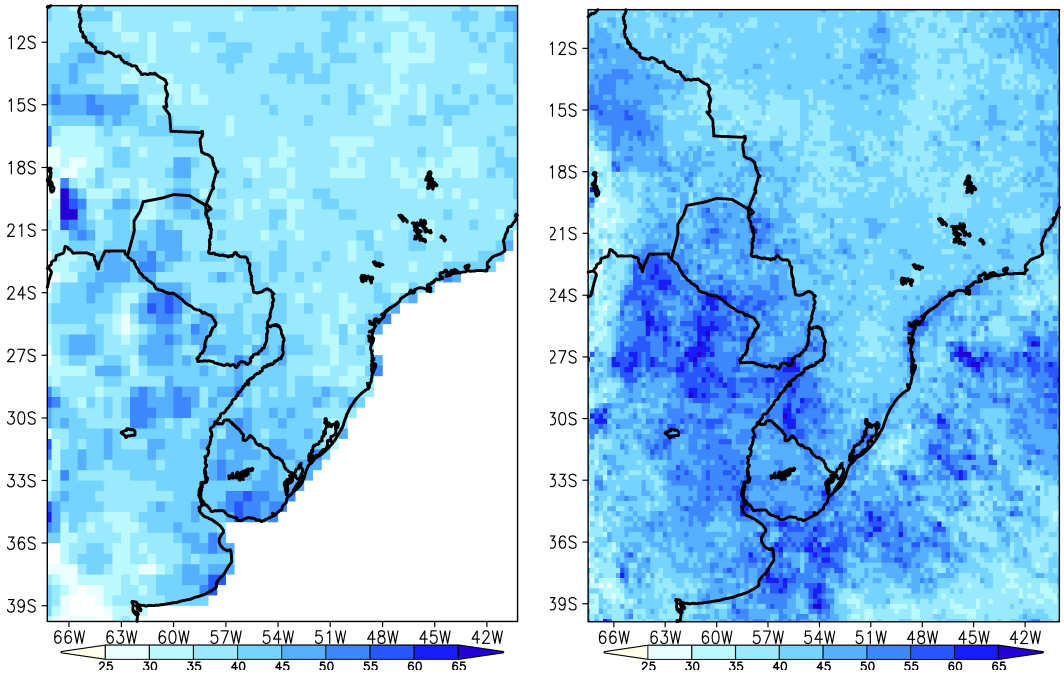

(a) CPCUNI, 0.5°×0.5° **(b)** TRMM, 0.25°×0.25°

Figure 4.11: Mean heavy precipitation events (rain $\geq$ 25 mm/day) during the austral summer of 1999-2008. The resolution of each dataset is indicated in the subcaptions.

Figure 4.12 shows the contribution of rainfall associated with the quasi-MCSs throughout the ten warm seasons. The rainfall percentage values are relative to the total rainfall in each grid box. Based on the observations, MCSs-associated rains contribute about 5–30% to the total summer precipitation. Corresponding to the simulated local minimum of OLR anomalies (Figure 4.9), REMO also shows local maximua of MCSs-associated precipitation with 25–30% contribution to the total summer precipitation located close to the Andes mountains.

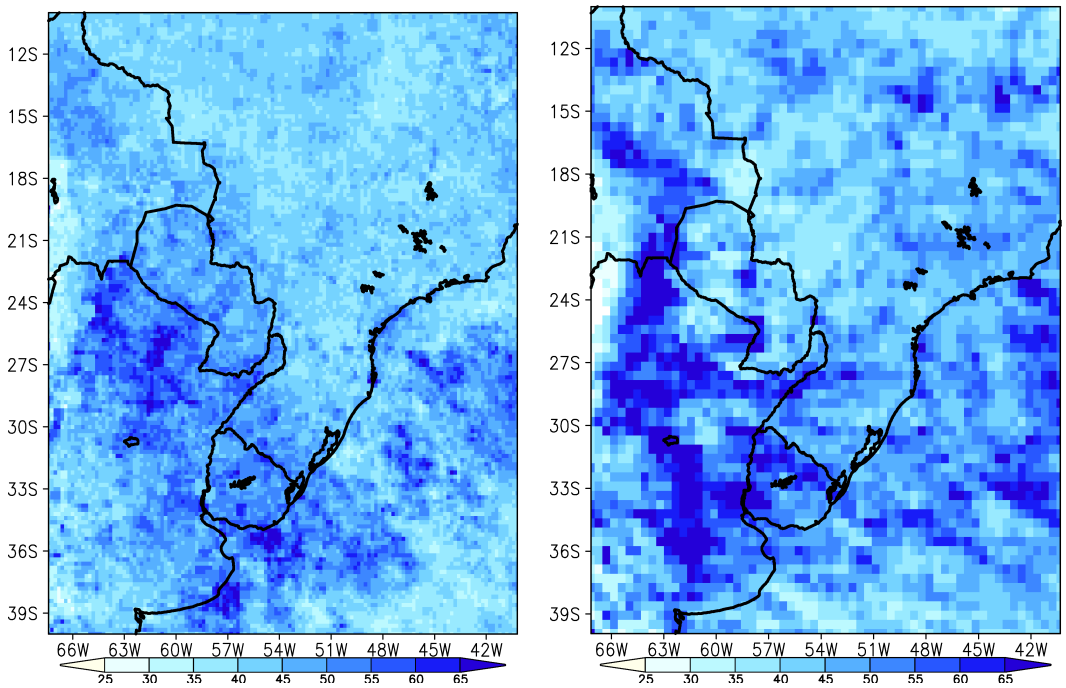

(c) MERGE, 0.22°×0.22° **(d)** REMO, 0.44°×0.44°

Figure 4.11: *cont.*

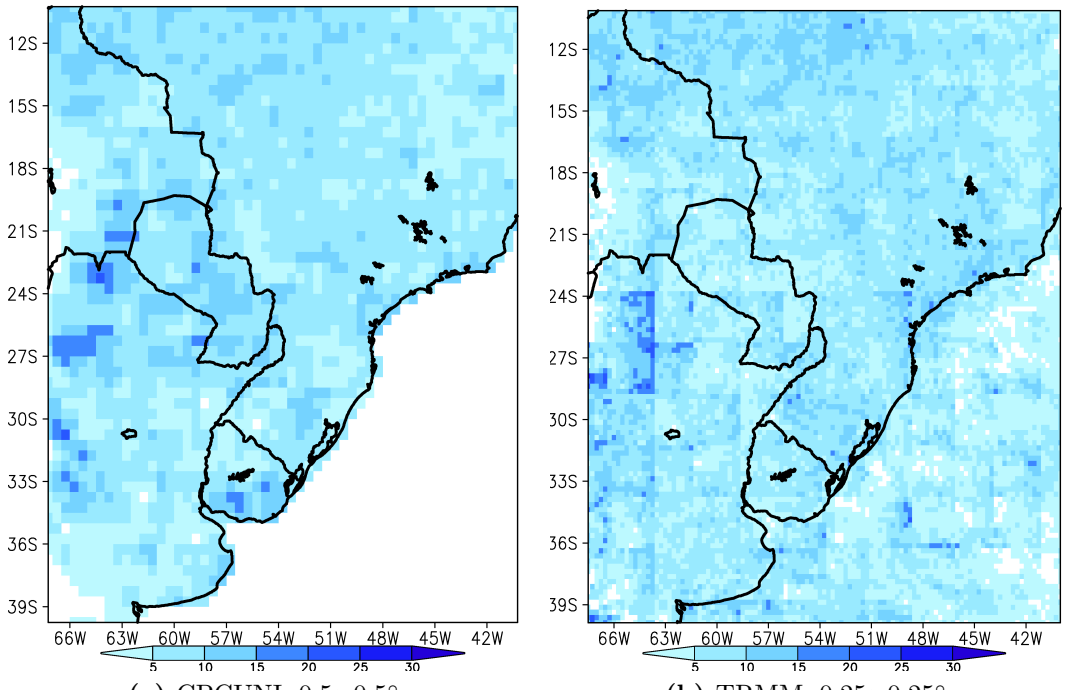

(a) CPCUNI, 0.5×0.5° **(b)** TRMM, 0.25×0.25°

Figure 4.12: Percentage of the accumulated rainfall from the heavy precipitation events associated with MCS (rainfall $\geq$ 25 mm/day) relative to the total accumulated rainfall during austral summer days for the period of 1999-2008. The resolution of each dataset is indicated in the subcaptions.

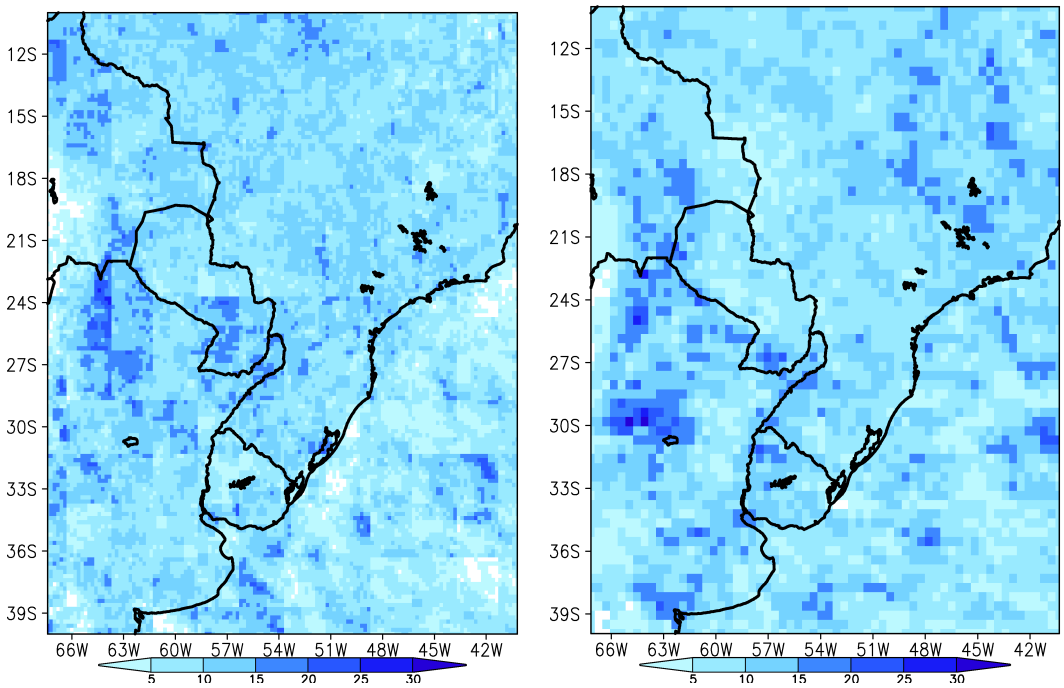

(c) MERGE, 0.22×0.22° **(d)** REMO, 0.44×0.44°

Figure 4.12: *cont.*

4.4 Summary and conclusions

The MCSs are the main drivers for the summertime precipitation over the La Plata Basin, which is important for the five surrounding countries. The spatial and temporal characteristics of MCSs are investigated because these systems contribute significantly to the hydrological cycle of the region. Gridded precipitation and outgoing longwave radiation (OLR) datasets derived from station observations and satellite estimates are used to evaluate the derived daily precipitation estimates and OLR values of the REMO simulations.

The results of the chapter are:

- REMO is able to represent the daily precipitation statistics over the La Plata Basin during the short SALLJEX period. Although the timing is inaccurate for some cases and the amplitude for the wet anomaly is lower than observed, the mean statistics of REMO is comparable with the observations over the defined MCS region.

- Negative anomalies of OLR are indicators for deep convection. The spatial patterns of REMO-derived OLR anomalies are similar to the NOAA OLR anomalies. The regions of deep convection are: La Plata Basin, Amazon Basin, and the South Atlantic Convergence Zone.

- The uncertainty in simulating the daily precipitation distribution, the mean, and extreme thresholds are analyzed using a seven member ensemble of regional climate models. Results from this intercomparison study indicate that REMO has a relatively high skill in simulating the distribution of warm season daily precipitation for regions with similar climate and hydrology characteristics.

- In order to select rainfall associated with MCSs, two criteria are established. One, using the OLR standard deviation and two, using heavy precipitation above or equal to 25 mm/day. With these criteria, regions of heavy precipitation are identified over the La Plata Basin. Based on the observations, MCSs-associated rains contribute about 30% of the total rainfall during the ten warm seasons. REMO generally simulates well the quantity and frequency of occurrences of observed precipitation during the quasi-MCSs events.

- The La Plata Basin is highly susceptible for the impacts of heavy rains associated with MCSs during the austral summer of 1999-2008.

The organization and structure of the MCSs are associated weak, midlevel troughs and the occurrence of low level jets. LLJs provide low-level warm air advection and moisture advection. Chapters 3 and 4 were the necessary precondition for the analysis of the link between MCS and LLJ in the next chapter.

5 Connections between MCSs and LLJs

5.1 Introduction

In the tropical and mid-latitude regions of South America, mesoscale convective systems (MCSs) are one of the main contributors to rainfall during the warm season. As shown in Chapter 4, precipitation associated with MCSs contributes up to 30% of the total summertime precipitation over the La Plata Basin. This is important for the water cycle of the basin, which has an area of about 3.2×10^6 km^2. The water resources in the basin are used for many human activities in Brazil, Argentina, Paraguay, Bolivia, and Uruguay (Berbery and Barros, 2002).

Several factors influence the development of MCSs such as the flow generated by a weak midlevel trough and the occurrence of low level jets (LLJs). These factors have been discussed in Chapter 3 including the spatial and temporal characteristics of LLJs east of the Andes mountain range. Furthermore, a study by Salio et al. (2007) has assessed the contribution of LLJs to the development of MCSs, using a compositing analysis for a 3-year austral summer (DJF) period. The compositing method revealed a dominant northerly flux with a duration of at least one full day before the organized convective systems is established. Based on their studies and references therein, the environmental conditions for the initiation of MCSs and their development to long-lived systems include the following:

- low-level convergence generated by a strong anomaly of northerly low-level jets transporting warm moist air and the incursion of cold and dry winds from the southeast;
- increasing areas of warm moist air transport via a low level jet;
- baroclinic zones with high low-level vertical wind shear and convective available potential energy; and
- upper-level divergence typically stronger and reinforced downstream flow as opposed to the weaker upstream divergence superimposed over the low-level convergence.

Figure 5.1 summarizes the conditions for the synergism between LLJs and MCSs near the LLJ exit region as proposed by Saulo et al. (2007). The hypothesis in their study states that the moist air of an LLJ leads to low level convergence because of the cold and dry air from the southeasterlies. Convection initiated in that region develops further and becomes organized. The upper level flow diverges as a result of the developing MCS. They have formulated their hypothesis on the interaction between the extratropical dynamics and convection in MCSs using comprehensive data collected during the 4-month campaign period of SALLJEX. As observations of upper air soundings were only intermittent during this campaign, also simulations using a regional model have been performed to verify the hypothesis. Rozante and Cavalcanti (2008) have performed sensitivity experiments using a regional model to identify the mechanisms of MCSs development. Their results have indicated that the model was able to determine the atmospheric characteristics such as the strong upper level flow, the LLJ, moisture transport and associated mechanisms 72 *hours* before the heavy precipitation events occur.

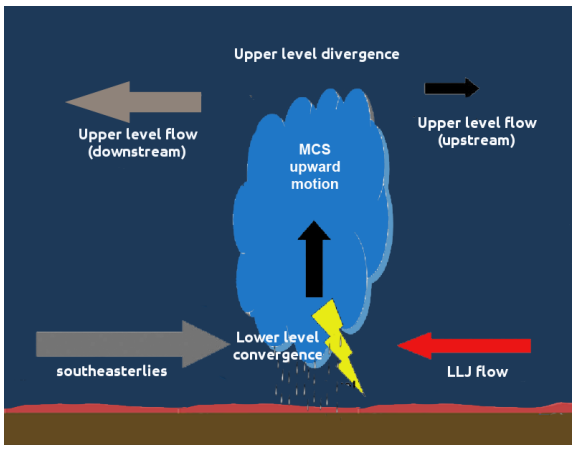

Figure 5.1: Schematic diagram of a typical structure during an MCS development influenced by an LLJ. The conceptual model is adapted from Saulo et al. (2007).

As heavy precipitation events sometimes have devastating consequences, studies all over the world are established to identify the precursors of these events using statistical methods such as the correlation analysis. Saeed et al. (2012) analyzed the predominant circulation patterns using atmospheric parameters such as geopotential heights to assess extreme precipitation events over South Asia. They defined extreme rainfall events as normalized rainfall anomalies that exceed more than one standard deviation for 3 consecutive days. Chen et al. (2005) defined heavy precipitation events as days with more than 50 mm/day of rainfall in the northern part

of Taiwan. In that study, 40% of LLJs were associated with heavy rain events. In South America, Rozante and Cavalcanti (2008) analyzed the relationship of MCSs and LLJs during the SALLJEX period. With the aid of observations and a regional model, they took the spatial average of precipitation over a region where the MCSs usually occur and found correlation between the preceding regional and synoptic conditions in the atmosphere.

Large-scale anomalies such as the El Niño Southern Oscillation (ENSO) strongly influence the climate variability of South America. Numerous studies based on observations and simulations such as from Garreaud et al. (2009); Barreiro and Diaz (2011); Saulo et al. (2000) among others, have investigated the modulation of ENSO on the region's climate, which in turn influences the activity of LLJs and MCSs. Vernekar et al. (2003) investigated the interannual variability of LLJs for five years. During the warm phase of ENSO, they found that the LLJs are stronger than during the ENSO cold phase. Marengo et al. (2004) also concluded similarly in their studies on LLJs using a 50-year reanalysis.

The atmospheric flows at different vertical levels and the spatial distribution of heavy precipitation occurrences have already been described in Chapter 3 and 4, respectively. In this chapter, the relationship of MCSs and LLJs is assessed to determine the vulnerability of the La Plata Basin to these systems during austral summer. Using observations and simulations from the regional model REMO, the physical processes leading to heavy precipitation events are investigated.

The aims of this chapter are to:

- analyze the moisture fluxes and instability indices during the mean austral summer and during the LLJ events;
- quantify the relationship of LLJs and MCSs using correlation analysis; and
- evaluate the importance of high northerly wind speeds preceding the heavy precipitation events during the austral summer of 1989-2008.

5.2 Data and methods

To analyze the relationship of MCSs and LLJs, the moisture fluxes at upper levels are analyzed followed by the correlation analysis during the austral summer from

1989 to 2008. The simulated (REMO) mean conditions for tropospheric circulations and moisture fluxes are evaluated using reanalysis (EITR). For precipitation, the CPCUNI dataset with 0.5×0.5° resolution is used. The details for each observational dataset are listed in Table D.1.

In addition to the mean summer conditions, the mean conditions during LLJ events are analyzed. This composite technique estimates the contribution of LLJs to the climate of the region. The detection of LLJ events is based on the first criterion of Bonner (c.f. Chapter 3.2). The events considered are large LLJ events, which are detected at the 5 stations within the LLJ core region. As illustrated in Figure 3.12, the composite of LLJ events are compared against the mean climate conditions of winds at 850 hPa level. During the austral summer, strong LLJ events occur in about 8% (12%) of the entire study period based on the 6-hourly reanalysis (simulation).

5.2.1 Moisture fluxes

The advection of warm moist air is evaluated using moisture fluxes and equivalent potential temperature during the austral summer. The 6-hourly moisture flux at the 850 hPa level ($\mathbf{MF_{850}}$) is calculated by multiplying the specific humidty q_d and wind speed:

$$\mathbf{MF_{850}} \approx q_d \vec{V} \tag{5.1}$$

with q_d in g/kg and $\vec{V}$ in m/s. In this formulation, the regions with intense moisture transport are identified during the mean climate conditions as well as during the composite of LLJ events.

As a measure of moisture advection, the equivalent potential temperature (Θ_e) is derived using the following:

$$\Theta_e \approx \Theta exp\left(\frac{l_v w}{c_p T}\right) \tag{5.2}$$

Θ_e is a function of the water vapor mixing ratio (w) and potential temperature (Θ) where $\Theta = T(1000/p)^{0.286}$, l_v is the latent heat of condensation or vaporization and c_p is the specific heat of air at constant pressure. After Stull (2000), Equation 5.2 can be approximated as:

$$\Theta_e \approx \Theta + \frac{l_v}{c_p} w \tag{5.3}$$

An increase of 6-hourly Θ_e in comparison to the daily mean indicates either an increase in moisture content or in temperature or of both. Relatively high Θ_e also indicates instability. During LLJ events, high wind speeds from a moisture source correspond to higher values of Θ_e.

5.2.2 Correlation method

As described in the previous section (Chapter 5.1), MCSs tend to develop after anomalously high northerly wind speeds. To evaluate the delayed response of rainfall, the lead-lag correlations between the meridional wind speed and 24-hour precipitation anomalies are calculated. The meridional wind speed time series is shifted relative to the daily precipitation. The link between the LLJs and MCSs is evaluated using the Pearson correlation (Wilks, 2006). The two-tailed t-test is used to test the significance of the correlation.

In this analysis, the accumulated daily precipitation is averaged over the MCS region, which is bounded by 67.5 to 55 °W and 30 to 20 °S as defined in Chapter 4. The average precipitation is then correlated with the the daily mean winds at each gridbox shifted by up to several days.

ENSO modulates the synoptic and climate variability of rainfall and LLJs over South America. In a feedback to the shifts in sea surface temperature patterns of the tropical Pacific Ocean, ENSO changes the precipitation and temperature anomaly patterns on the continent (Hobbs et al., 1998). During the warm phase or El Niño, the precipitation is higher than normal and the surface temperature is above average over the La Plata Basin. During the cold phase or La Niña, there is no clear, however, there is a general tendency of below average temperature over the La Plata Basin. Due to this large-scale influence of ENSO, several periods are considered for the lead-lag correlation analysis. Table 5.1 lists the austral summer seasons when ENSO influences the region.

Table 5.1: List of the normal, El Niño, and La Niña years for the 1989 to 2008 period based on the Oceanic Niño Index (ONI). Source: Climate Prediction Center. *Note that the 1st month of simulation (January 1989) is not included in the lead-lag correlation analysis.

	Seasons	DJF Years
Normal	7	1989-90, 1990-91, 1992-93, 1993-94, 1996-97, 2001-02, 2003-04
El Niño	6	1991-92, 1994-95, 1997-98, 2002-03, 2004-05, 2006-07
La Niña	7	1989*, 1995-96, 1998-99, 1999-2000, 2000-01, 2003-04, 2005, 2007

5.3 Results and discussion

5.3.1 Moisture fluxes

The mean moisture flux conditions during the austral summer as well as the contributions of LLJ events are investigated. The moisture fluxes (**MF**) and equivalent potential temperature (Θ_e) at 850 hPa represent the moisture advection. As shown in Chapter 3.3, the wind speeds at 850 hPa intensify over Bolivia during LLJ events compared to the mean summer conditions. These high wind speeds generally advect the warm and moist air from the Amazon Basin further south towards the La Plata Basin. The above conditions essentially favor the development of convection that produces heavy precipitation events.

Figure 5.2 shows the low-level moisture advection during summer conditions and during the LLJ events. For the mean austral summer in the reanalysis (EITR), the highest values of moisture advection are present at the northeast coast of Brazil (Figure 5.2a). The contours of Θ_e indicate regions of warm moist air and a local maximum is located over the Amazon Basin. The Θ_e values decrease further south. For the composite of LLJ events (Figure 5.2c), the low-level flow is enhanced in the region between 70–50 $°W$ and 10–30 $°S$. In this region, the higher wind speeds transport moisture from Bolivia towards the La Plata Basin and the moisture flux increases by about 50% in comparison to the mean conditions.

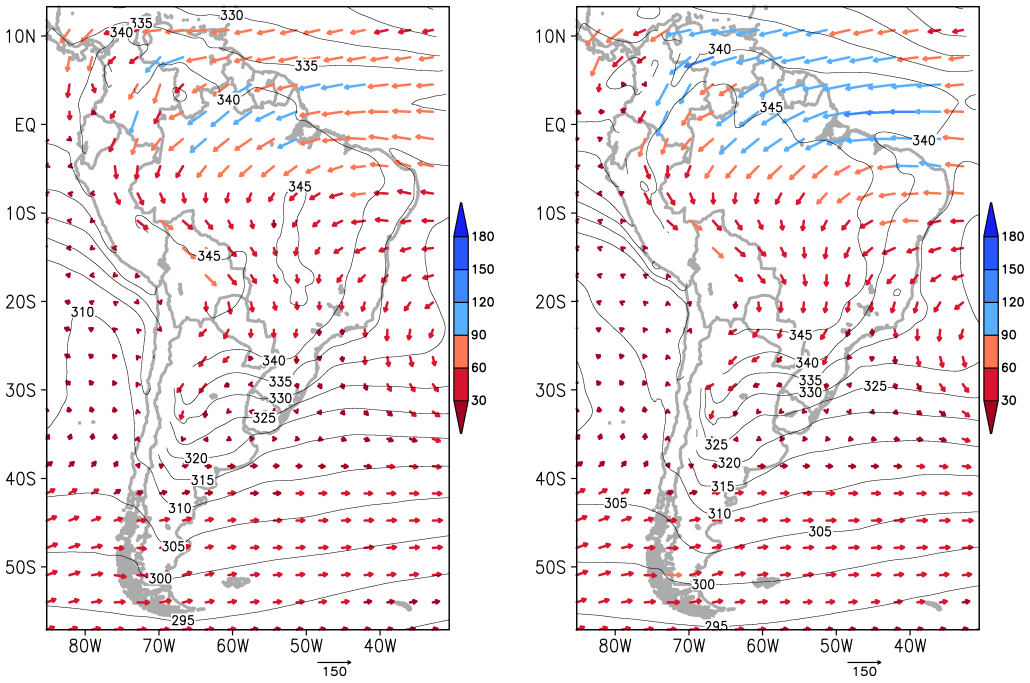

(a) EITR, mean DJF **(b)** REMO, mean DJF

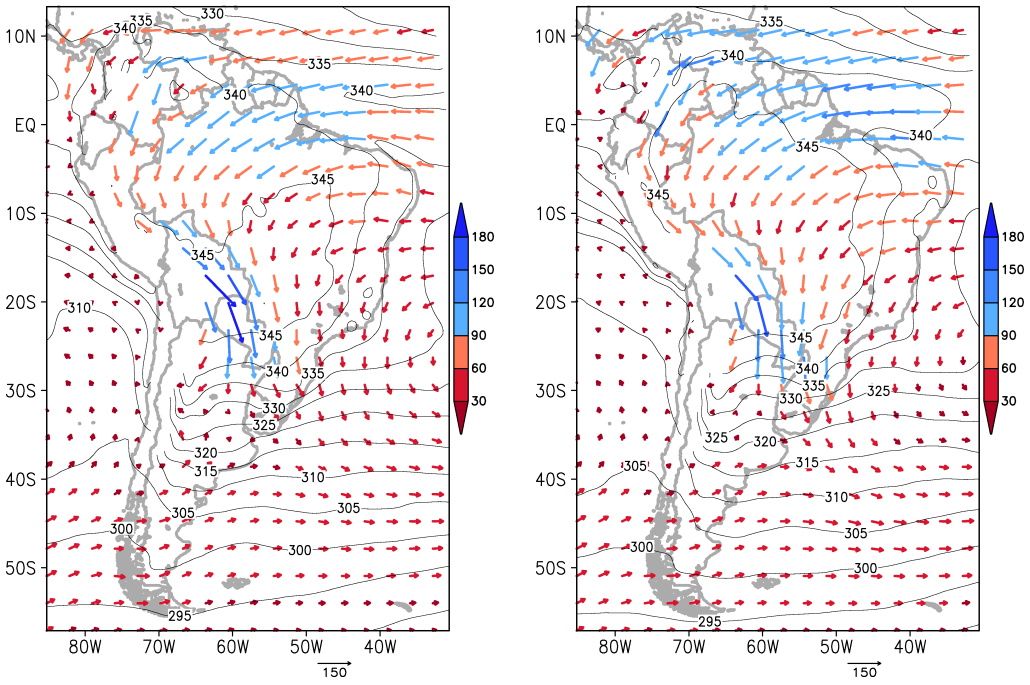

(c) EITR, mean LLJ during DJF **(d)** REMO, mean LLJ during DJF

Figure 5.2: Mean moisture flux (**MF**) and equivalent potential temperature (Θ_e) at 850 hPa for the mean austral summer (a,b) and for the mean LLJ events (c,d) from 1989 to 2008 period. **MF** in coloured vectors ($g/kg \times m/s$). Θ_e in isolines, interval of 5 K. The reanalysis (EITR) on the left panels and the regional model (REMO) on the right panels.

Comparing the reanalysis with the simulation, REMO also simulates the advection of moisture in both period (Figure 5.2b and 5.2d), however the Θ_e values tend to be higher over Bolivia and southern Brazil compared to EITR. The warm moist air can be an indication of the overestimation of surface temperature over the Amazon Basin (cf. Chapter 2) and the tendency of REMO to simulate higher wind speeds especially at 1800 UTC or 2PM local time (cf. Chapter 3.3.2) compared to observations. The implication of the warm bias and overestimation of wind speeds are investigated further by evaluating the vertical profile of meridional wind speed (v) and equivalent potential temperature (Θ_e).

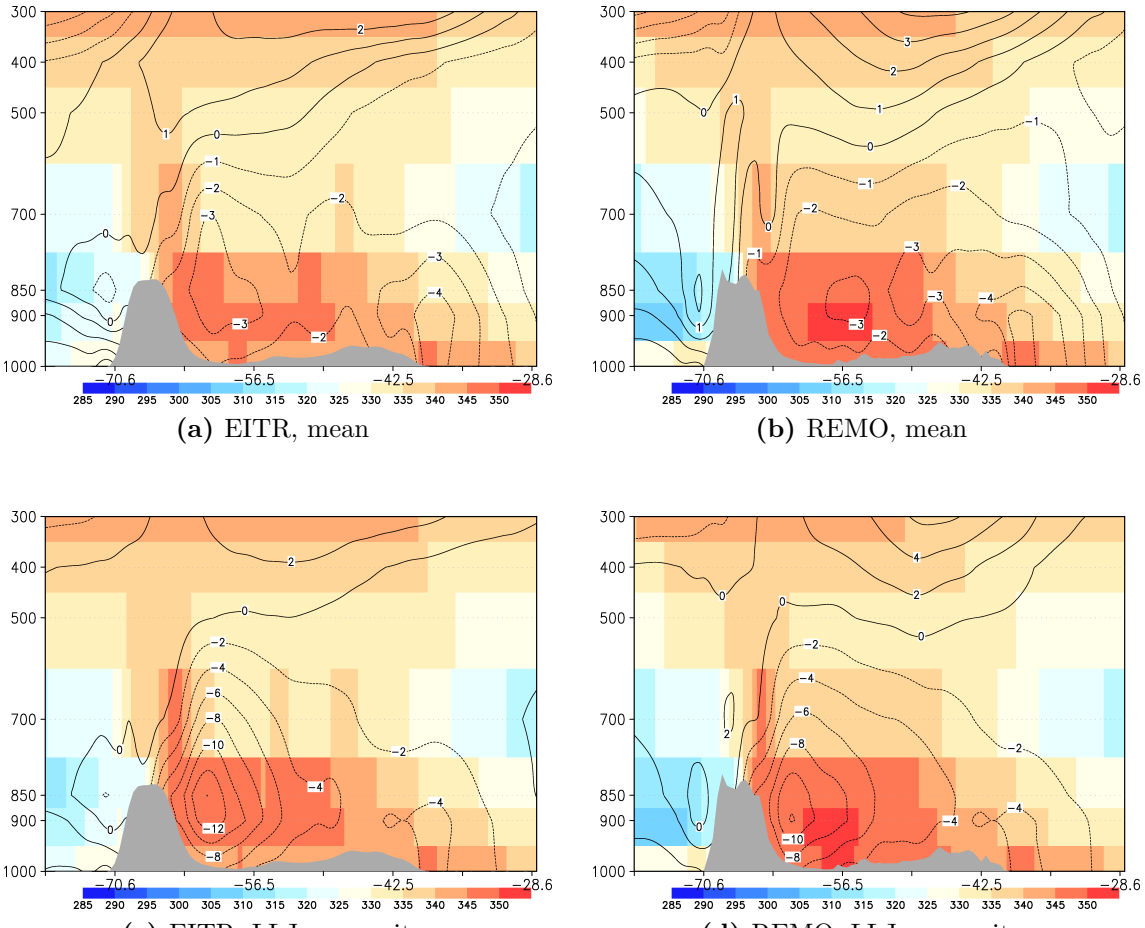

(a) EITR, mean

(b) REMO, mean

(c) EITR, LLJ composite

(d) REMO, LLJ composite

Figure 5.3: Height-longitude cross-section of meridional winds (v) and equivalent potential temperature (Θ_e) along 17.76 °S for (a&b) the seasonal mean and (c&d) LLJ composite. EITR reanalysis (left panels) and REMO simulation (right panels) during the austral summer of 1989 to 2008. Gray area indicates the terrain. v indicated by contour lines in m/s and Θ_e indicated by shaded contours in K.

Figure 5.3 shows the vertical cross-section of the seasonal mean v and Θ_e and the corresponding composite during the LLJ events in the region of maximum LLJ occurrences (17.76 $^\circ S$). The LLJ core is not depicted clearly in the seasonal mean meridional wind speed (Figure 5.3a and 5.3b) but is evident in the seasonal LLJ composite (Figure 5.3c and 5.3d). The LLJ core is indicated by the region of maximum v at 850 hPa and is located near 56.5°W for both EITR reanalysis and REMO simulation. Within the LLJ core, the simulated v and Θ_e are comparable to the reanalysis. REMO slightly underestimate the wind speeds by 1 to 1.5 m/s during the LLJ composite since the model detects more LLJ events than the reanalysis (c.f. Chapter 3).

5.3.2 Correlation analysis

The relationship between the daily precipitation anomalies averaged over the MCS region and the mean daily meridional winds at each grid point are evaluated using the correlation analysis. The correlation coefficients are calculated at least $+/-3$ days leading/lagging to the heavy precipitation events in the La Plata Basin. Positive (negative) correlation coefficient at each grid box implies that the increase of rainfall anomalies over the MCS region corresponds to southerly (northerly) meridional wind speed. In addition, the correlation of winds and heavy precipitation events are analyzed for four time periods, namely the 4-month SALLJEX period, 20-year austral summer, normal years, and ENSO years. Normal years are defined as years without the influence of ENSO. The ENSO and normal years are listed in Table 5.1. The correlation plots show only values that are significant at the 99% confidence level ($p = 0.01$).

During the SALLJEX period, the LLJ occurrences and rainfall anomalies have been described separately in Sections 3.3.1 and 4.3.1, respectively. The reanalyses (NCEP, EITR) and the simulations (REMO) detect the LLJs near the Santa Cruz station in Bolivia (cf. Figure 3.5). Concurrently, the area-averaged precipitation over the MCS region exhibits positive rainfall anomalies (cf. Figure 4.3). Here, Figure 5.4 shows the observed and simulated correlation of precipitation anomaly and 850-hPa meridional wind speed anomaly. The results show a correlation starting from two days before the heavy precipitation events (Days 2 to 0) with the highest negative correlation on Day 1. This strong correlation of northerly wind speeds a day before the heavy precipitation events is similar to the results found by Zipser et al. (2004).

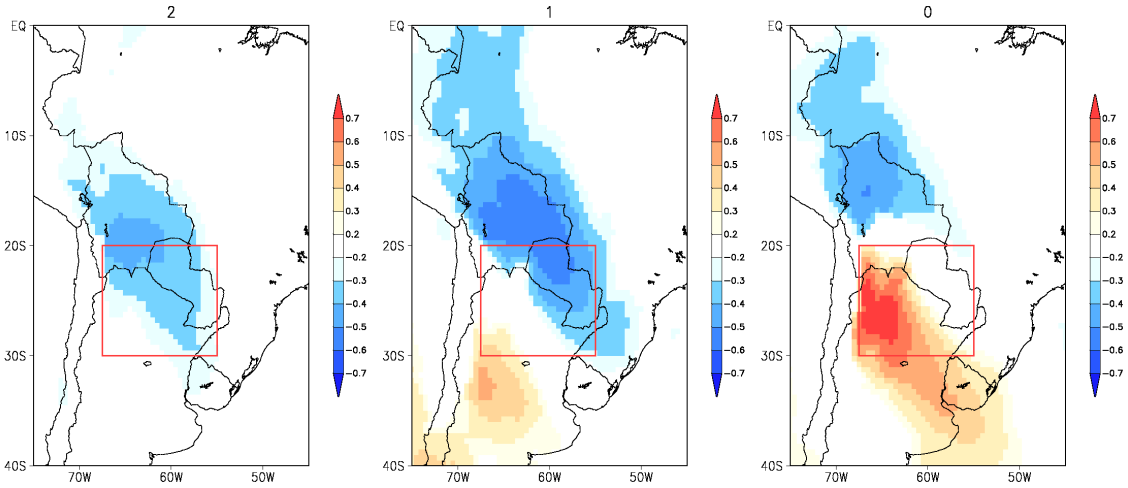

(a) Precipitation (CPCUNI), v_{850hPa} (EITR)

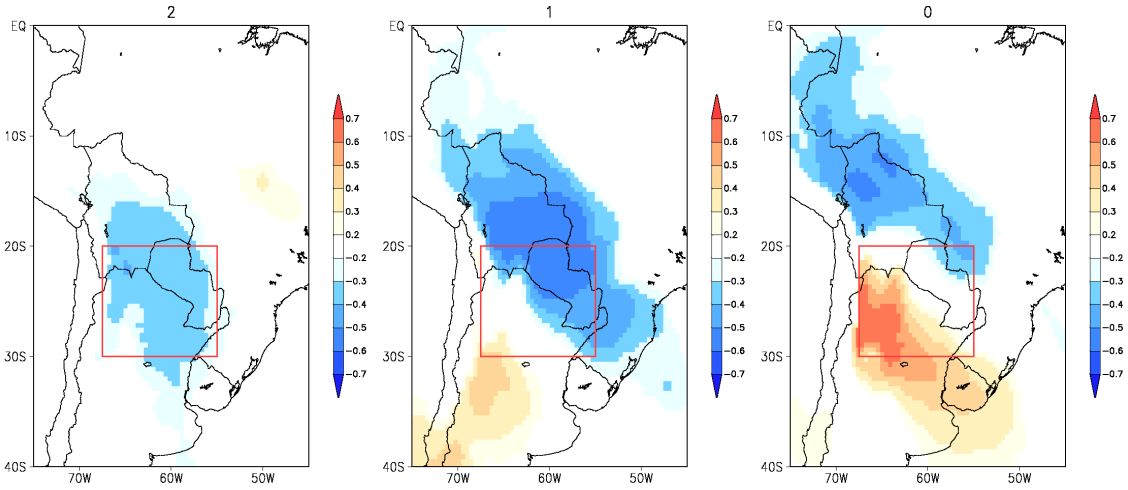

(b) Precipitation and v_{850hPa} (REMO)

Figure 5.4: Lead-lag correlation coefficients between precipitation and meridional wind speed at 850 hPa from (a) CPCUNI and EITR and (b) REMO during the austral summer of 2002 to 2003. The spatial coverage of the area-averaged daily precipitation are indicated in the red box. The numbers above each subfigure indicate the shift in days until the precipitation anomaly. Values range from -0.7 to $+0.7$.

On Day 2, negative correlation coefficients are found over the LLJ region. The magnitude of the anticorrelation ($p = 0.01$) is between 0.4 and 0.5. On the day before (Day 1), the anticorrelation increases and the spatial coverage extends further to the northwest and southwest. In addition, a region of positive correlation appears in Central Argentina. On Day 0, the region of positive correlation intensifies and shifts northwards to the MCS region while the region of negative correlation shifts

further towards Bolivia. The positive and negative correlation coefficients between the meridional wind speeds and daily precipitation during the three day interval indicate a convergence of warm and cold air, which is one of the mechanisms for LLJ and MCS indicated by Saulo et al. (2007).

Figure 5.4b illustrates correlation plots for the simulated daily precipitation and meridional winds from REMO during the SALLJEX period. The magnitude and the spatial coverage of the positive and negative correlation values are strongly similar to the observed ones (Figure 5.4a).

Based on this short-term analysis, now the correlation between the daily precipitation and the meridional winds at 850 hPa are determined for the entire period. The magnitude of the negative correlation is highest at Day 1 while the positive correlation is highest at Day 0. From here onwards, the correlation of 850 hPa meridional winds from two days before the precipitation anomalies are shown.

Figure 5.5 shows the lead-lag correlation of rains and near surface meridional winds during the austral summer for twenty years. The subfigures illustrate that the regions of positive and negative correlation are quasi-stationary throughout the three days. The results differ from the distinct progression of correlation values during the short-term analysis of a single year (Figure 5.4).

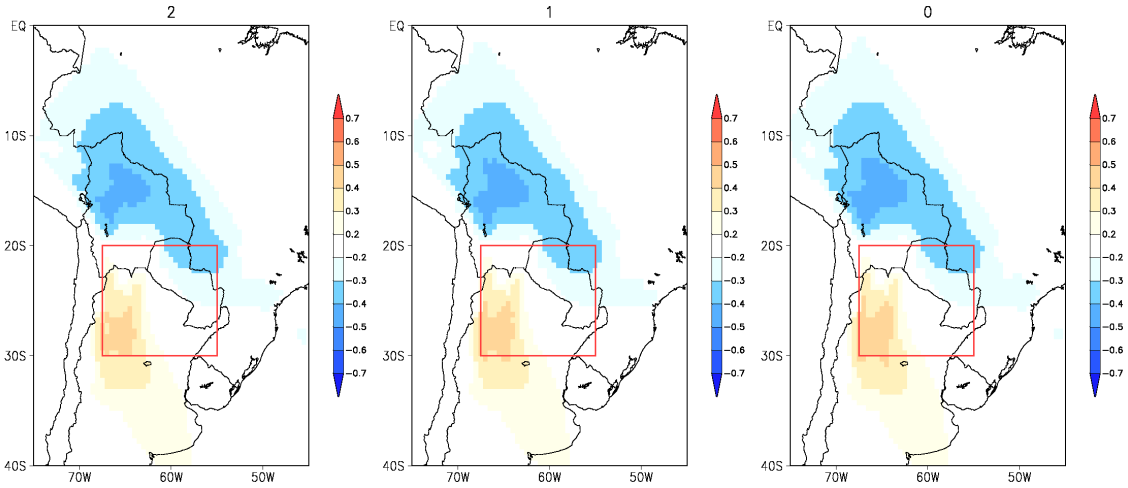

(a) Precipitation (CPCUNI), v_{850hPa} (EITR)

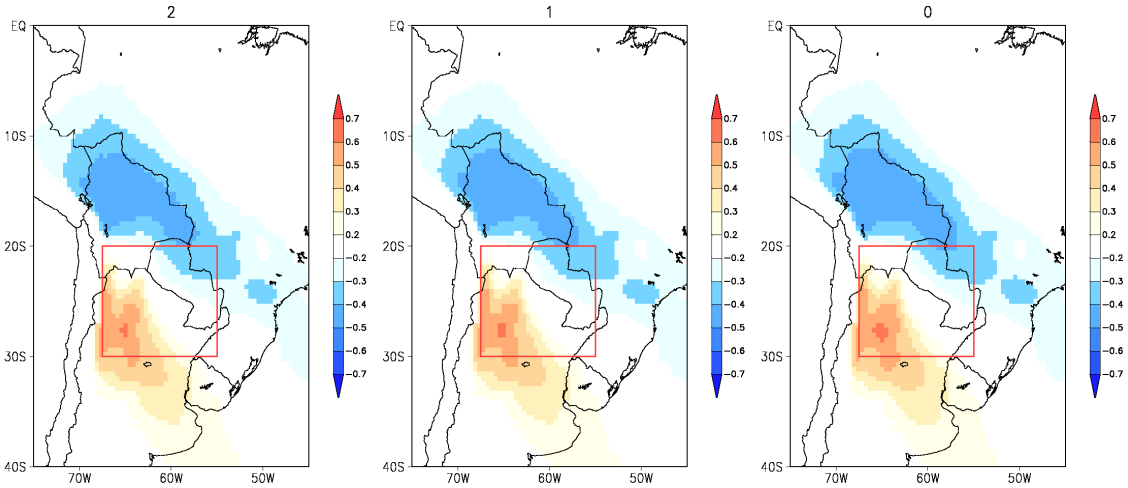

(b) Precipitation and v_{850hPa} (REMO)

Figure 5.5: Same as Figure 5.4 but during the austral summer for the 1989 to 2008 period.

The correlation during the twenty summer seasons indicates a semi-permanent relationship between the meridional winds and precipitation. The highest negative (positive) correlation values are up to -0.5 (0.7), which are slightly lower than during the SALLJEX Period (Figure 5.4).

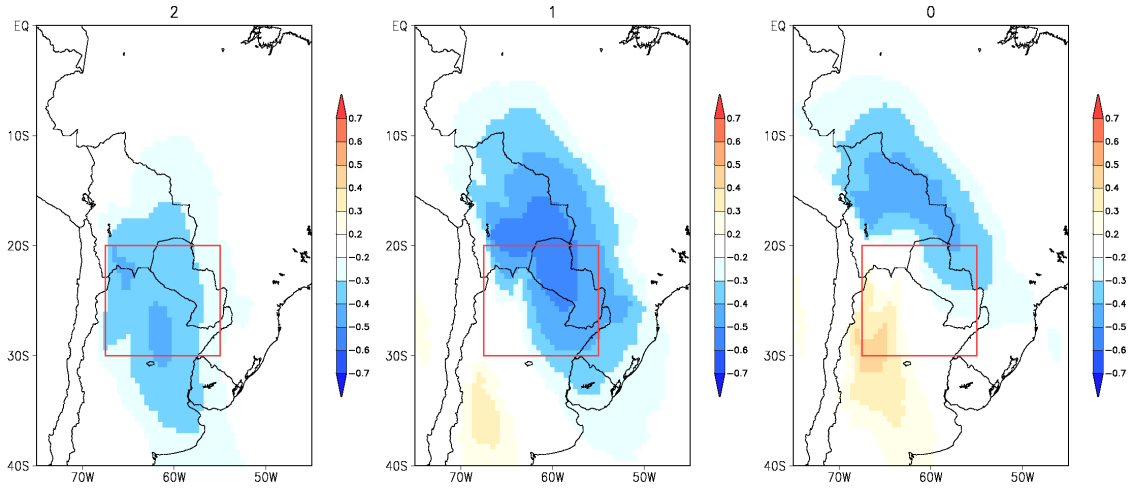

(a) Precipitation (CPCUNI), v_{850hPa} (EITR)

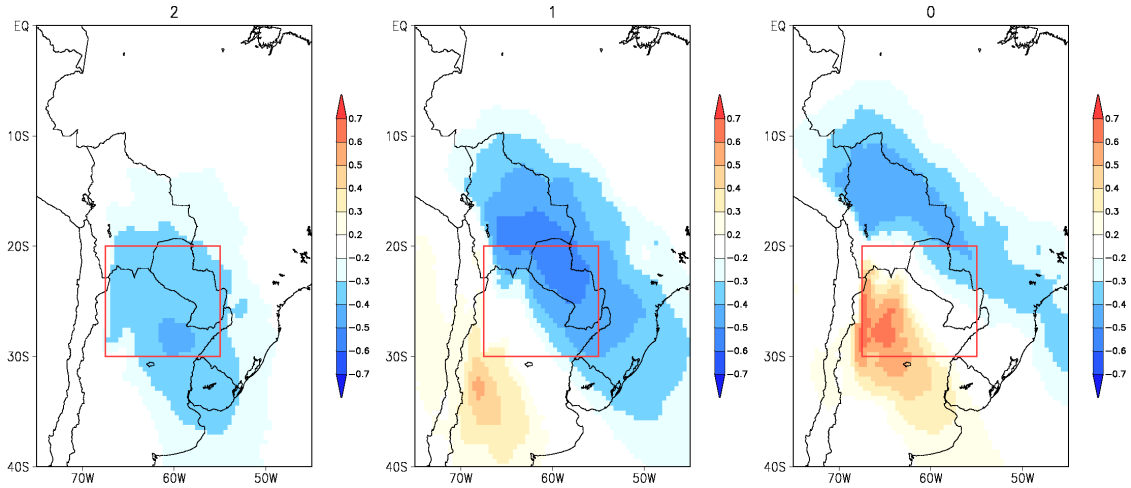

(b) Precipitation and v_{850hPa} (REMO)

Figure 5.6: same as Figure 5.4 but during the austral summer for the normal years listed in Table 5.1.

During the non-ENSO or normal years (Figure 5.6), the correlation during the seven seasons shows similar behavior with the correlation during the SALLJEX period . The two previous days leading to the anomalous precipitation events show significant correlation with the anomalous meridional wind speeds. On Day 2, the regions with the anticorrelation meridional wind speeds are further south of Bolivia. On Day 1, the region shifted towards the north and becomes more pronounced. Additionally, a region of positive correlation becomes visible over central Argentina, which indicates incursion of cold and dry southeasterlies. On the day of the event (Day 0), a strong

positive and negative correlation of meridional winds illustrate the convergence of two air masses, which leads to the daily precipitation anomalies in the MCS region.

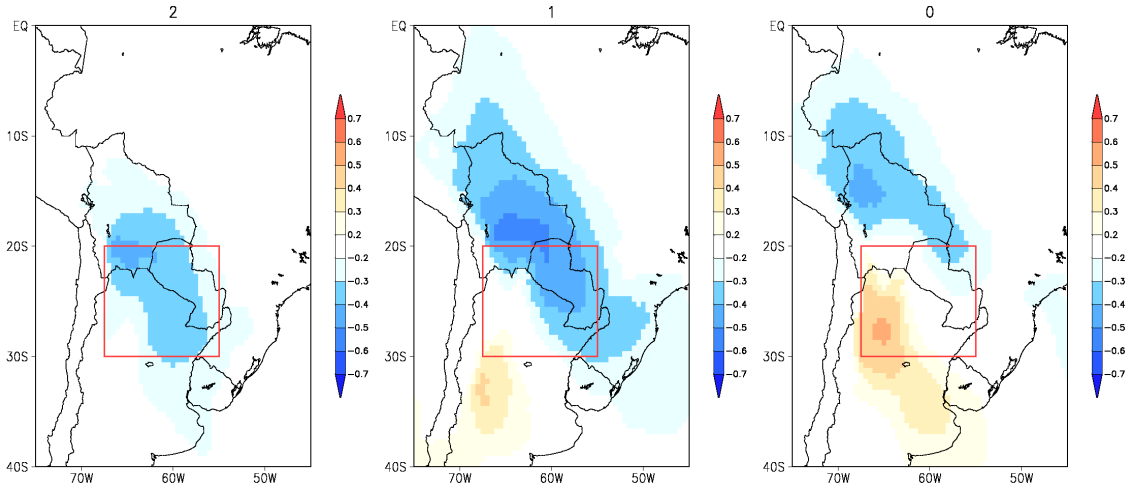

(a) Precipitation (CPCUNI), v_{850hPa} (EITR)

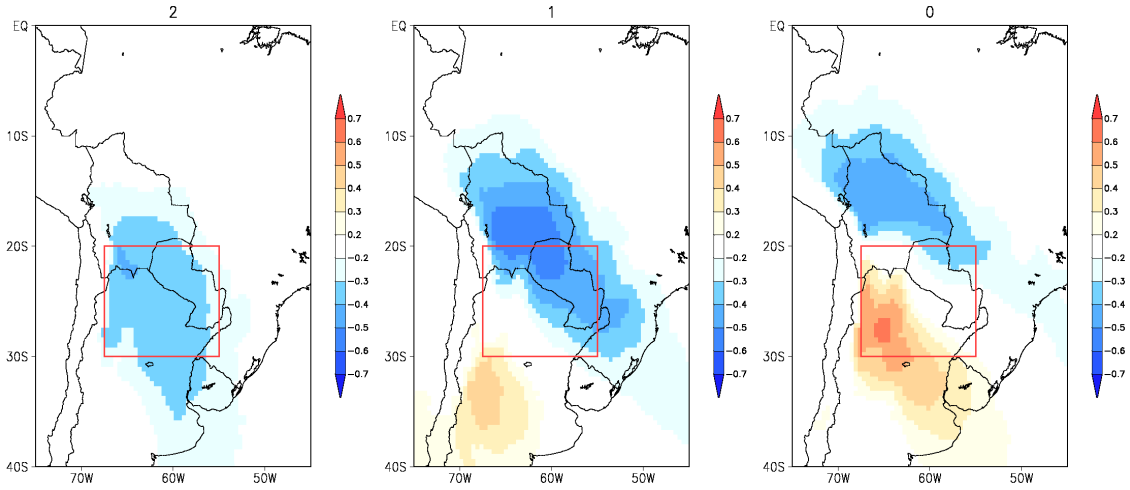

(b) Precipitation and v_{850hPa} (REMO)

Figure 5.7: Same as Figure 5.4 but during the austral summer with the warm phase of ENSO listed in Table 5.1.

During the warm phase of ENSO or El Niño years (Figure 5.7), the correlation during the six seasons shows similar behavior with the correlation during the SALLJEX period. The regions of correlation are smaller compared to Figure 5.6. The correlation plots during the cold phase of ENSO or La Niña have similar characteristics as during the El Niño years (figure not shown).

5.4 Summary and conclusions

The connections between low level jets and mesoscale convective systems are analyzed using moisture fluxes, equivalent potential temperature and correlation of anomalous meridional winds and daily precipitation. In this chapter, the relationship of MCSs and LLJs is assessed using the correlation analysis in order to determine the vulnerability of La Plata Basin to these systems during austral summer. Using observations and simulations with the regional model REMO, the physical processes leading to heavy precipitation events are investigated.

The chapter is summarized as follows:

- The moisture flux from the Amazon Basin towards the La Plata Basin is enhanced during the LLJ events both in the EITR reanalysis and REMO simulation data.
- During the SALLJEX period and during the normal years (without the influence of ENSO), the lead-lag correlation indicates that the occurrence of anomalous meridional winds is negatively correlated with the anomalous rainfall events over La Plata Basin two days before. The correlation is -0.6 at 99% significance level, which indicates the strong relationship between northerly winds and heavy precipitation events. A day before the heavy precipitation event, the correlation plots show negative values over Bolivia and a local maximum of positive values over central Argentina. These opposing values show the convergence of the warm moist air from the north and the cold and dry air from the southeast. The correlation intensifies during the co-occurence day of heavy precipitation events and strong northerly flow.
- Considering the 20-year period, the correlation values are constant throughout the 3 days indicating a stationary system. This result indicates the dependence of the system on the large-scale influences of ENSO. During ENSO, the correlation values are similar to the SALLJEX period and the normal years.

6 Conclusions and Outlook

The relationship between mesoscale convective systems (MCSs) and low level jets (LLJs) in South America has been investigated using observational datasets and the high resolution simulation from the regional model REMO. Chapter 1 introduces the motivation of studying the connections of LLJs and MCSs as well as the climate of South America. Chaper 2 describes REMO, the state-of-the-art regional climate modelling tool used in this study. A parameter in the land surface scheme of the default model version of REMO has been modified in order to have a realistic representation of the deep rooting depths in the Amazon rainforest. Chapters 3 and 4 comprehensively describe the spatial and temporal characteristics of the LLJs east of the Andes and the MCSs over La Plata Basin, respectively. Finally, Chapter 5 investigates the correlation of the LLJs and MCSs during austral summer. The results have been summarized at the end of each chapter and the major findings, conclusions, and outlook are emphasized in the succeeding sections.

6.1 Major findings

Before the analysis of the LLJs and MCSs, the regional model REMO has been adapted to have a better representation of the physical processes as well as the climate of South America. In modifying the rooting depth via the permanent wilting point parameter, the known springtime warm bias in the Amazon basin has been reduced by about 3 K. In this modified version, REMO exhibits a relatively high skill in simulating the climate of the region compared to observational datasets and simulation results from other regional models.

The research questions posted in Section 1.3 are briefly summarized in the following:

- *What are the spatial and temporal characteristics of low level jets east of the central Andes? How do they modulate the climate of South America?*
  The LLJs are an important feature in the South American climate especially during the warm seasons. Based on the new LLJ climatology constructed from

a high resolution 20-year reanalysis and simulation data, it has been found that the strong low-level flow at 850 hPa occurs throughout the year with peak LLJ occurrences in the Gran Chaco region (62.3 $°W$, 20.1 $°S$) near the border of Bolivia and Paraguay. The Santa Cruz, Robore, Mariscal Estigarribia, Asuncion and Foz do Iguassu station locations are near the axis of this strong low-level flow. Due mainly to a higher resolution that better resolves the orography, REMO data simulates more LLJs than EITR reanalysis data and the simulated diurnal cycle tends to show more LLJ events at 18 UTC than the reanalysis. Although the highest frequency of LLJs occurs during austral winter, the LLJs modulate the climate more during austral summer as they transport warm and moist air from the Amazon to the La Plata Basin. The variability in the location and intensity of LLJs during summer have a great impact on the development of MCSs.

- *What are the spatial and temporal characteristics of the mesoscale convective systems over the La Plata Basin?*
  The La Plata Basin is highly susceptible for the impacts of heavy rains associated by MCSs during the austral summer of 1999-2008. Within the SALLJEX Period, the spatially averaged precipitation of REMO coincides with the timing of observed precipitation anomalies during the intensive SALLJEX period. Results from an intercomparison study indicate that REMO has a relatively high skill in simulating the distribution of daily precipitation at regions with certain climate characteristics. In order to select rainfall associated with MCSs, two criteria are established using the OLR and heavy precipitation threshold of rain intensity at least 25 mm/day. With these criteria, regions of heavy precipitation are identified over the La Plata Basin. Based on the observations, MCSs-associated rains contribute about 30% of the total rainfall during the 10 warm seasons. REMO generally simulates the quantity and frequency of the observed heavy precipitation events associated with MCSs events.

- *What are the connections of the mesoscale convective systems and low level jets in South America?*
  The connections between LLJs and MCSs have been analyzed using moisture fluxes, equivalent potential temperature and correlation of anomalous meridional winds and daily precipitation. The moisture fluxes from the Amazon Basin towards the La Plata Basin are enhanced during the LLJ events.

The lead-lag correlation indicates that the occurrence of anomalous meridional winds is negatively correlated with the anomalous rainfall events over La Plata Basin two days before. The correlation values are about -0.5 at 99% significant level, which indicate a weak but significant negative correlation between the northerly wind speeds and anomalous precipitation events. A day before the strong precipitation event, the correlation plots show negative values over Bolivia and a local maximum of positive values over central Argentina. These opposing values show the convergence of the warm moist air from the north and the cold and dry air from the southeast. The correlation intensifies during the cooccurrence of the two systems and dissipates the following days. The correlation values are also dependent on the large-scale influences of ENSO.

6.2 Outlook

Large MCSs are resolved in REMO, however to be able to represent the lifecycles of MCSs from individual deep convective clouds to organized systems, the use of a nonhydrostatic version of the REMO model is highly recommended.

In the last IPCC AR4 Report, the global simulations have predicted an increase likelihood of the extreme precipitation events over the La Plata basin. With the high resolution REMO, the effects of climate change due to anthropogenic sources on the relationship between MCSs and LLJs can be predicted using the available climate change simulations.

As mentioned in Chapter 2, the sensitivity studies have been done to mitigate the overestimation of surface temperature in the Amazon Basin during austral spring. In order to simulate the complexity of the land-atmosphere interactions, particularly the role of the Amazon rainforest and the swelling and falling of the rivers in the Amazon Basin, further studies must be conducted. Additionally, a smooth function of the permanent wilting point instead of the step-function (Equation 2.2) could be used to avoid sharp transitions at the edge of the forests. The results of these studies could potentially reduce further the warm bias over the Amazon Basin as well as a better representation of the hydrological cycle in the region.

6.3 Concluding remarks

With the high resolution simulation, the understanding of the LLJs and MCSs relationship are enhanced. A weak but significant anticorrelation between the meridional wind speed and precipitation develops two days before the heavy precipitation events. The day before the anomalous precipitation occur, high northerly wind speeds develop east of the Andes in Bolivia. The significantly strong correlation between the meridional wind speeds and precipitation the day before the occurrence of heavy rainfall events can aid in monitoring severe weather events over La Plata Basin.

References

Aldrian, E., D. Sein, D. Jacob, L. D. Gates and R. Podzun (2005). Modelling Indonesian rainfall with a coupled regional model. *Climate Dynamics*, **25**(1), 1–17. doi: 0.1007/s00382-004-0483-0.

Arakawa, A. (1988). Finite-difference methods in climate modeling. *Physically-Based Modelling and Simulation of Climate and Climatic Change NATO ASI Series*, **243**, 79–168. doi: 0.1007/978-94-009-3041-4_3.

Asselin, R. (1972). Frequency filter for time integrations. *Monthly Weather Review*, **100**(6), 487–490.

Bader, D., C. Covey, W. Gutowski, I. Held, K. Kunkel, R. Miller, R. Tokmakian and M. Zhang (2008). Climate models: an assessment of strengths and limitations. Technical report, U.S. Climate Change Science Program and the Subcommittee on Global Change Research, Department of Energy, Office of Biological and Environmental Research, Washington, D.C., USA.

Barreiro, M. and N. Diaz (2011). Land-atmosphere coupling in El Niño influence over South America. *Atmospheric Science Letters*, **12**(4), 351–355. doi: 0.1002/asl.348.

Barros, V., R. Clarke and P. Dias (2006). Climate Change in the La Plata Basin. Inter American Institute on Global Change, 221 pp.

Basara, J. B. and K. C. Crawford (2002). Linear relationships between root-zone soil moisture and atmospheric processes in the planetary boundary layer. *Journal of Geophysical Research*, **107**(D15), 4274. doi: 0.1029/2001JD000633.

Berbery, E. and V. Barros (2002). The hydrologic cycle of the La Plata basin in South America. *Journal of Hydrometeorology*, **3**, 630–645.

Berbery, E. H., J.-P. Boulanger and C. Ereno (2011). Special Issue on LPB. *CLIVAR Exchanges No. 57 (Vol. 16, No.3)*, **16**(57), 1–44.

Blackadar, A. (1957). Boundary layer wind maxima and their significance for the growth of nocturnal inversions. *Bulletin of the American Meteorological Society*, **38**(5), 283–290.

Bonner, W. D. (1968). Climatology of the Low Level Jet. *Monthly Weather Review*, **96**(12), 833–850.

Boulanger, J.-P., G. Brasseur, A. F. Carril, M. de Castro, N. Degallier, C. Ereño, H. Le Treut, J. A. Marengo, C. G. Menendez, M. N. Nuñez, O. C. Penalba, A. L. Rolla, M. Rusticucci and R. Terra (2009). A Europe–South America network for climate change assessment and impact studies. *Climatic Change*, **98**(3-4), 307–329. doi: 0.1007/s10584-009-9734-8.

Carril, A. F., C. G. Menéndez, A. R. C. Remedio, F. Robledo, A. Sörensson, B. Tencer, J.-P. Boulanger, M. Castro, D. Jacob, H. Treut, L. Z. X. Li, O. Penalba, S. Pfeifer, M. Rusticucci, P. Salio, P. Samuelsson, E. Sanchez and P. Zaninelli (2012). Performance of a multi-RCM ensemble for South Eastern South America. *Climate Dynamics*. doi: 0.1007/s00382-012-1573-z.

Carson, D., R. Mechoso and H. Cattle (2004). South American Low Level Jet Experiment SALLJEX. *CLIVAR Exchanges No. 29 (Vol. 9, No. 1)*, (July), 1–32.

Carvalho, L., C. Jones and B. Liebmann (2004). The South Atlantic convergence zone: Intensity, form, persistence, and relationships with intraseasonal to interannual activity and extreme rainfall. *Journal of Climate*, **17**, 88–108.

Cavalcanti, I., A. Carril, M. Barreiro, M. Bettolli, A. Cherchi, A. Grimm, R. Tedeschi, D. Jacob, C. Menéndez, O. Penalba, N. Pessacg, S. Pfeifer, A. Remedio, M. Renom, J. Rivera, F. Robledo, R. Ruscica, S. Solman, A. Sorensson, B. Tencer and P. Zaninelli (2011). CLARIS LPB WP6: Processes and Future Evolution of Extreme Climate Events in La Plata Basin. *CLIVAR Exchanges No. 57 (Vol. 16, No.3): Special Issue on LPB*, pp. 22–24.

Cavalcanti, I. F. A. (2012). Large scale and synoptic features associated with extreme precipitation over South America: A review and case studies for the first decade of the 21st century. *Atmospheric Research*, **118**, 27–40. doi: 0.1016/j.atmosres.2012.06.012.

Chen, G. T.-J. G., C.-C. C. Wang and D. D. T.-W. Lin (2005). Characteristics of Low-Level Jets over Northern Taiwan in Mei-Yu Season and Their Relationship to

Heavy Rain Events. *Monthly Weather Review*, **133**(1), 20–43. doi: 0.1175/MWR-2813.1.

Chen, J. L., C. R. Wilson, B. D. Tapley, L. Longuevergne, Z. L. Yang and B. R. Scanlon (2010). Recent La Plata basin drought conditions observed by satellite gravimetry. *Journal of Geophysical Research*, **115**(D22), D22108. doi: 0.1029/2010JD014689.

Chen, M., W. Shi, P. Xie, V. B. S. Silva, V. E. Kousky, R. Wayne Higgins and J. E. Janowiak (2008). Assessing objective techniques for gauge-based analyses of global daily precipitation. *Journal of Geophysical Research*, **113**(D4), D04110. doi: 0.1029/2007JD009132.

Christensen, J., B. Hewitson, A. Busuloc, A. Chen, X. Gao, I. Held, R. Jones, R. Kolli, W.-T. Kwon, R. Laprise, V. Magana Rueda, L. Mearns, C. G. Menendez, J. Raisanen, A. Rinke, A. Sarr and P. Whetton (2007). Regional climate projections. In *Climate Change, 2007: The Physical Science Basis. Contribution of Working Group I to the Fourth Assessment Report of the Intergovernmental Panel on Climate Change.* (edited by S. Solomon, D. Qin, M. Manning, Z. Chen, M. Marquis, K. B. Averyt, M. Tignor and H. L. Miller), chapter 11, pp. 846–940. Cambridge University Press, Cambridge, United Kingdom.

Cotton, W. R., G. Bryan and S. C. van den Heever (2011). Chapter 9: Mesoscale Convective Systems. In *Storm and Cloud Dynamics*, Vol. 99 of *International Geophysics*, pp. 455–526. Elsevier, San Diego, USA. ISBN 9780120885428.

CRU (2011). Viewing Climatic Research Unit (CRU) time-series datasets of variations in climate with variations in other phenomena.

da Silva, M. C. L., R. P. Rocha and R. Y. Ynoue (2010). Climatic simulations of the eastern Andes low-level jet and its dependency on convective parameterizations. *Meteorology and Atmospheric Physics*, **108**(1-2), 9–27. doi: 0.1007/s00703-010-0077-9.

Dai, A. (2001). Global precipitation and thunderstorm frequencies. Part I: Seasonal and interannual variations. *Journal of climate*, **14**, 1092–1111.

Davies, H. C. (1976). A lateral boundary formulation for multi-level prediction models. *Quarterly Journal of the Royal Meteorological Society*, **102**, 405–418.

Dee, D. P., S. M. Uppala, A. J. Simmons, P. Berrisford, P. Poli, S. Kobayashi, U. Andrae, M. A. Balmaseda, G. Balsamo, P. Bauer, P. Bechtold, A. C. M. Beljaars, L. van de Berg, J. Bidlot, N. Bormann, C. Delsol, R. Dragani, M. Fuentes, A. J. Geer, L. Haimberger, S. B. Healy, H. Hersbach, E. V. Hólm, L. Isaksen, P. Kå llberg, M. Köhler, M. Matricardi, A. P. McNally, B. M. Monge-Sanz, J.-J. Morcrette, B.-K. Park, C. Peubey, P. de Rosnay, C. Tavolato, J.-N. Thépaut and F. Vitart (2011). The ERA-Interim reanalysis: configuration and performance of the data assimilation system. *Quarterly Journal of the Royal Meteorological Society*, **137**(656), 553–597. doi: 0.1002/qj.828.

Durkee, J. D. and T. L. Mote (2009). A climatology of warm-season mesoscale convective complexes in subtropical South America. *International Journal of Climatology*, **30**(3), 418–431. doi: 0.1002/joc.1893.

Elizalde, A. (2011). The Water Cycle in the Mediterranean Region and the Impacts of Climate Change. PhD thesis, Universitaet Hamburg.

Fiedler, S., K. Schepanski, B. Heinold, P. Knippertz and I. Tegen (2012). A climatology of Nocturnal Low-level Jets over North-Africa and implications for simulating mineral dust emission. *EGU General Assembly Conference Abstracts*, **14**, 4529.

Garreaud, R. D., M. Vuille, R. Compagnucci and J. Marengo (2009). Present-day South American climate. *Palaeogeography, Palaeoclimatology, Palaeoecology*, **281**(3-4), 180–195. doi: 0.1016/j.palaeo.2007.10.032.

Giorgi, F., N. Diffenbaugh, X. Gao, E. Coppola, S. Dash, O. Frumento, S. Rauscher, A. Remedio, I. Sanda, A. Steiner, M. Sylla and A. Zakey (2008). The Regional Climate Change Hyper-Matrix Framework. *Eos, Transactions American Geophysical Union*, **89**(45), 445. doi: 0.1029/2008EO450001.

Giorgi, F., C. Jones and G. Asrar (2009). Addressing climate information needs at the regional level: the CORDEX framework. *WMO Bulletin*, **58**(3), 175–183.

Grimm, A. M. and R. G. Tedeschi (2009). ENSO and Extreme Rainfall Events in South America. *Journal of Climate*, **22**(7), 1589–1609. doi: 0.1175/2008JCLI2429.1.

Haensler, A., S. Hagemann and D. Jacob (2011). Dynamical downscaling of ERA40 reanalysis data over southern Africa: added value in the simulation of the seasonal rainfall characteristics. *International Journal of Climatology*, **31**(15), 2338–2349. doi: 0.1002/joc.2242.

Hagemann, S., M. Botzet, L. Dümenil and B. Machenhauer (1999). No. 289. Derivation of global GCM boundary conditions from 1 km land use satellite data. Technical Report 289, Max Planck Institute for Meteorology, Hamburg, Germany.

Hagemann, S. and L. Dümenil (2003). Improving a subgrid runoff parameterization scheme for climate models by the use of high resolution data derived from satellite observations. *Climate Dynamics*, **21**(3-4), 349–359. doi: 0.1007/s00382-003-0349-x.

Hobbs, J. E., J. A. Lindesay and H. A. Bridgman (1998). Climates of the Southern Continents: Present, Past and Future. John Wiley & Sons, Ltd, West Sussex, England. ISBN 978-0-471-94926-8, 318 pp.

Holton, J. (1967). The diurnal boundary layer wind oscillation above sloping terrain. *Tellus*, **19**(2), 199–205.

Houze, R. A. (2004). Mesoscale convective systems. *Reviews of Geophysics*, **42**(4), RG4003. doi: 0.1029/2004RG000150.

Hoyos, I., A. Baquero-Bernal and S. Hagemann (2013). How accurately are climatological characteristics and surface water and energy balances represented for the Colombian Caribbean Catchment Basin? *Climate Dynamics*. doi: 0.1007/s00382-013-1685-0.

Huffman, G. J., D. T. Bolvin, E. J. Nelkin, D. B. Wolff, R. F. Adler, G. Gu, Y. Hong, K. P. Bowman and E. F. Stocker (2007). The TRMM Multisatellite Precipitation Analysis (TMPA): Quasi-Global, Multiyear, Combined-Sensor Precipitation Estimates at Fine Scales. *Journal of Hydrometeorology*, **8**(1), 38–55. doi: 0.1175/JHM560.1.

Jacob, D. (2001). A note to the simulation of the annual and inter-annual variability of the water budget over the Baltic Sea drainage basin. *Meteorology and Atmospheric Physics*, **77**(1-4), 61–73. doi: 0.1007/s007030170017.

Jacob, D., A. Elizalde, A. Haensler, S. Hagemann, P. Kumar, R. Podzun, D. Rechid, A. R. Remedio, F. Saeed, K. Sieck, C. Teichmann and C. Wilhelm (2012). Assessing the Transferability of the Regional Climate Model REMO to Different COordinated Regional Climate Downscaling EXperiment (CORDEX) Regions. *Atmosphere*, **3**(4), 181–199. doi: 0.3390/atmos3010181.

Jacob, D. and R. Podzun (1997). Sensitivity studies with the regional climate model REMO. *Meteorology and Atmospheric Physics*, **63**, 119–129.

Jacob, D., B. J. J. M. Van den Hurk, U. Andrae, G. Elgered, C. Fortelius, L. P. Graham, S. D. Jackson, U. Karstens, C. Koepken, R. Lindau, R. Podzun, B. Rockel, F. Rubel, B. H. Sass, R. N. B. Smith and X. Yang (2001). A comprehensive model inter-comparison study investigating the water budget during the BALTEX-PIDCAP period. *Meteorology and Atmospheric Physics*, **77**(1-4), 19–43. doi: 0.1007/s007030170015.

Kanamitsu, M., W. Ebisuzaki, J. Woollen, S.-K. Yang, J. J. Hnilo, M. Fiorino and G. L. Potter (2002). NCEP–DOE AMIP-II Reanalysis (R-2). *Bulletin of the American Meteorological Society*, **83**(11), 1631–1643. doi: 0.1175/BAMS-83-11-1631.

Kjellström, E., F. Boberg, M. Castro, J. Christensen, G. Nikulin and E. Sánchez (2010). Daily and monthly temperature and precipitation statistics as performance indicators for regional climate models. *Climate Research*, **44**(2-3), 135–150. doi: 0.3354/cr00932.

Kleidon, A. and M. Heimann (2000). Assessing the role of deep rooted vegetation in the climate system with model simulations: mechanism, comparison to observations and implications for Amazonian deforestation. *Climate Dynamics*, **16**(2-3), 183–199. doi: 0.1007/s003820050012.

Kotlarski, S. (2007). A Subgrid Glacier Parameterisation for Use in Regional Climate Modelling. PhD thesis, Universitaet Hamburg.

Laing, A. and J. M. Fritsch (1997). The global population of mesoscale convective complexes. *Quarterly Journal of the Royal Meteorological Society*, **123**, 389–405.

Laprise, R., D. Kornic, M. Rapaić, L. Šeparović, M. Leduc, O. Nikiema, A. Luca, E. Diaconescu, A. Alexandru, P. Lucas-Picher, R. El´ia, D. Caya and S. Biner (2012). Considerations of Domain Size and Large-Scale Driving for Nested Regional Climate Models: Impact on Internal Variability and Ability at Developing Small-Scale Details. In *Climate Change* (edited by A. Berger, F. Mesinger and D. Sijacki), pp. 181–199. Springer Vienna. ISBN 978-3-7091-0972-4.

Lenters, J. and K. Cook (1997). On the origin of the Bolivian high and related circulation features of the South American climate. *Journal of the Atmospheric Sciences*, **54**, 656–678.

Li, W. and R. Fu (2004). Transition of the large-scale atmospheric and land surface conditions from the dry to the wet season over Amazonia as diagnosed by the ECMWF re-analysis. *Journal of Climate*, **17**, 2637–2651.

Liebmann, B. (1996). Description of a complete (interpolated) outgoing longwave radiation dataset. *Bulletin of the American Meteorological Society*, **77**(6), 1275–1277.

Lin, Y.-L. (2007). Mesoscale Dynamics. Cambridge University Press. ISBN 0521808758, 630 pp.

Lohmann, U. and E. Roeckner (1996). Design and performance of a new cloud microphysics scheme developed for the ECHAM general circulation model. *Climate Dynamics*, **12**(8), 557–572. doi: 0.1007/BF00207939.

Louis, J.-F. (1979). A parametric model of vertical eddy fluxes in the atmosphere. *Boundary-Layer Meteorology*, **17**(2), 187–202. doi: 0.1007/BF00117978.

Maddox, R. A. (1980). Mesoscale Convective Complexes. *Bulletin of the American Meteorological Society*, **61**(11), 1374–1387. doi: 0.1175/1520-0477(1980)061.

Majewski, D. (1991). The Europa-Modell of the Deutscher Wetterdienst. In *ECMWF Seminar Proceedings*, Vol. 2, pp. 147–191.

Marengo, J. (1995). Interannual variability of deep convection over the tropical South American sector as deduced from ISCCP C2 data. *International Journal of Climatology*, **15**, 995–1010.

Marengo, J., W. Soares, C. Saulo and M. Nicolini (2004). Climatology of the low-level jet east of the Andes as derived from the NCEP-NCAR reanalyses: Characteristics and temporal variability. *Journal of Climate*, **17**(12), 2261–2280.

Menéndez, C. G., M. Castro, J.-P. Boulanger, a. D'Onofrio, E. Sanchez, a. a. Sörensson, J. Blazquez, a. Elizalde, D. Jacob, H. Le Treut, Z. X. Li, M. N. Núñez, N. Pessacg, S. Pfeiffer, M. Rojas, a. Rolla, P. Samuelsson, S. a. Solman and C. Teichmann (2009). Downscaling extreme month-long anomalies in southern South America. *Climatic Change*, **98**(3-4), 379–403. doi: 0.1007/s10584-009-9739-3.

Menéndez, C. G., M. de Castro, A. Sorensson and J. P. Boulanger (2010). CLARIS Project: towards climate downscaling in South America. *Meteorologische Zeitschrift*, **19**(4), 357–362. doi: 0.1127/0941-2948/2010/0459.

Mitchell, T. D. and P. D. Jones (2005). An improved method of constructing a database of monthly climate observations and associated high-resolution grids. *International Journal of Climatology*, **25**(6), 693–712. doi: 0.1002/joc.1181.

Morcrette, J.-J., L. Smith and Y. Fourquart (1986). Pressure and temperature dependence of the absorption in longwave radiation parameterizations. *Beiträge zur Atmosphärenphysik*, **59**, 455–469.

Nesbitt, S., E. Zipser and D. Cecil (2000). A census of precipitation features in the Tropics using TRMM: Radar, ice scattering, and lightning observations. *Journal of Climate*, **13**, 4087–4106.

Nicolini, M., P. Salio and P. Borque (2006). Thermodynamic and kinematic characterization of the low-level troposphere during SALLJEX under different large-scale environments. In *Proceedings of International Conference on Southern Hemisphere Meteorology and Oceanography (ICSHMO), 8*, No. 1428, pp. 1141–1148. INPE, São José dos Campos, Brazil. ISBN 85-17-00023-4.

Nordeng, T. (1994). Extended versions of the convective parametrization scheme at ECMWF and their impact on the mean and transient activity of the model in the tropics. Technical report, European Center for Medium-Range Weather Forecasts.

Orlanski, I. (1975). A rational subdivision of scales for atmospheric processes. *Bulletin of the American Meteorological Society*, **56**(5), 527–530.

Pal, J. S., F. Giorgi, X. Bi, N. Elguindi, F. Solmon, S. a. Rauscher, X. Gao, R. Francisco, A. Zakey, J. Winter, M. Ashfaq, F. S. Syed, L. C. Sloan, J. L. Bell, N. S. Diffenbaugh, J. Karmacharya, A. Konaré, D. Martinez, R. P. da Rocha and A. L. Steiner (2007). Regional Climate Modeling for the Developing World: The ICTP RegCM3 and RegCNET. *Bulletin of the American Meteorological Society*, **88**(9), 1395–1409. doi: 0.1175/BAMS-88-9-1395.

Perkins, S. E., a. J. Pitman, N. J. Holbrook and J. McAneney (2007). Evaluation of the AR4 Climate Models' Simulated Daily Maximum Temperature, Minimum Temperature, and Precipitation over Australia Using Probability Density Functions. *Journal of Climate*, **20**(17), 4356–4376. doi: 0.1175/JCLI4253.1.

Pesquero, J. F., S. C. Chou, C. A. Nobre and J. A. Marengo (2009). Climate downscaling over South America for 1961–1970 using the Eta Model. *Theoretical and Applied Climatology*, **99**(1-2), 75–93. doi: 0.1007/s00704-009-0123-z.

Pfeifer, S. (2006). Modeling cold cloud processes with the regional climate model REMO. PhD thesis, Universitaet Hamburg.

Rechid, D. (2009). On biogeophysical interactions between vegetation phenology and climate simulated over Europe. PhD thesis, Universitaet Hamburg.

Rechid, D. and D. Jacob (2006). Influence of monthly varying vegetation on the simulated climate in Europe. *Meteorologische Zeitschrift*, **15**(1), 99–116. doi: 0.1127/0941-2948/2006/0091.

Roeckner, E., K. Arpe, L. Bengtsson, M. Christoph, M. Claussen, L. Dueminil, M. Esch, M. Giorgetta, U. Schlese and U. Schulzweida (1996). Report No. 218: The atmospheric general circulation model ECHAM-4: Model description and simulation of present-day climate. Technical Report 218, Max Planck Institute for Meteorology, Hamburg, Germany.

Roeckner, E., G. Bäuml, L. Bonaventura, R. Brokopf, M. Esch, M. Giorgetta, S. Hagemann, I. Kirchner, L. Kornblueh, E. Manzini, A. Rhodin, U. Schlese, U. Schulzweida and A. Tompkins (2003). Report No. 349. The Atmospheric General Circulation Model ECHAM5, Part 1: Model Description. Technical Report 349, Max Planck Institute for Meteorology, Hamburg, Germany.

Rossow, W. and R. Schiffer (1999). Advances in understanding clouds from ISCCP. *Bull. Amer. Meteor. Soc*, **80**, 2261–2288.

Rozante, J. R. and I. F. A. Cavalcanti (2008). Regional Eta model experiments: SALLJEX and MCS development. *Journal of Geophysical Research*, **113**(D17), D17106. doi: 0.1029/2007JD009566.

Rozante, J. R., D. S. Moreira, L. G. G. de Goncalves and D. a. Vila (2010). Combining TRMM and Surface Observations of Precipitation: Technique and Validation over South America. *Weather and Forecasting*, **25**(3), 885–894. doi: 0.1175/2010WAF2222325.1.

Saeed, F., S. Hagemann, S. Saeed and D. Jacob (2012). Influence of mid-latitude circulation on upper Indus basin precipitation: the explicit role of irrigation. *Climate Dynamics*, **40**(1-2), 21–38. doi: 0.1007/s00382-012-1480-3.

Salio, P., M. Nicolini and A. Saulo (2002). Chaco low-level jet events characterization during the austral summer season. *Journal of Geophysical Research*, **107**(D24), 4816. doi: 0.1029/2001JD001315.

Salio, P., M. Nicolini and E. J. Zipser (2007). Mesoscale Convective Systems over Southeastern South America and Their Relationship with the South American Low-Level Jet. *Monthly Weather Review*, **135**(4), 1290–1309. doi: 0.1175/MWR3305.1.

Samuelsson, P., S. Solman, E. Sanchez, R. Rocha and L. Li (2013). Regional climate change projections over South America based on the CLARIS-LPB RCM ensemble. In *European Geosciences Union*, Vol. 15, p. 5800.

Satyamurty, P., C. A. Nobre and P. L. Silva Dias (1998). South America. *Meteorological Monographs*, **27**(49), 119–139.

Saulo, A., M. Nicolini and S. Chou (2000). Model characterization of the South American low-level flow during the 1997–1998 spring–summer season. *Climate Dynamics*, **16**, 867–881.

Saulo, C., J. Ruiz and Y. G. Skabar (2007). Synergism between the Low-Level Jet and Organized Convection at Its Exit Region. *Monthly Weather Review*, **135**(4), 1310–1326. doi: 0.1175/MWR3317.1.

Schumacher, C. and R. A. Houze (2003). Stratiform Rain in the Tropics as Seen by the TRMM Precipitation Radar*. *Journal of Climate*, **16**(11), 1739–1756. doi: 0.1175/1520-0442(2003)016.

Semmler, T. (2002). Der Wasser- und Energiehaushalt der arktischen Atmosphäre. PhD thesis, Universitaet Hamburg.

Silvestri, G., C. Vera, D. Jacob, S. Pfeifer and C. Teichmann (2008). A high-resolution 43-year atmospheric hindcast for South America generated with the MPI regional model. *Climate Dynamics*, **32**(5), 693–709. doi: 0.1007/s00382-008-0423-5.

Simmons, A. and D. Burridge (1981). An energy and angular-momentum conserving vertical finite-difference scheme and hybrid vertical coordinates. *Monthly Weather Review*, **109**(4), 758–766.

Solman, S., E. Sanchez, P. Samuelsson, E. Berbery, A. Remedio, R. da Rocha, S. Chou and L. Li (2011). CLARIS LPB WP5: Regional Climate Change assessments for La Plata Basin. *CLIVAR Exchanges No. 57 (Vol. 16, No.3): Special Issue on LPB*, pp. 19–21.

Solman, S. A. and N. L. Pessacg (2011). Regional climate simulations over South America: sensitivity to model physics and to the treatment of lateral boundary conditions using the MM5 model. *Climate Dynamics*, **38**(1-2), 281–300. doi: 0.1007/s00382-011-1049-6.

Solman, S. A., E. Sanchez, P. Samuelsson, R. P. Rocha, L. Li, J. Marengo, N. L. Pessacg, A. R. C. Remedio, S. C. Chou, H. Berbery, H. Treut, M. Castro and D. Jacob (2013). Evaluation of an ensemble of regional climate model simulations over South America driven by the ERA-Interim reanalysis: model performance and uncertainties. *Climate Dynamics*. doi: 0.1007/s00382-013-1667-2.

Stensrud, D. J. (1996). Importance of Low-Level Jets to Climate: A Review. *Journal of Climate*, **9**(8), 1698–1711. doi: 0.1175/1520-0442(1996)009.

Stensrud, D. J. (2007). Parameterization Schemes: Keys to Understanding Numerical Weather Prediction Models. Cambridge University Press, Cambridge, United Kingdom. ISBN 9780521865401, 459 pp.

Stull, R. (2000). Meteorology for scientists and engineers : a technical companion book with Ahrens' Meteorology Today. Brooks/Cole, Pacific Grove, CA. ISBN 0534372147.

Sturm, C., G. Hoffmann and B. Langmann (2007). Simulation of the Stable Water Isotopes in Precipitation over South America: Comparing Regional to Global Circulation Models. *Journal of Climate*, **20**(15), 3730–3750. doi: 0.1175/JCLI4194.1.

Sugahara, S., R. P. da Rocha and M. Rodrigues (1994). Condicoes atmosfericas de grande escala associadas a jato de baixos niveis na America do Sul. In *Anais do VIII Congresso Brasileiro de Meteorologia*, pp. 1383–1387. SBMET.

Teichmann, C. (2010). Climate and Air Pollution Modelling in South America with Focus on Megacities. PhD thesis, Universitaet Hamburg.

Teichmann, C., B. Eggert, A. Elizalde, A. Haensler, D. Jacob, P. Kumar, C. Moseley, S. Pfeifer, D. Rechid, A. R. C. Remedio, H. Ries, J. Petersen, S. Preuschmann, T. Raub, F. Saeed, K. Sieck and T. Weber (2013). How does a regional climate model modify the projected climate change signal of the driving GCM: A study over different CORDEX regions using REMO. *Atmosphere*, **submitted**.

Thunis, P. and R. Bornstein (1996). Hierarchy of Mesoscale Flow Assumptions and Equations. *Journal of the Atmospheric Sciences*, **53**(3), 380–397.

Tiedtke, M. (1989). A comprehensive mass flux scheme for cumulus parameterization in large-scale models. *Monthly Weather Review*, **117**, 1779–1800.

Town, M. S., V. P. Walden and S. G. Warren (2007). Cloud cover over the South Pole from visual observations, satellite retrievals, and surface-based infrared radiation measurements. *Journal of Climate*, **20**(3), 544–559. doi: 0.1175/JCLI4005.1.

Trewartha, G. T. (1954). An Introduction to Climate, Vol. 3rd ed. McGraw-Hill, New York, USA.

Velasco, I. and J. Fritsch (1987). Mesoscale convective complexes in the Americas. *Journal of Geophysical Research*, **92**(8), 9591–9613.

Vera, C., J. Baez, M. Douglas, C. B. Emmanuel, J. Marengo, J. Meitin, M. Nicolini, J. Nogues-Paegle, J. Paegle, O. Penalba, P. Salio, C. Saulo, M. a. Silva Dias, P. Silva Dias and E. Zipser (2006a). The South American Low-Level Jet Experiment. *Bulletin of the American Meteorological Society*, **87**(1), 63–77. doi: 0.1175/BAMS-87-1-63.

Vera, C., W. Higgins, J. Amador, T. Ambrizzi, R. Garreaud, D. Gochis, D. Gutzler, D. Lettenmaier, J. Marengo, C. R. Mechoso, J. Nogues-Paegle, P. L. S. Dias and C. Zhang (2006b). Toward a Unified View of the American Monsoon Systems. *Journal of Climate*, **19**(20), 4977–5000. doi: 0.1175/JCLI3896.1.

Vera, C., G. Silvestri, V. Barros and A. Carril (2004). Differences in el nino response over the southern hemisphere. *Journal of climate*, **17**, 1741–1754.

Vernekar, A. D., B. P. Kirtman and M. J. Fennessy (2003). Low-Level Jets and Their Effects on the South American Summer Climate as Simulated by the NCEP Eta Model*. *Journal of Climate*, **16**(2), 297–311. doi: 0.1175/1520-0442(2003)016.

Whiteman, C., X. Bian and S. Zhong (1997). Low-level jet climatology from enhanced rawinsonde observations at a site in the southern Great Plains. *Journal of Applied Meteorology*, **36**, 1363–1376.

Wilks, D. S. (2006). Statistical Methods in the Atmospheric Sciences: An Introduction. Elsevier, San Diego, California. ISBN 0127519661, 627 pp.

Zipser, E. J., C. Liu, D. J. Cecil, S. W. Nesbitt and D. P. Yorty (2006). Where Are the Most Intense Thunderstorms on Earth? *Bulletin of the American Meteorological Society*, **87**(8), 1057–1071. doi: 0.1175/BAMS-87-8-1057.

Zipser, E. J., P. Salio and M. Nicolini (2004). Mesoscale Convective Systems activity during SALLJEX and the relationship with SALLJ. *CLIVAR Exchanges No. 29 (Vol. 9, No. 1)*, pp. 14–19.

A List of Abbreviations and Acronyms

CLARIS-LPB	A Europe South-America Network for Climate Change Assessment and Impact Studies in the La Plata Basin
CORDEX	COordinated Regional Downscaling EXperiment
CPCUNI	NOAA Climate Prediction Center for Unified Precipitation
CRU	University of East Anglia Climate Research Unit
ECHAM	Atmospheric General Circulation Model developed at the Max Planck Institute for Meteorology
ECMWF	European Centre for Medium-Range Weather Forecasts
ERA40	ECMWF ERA 40-year Reanalysis
EITR	ECMWF ERA-Interim Reanalysis
ENSO	El Niño Southern Oscillations
IPCC	Integovernmental Panel on Climate Change
ISCCP	International Satellite Cloud Climatology
ITCZ	Intertropical Convergence Zone
LLJ	Low-level jet
MCS	Mesoscale convective system
MERGE	Merged TRMM and raingauge datasets over South America
NASA	National Aeronautics and Space Administration
NOAA	National Oceanic and Atmospheric Administration
NCEP	The United States National Center for Environmental Prediction – National Center for Atmospheric Research reanalysis
OLR	Outgoing Longwave Radiation
ONI	Oceanic Niño Index (ONI)
PACS-SONET	Pan American Climate Studies–SOunding NETwork
RCM	Regional Climate Model
REMO	REgional MOdel
SACZ	South Atlantic Convergence Zone
SALLJEX	South America Low-level Jet Experiment
TRMM	Tropical Rainfall Measuring Mission

B Remo Model Runs

REMO model simulations performed within this study are listed in the table. The table also shows a brief description of the runs and the simulation period.

Name	Description	Period
REMO_{CTRL}	REMO control run, standard REMO2009	1989-2008
$\text{REMO}_{0.25}$	25% f_{pwp} reduction over the whole domain	1989-1990
$\text{REMO}_{0.10}$	10% f_{pwp} reduction over the whole domain	1989-1990
$\text{REMO}_{0.10forest}$	10% f_{pwp} reduction over the forested region only	1989-2008
REMO A1B	REMO driven by ECHAM5 A1B Run 3	1950-2100
REMO RCP2.6	REMO driven by MPI-ESM RCP2.6	1950-2100
REMO RCP4.5	REMO driven by MPI-ESM RCP4.5	1950-2100
REMO RCP8.5	REMO driven by MPI-ESM RCP8.5	1950-2100

C CLARIS-LPB Regional Climate Simulations

Regional Climate Model Simulations (RCMs) within the framework of the EU FP7 CLARIS-LPB Project are listed in Table C.1.

Model version (abbrev)	Institution & Country	Grid type, size	Vertical coordinate, levels	*LBC**, sponge zone	Convection scheme	Land surface scheme	Spin-up period	Basic references
RCA3.5 (SMHI-RCA)	Swedish Meteorological & Hydrological Institude SWEDEN	Rotated lat/lon 134x155	Hybrid 40	Davies (1976), 8 pts	Kain & Fritsch (1990, 1993), Kain (2004), Jones & Sanchez (2002)	Samuelsson et al. (2006)	11 mos.	Samuelsson et al. (2010), Samuelsson et al. (2011)
REMO2009 (MPIM-REMO)	Max-Planck-Institute for Meteorology GERMANY	Rotated lat/lon 151x181	Hybrid 31	Davies (1976), 8 pts	Tiedtke (1989), Nordeng (1994)	Dümenil & Todini (1992) Rechid & Jacob (2006)	20 yrs.	Jacob et al. (2001) Jacob et al. (2012)
PROMES2.4 (UCLM-PROMES)	Universidad Castilla-La Mancha SPAIN	Lambert conformal 145x163	Pressure-based sigma 37	Davies (1976), 10 pts	Kain & Fritsch (1993) Kain (2004)	Krinner et al. (2005), De Rosnay & Polder (1998), Sitch et al. (2003)	3 yrs.	Sanchez et al. (2007) Dominguez et al. (2010)
RegCM3 (USP-RegCM3)	Universidade de São Paulo BRAZIL	Rotated Mercator 190x202	Terrain-following sigma 18	Davies (1976), 12 pts	Grell (1993)	Dickinson et al. (1993)	12 mos.	Pal et al. (2007) da Rocha et al (2009)
MM5V3.7 (CIMA-MM5)	Centro de Investigaciones del Mar y la Atmósfera ARGENTINA	Mercator 150x203	sigma 23	Stauffer and Seaman, 1990) 8 pts	Grell (1993)	Chen & Dudhia (2001)	2 mos.	Grell et al. (1993) Solman and Pessacg (2011)
LMDZ4 (IPSL-LMDZ)	Institute Pierre - Simon Laplace FRANCE	Irregular rectangular lat/lon 184x180	Hybrid σ-p 19	32 pts	Emanuel (1991, 1993)	Krinner et al. (2005)	12 mos.	Hourdin et al. (2006) Li (1999)
ETA-CC** V1.0 (INPE-ETA)	Instituto Nacional de Pesquisas Espaciais BRAZIL	Regular lat/lon 123x245	Eta 38	Messinger (1977) 1 pt	Betts & Miller (1986)	Ek et al (2003)	12 mos.	Pesquero et al. (2009) Chou et al. (2011)

Table C.1: Summary of regional climate models used in the CLARIS-LPB. The model abbrevations in parentheses e.g. **MPIM-REMO** are generally used as short names for the models. **Lateral Boundary Conditions.* ***Climate Change*

D Observational datasets

The observational datasets and parameters used throughout the study from various sources are listed in Table D.1.

Table D.1: List of observations and reanalysis datasets used to evaluate the REMO simulation. The variables used are the wind components (u, v), temperature (t), geopotential height (gpm), pressure (p), precipitation $(prec)$, total cloud cover (clt), and outgoing longwave radiation (OLR).

Acronym	Dataset	Variables	Resolution & coverage	Available Period	References
EITR	ECMWF ERA-Interim Reanalysis	$u, v,$ gpm, t, p	T255 (0.7 °) resolution, 37 model levels, 6-hourly	1979-present	Dee et al. (2011)
NCEP	NCEP Reanalysis	u, v	2.5 ° resolution, 17 model levels, 6-hourly	1979-present	Kanamitsu et al. (2002)
SALLJEX	South American Low Level Jet Experiment	u, v	station data, intermittent frequency	Nov 2002 to Feb 2003	Vera et al. (2006a)
CRU*	UEA CRU Version TS3.0 Version TS3.1	$t, prec$	0.5 ° resolution global, land only, monthly	1901-2006 1901-2008	Mitchell and Jones (2005)
NOAA	NOAA OLR	OLR	2.5 ° resolution, daily and monthly	June 1974 to present	Liebmann (1996)
ISCCP	NOAA/ NESDIS/ NCDCC	clt	280 km resolution, daily and monthly	July 1983 to June 2008	Rossow and Schiffer (1999)
CPCUNI	NOAA Climate Prediction Center Unified Precipitation Analysis	$prec$	0.5°, land only, daily	1979-present	Chen et al. (2008)
TRMM	Tropical Rain Measuring Mission	$prec$	0.25°, 50 °S to 50 °N satellite estimates, 3-hourly	1998-2008	Huffman et al. (2007)
MERGE	Merged TRMM and rain gauge	$prec$	0.22°, South America, land only, daily	1998-2008	Rozante and Cavalcanti (2008)

*The sensitivity experiments use the available CRU Version TS3.0. For the long term simulations, the latest version was used. No significant differences between the two datasets (CRU, 2011) exist.

E Published Manuscript I

Silvina A. Solman[1], E. Sanchez[2], P. Samuelsson[3], R. P. da Rocha[4], L. Li[5], J. Marengo[6], N. L. Pessacg[7], **A.R. C. Remedio**[8], S. C. Chou[9], H. Berbery[10], H. Le Treut[2], M. de Castro[2], D. Jacob[8,11], 2013. Evaluation of an ensemble of regional climate model simulations over South America driven by the ERA-Interim reanalysis: model performance and uncertainties. *Climate Dynamics*. doi: 0.1007/s00382-013-1667-2.

Author's contributions: **ARCR** performed the REMO simulations, prepared and analyzed the data, and revised the paper in response to peer-reviewers' comments. All authors participated in the discussion of results, writing, and revision process of the manuscript.

[1]Centro de Investigaciones del Mar y la Atmosfera, CIMA/CONICET-UBA, DCAO/FCEN-UBA,UMI IFAECI/CNRS, Ciudad Universitaria Pabellon II Piso 2, C1428EGA Buenos Aires, Argentina

[2]Facultad Ciencias Ambientales y Bioquimica, Universidad de Castilla-La Mancha, Toledo, Spain

[3]Rossby Centre, SMHI, 601 76 Norrkoping, Sweden

[4]Departamento de Ciencias, Atmosfericas, Instituto de Astronomia, Geofi sica e Ciencia Atmosfericas, Universidade de Sao Paulo, Sao Paulo, Brazil

[5]Laboratoire de Meteorologie, Dynamique, IPSL, CNRS/UPMC, Paris, France

[6]Centro de Ciencia do Sistema Terrestre-Instituto Nacional de Pesquisas Espaciais (CCST INPE), Rodovia Dutra km, 40, 12630-000 Cachoeira Paulista, Sao Paulo, Brazil

[7]Centro Nacional Patagonico (CENPAT/CONICET), U9120ACF Puerto Madryn, Chubut, Argentina

[8]Max Planck Institute for Meteorology, 20146 Hamburg, Germany

[9]Centro de Previsao de Tempo e Estudos Climaticos-Instituto Nacional de Pesquisas Espaciais (CPTEC INPE), Rodovia Dutra km, 40, Cachoeira Paulista, Sao Paulo 12630-000, Brazil

[10]Earth System Science Interdisciplinary Center (ESSIC), University of Maryland, 5825 University Research Court, Suite 4001, College Park, MD 20740-3823, USA

[11]Climate Service Center, 20095 Hamburg, Germany

Abstract

The capability of a set of 7 coordinated regional climate model simulations performed in the framework of the CLARIS-LPB Project in reproducing the mean climate conditions over the South American continent has been evaluated. The model simulations were forced by the ERA-Interim reanalysis dataset for the period 1990–2008 on a grid resolution of 50 km, following the CORDEX protocol. The analysis was focused on evaluating the reliability of simulating mean precipitation and surface air temperature, which are the variables most commonly used for impact studies. Both the common features and the differences among individual models have been evaluated and compared against several observational datasets. In this study the ensemble bias and the degree of agreement among individual models have been quantified. The evaluation was focused on the seasonal means, the area-averaged annual cycles and the frequency distributions of monthly means over target subregions. Results show that the Regional Climate Model ensemble reproduces adequately well these features, with biases mostly within $\pm$ 2 $^{\circ}C$ and $\pm$ 20 % for temperature and precipitation, respectively. However, the multi-model ensemble depicts larger biases and larger uncertainty (as defined by the standard deviation of the models) over tropical regions compared with subtropical regions. Though some systematic biases were detected particularly over the La Plata Basin region, such as underestimation of rainfall during winter months and overestimation of temperature during summer months, every model shares a similar behavior and, consequently, the uncertainty in simulating current climate conditions is low. Every model is able to capture the variety in the shape of the frequency distribution for both temperature and precipitation along the South American continent. Differences among individual models and observations revealed the nature of individual model biases, showing either a shift in the distribution or an overestimation or underestimation of the range of variability.

F Published Manuscript II

Jacob, D.[1,2], A. Elizalde[2], A. Haensler[1], S. Hagemann[2], P. Kumar[2], R. Podzun[2], D. Rechid[2], **A.R. C. Remedio**[2], F. Saeed[1] K. Sieck[2], C. Teichmann[2], C. Wilhelm[2], (2012). Assessing the Transferability of the Regional Climate Model REMO to Different COordinated Regional Climate Downscaling EXperiment (CORDEX) Regions. *Atmosphere*, 3(1), 181–199. doi: 0.3390/atmos3010181.

Author's contributions: **ARCR** simulated the South America domain using REMO, prepared and analyzed observational data and model simulations, performed statistical analysis using probability distribution functions, prepared the manuscript and revised it in response to reviewers' comments. All authors participated in the discussion of results, writing, and revision process of the manuscript.

[1]Climate Service Center, 20095 Hamburg, Germany
[2]Max Planck Institute for Meteorology, 20146 Hamburg, Germany

Abstract

The transferability of the regional climate model REMO with a standard setup over different regions of the world has been evaluated. The study is based on the idea that the modeling parameters and parameterizations in a regional climate model should be robust to adequately simulate the major climatic characteristic of different regions around the globe. If a model is not able to do that, there might be a chance of an "overtuning" to the "home-region", which means that the model physics are tuned in a way that it might cover some more fundamental errors, e.g., in the dynamics. All simulations carried out in this study contribute to the joint effort by the international regional downscaling community called COordinated Regional climate Downscaling EXperiment (CORDEX). REMO has been integrated over six CORDEX domains forced with the so-called perfect boundary conditions obtained from the global reanalysis dataset ERA-Interim for the period 1989 to 2008. These six domains include Africa, Europe, North America, South America, West Asia and the Mediterranean region. Each of the six simulations was conducted with the identical model setup which allows investigating the transferability of a single model to regions with substantially different climate characteristics. For the consistent evaluation over the different domains, a new evaluation framework is presented by combining the Köppen-Trewartha climate classification with temperature-precipitation relationship plots and a probability density function (PDF) skill score method. The evaluation of the spatial and temporal characteristics of simulated precipitation and temperature, in comparison to observational datasets, shows that REMO is able to simulate the mean annual climatic features over all the domains quite reasonably, but still some biases remain. The regions over the Amazon and near the coast of major upwelling regions have a significant warm bias. Wet and dry biases appear over the mountainous regions and East Africa, respectively. The temperature over South America and precipitation over the tundra and highland climate of West Asia are misrepresented. The probable causes leading to these biases are discussed and ideas for improvements are suggested. The annual cycle of precipitation and temperature of major catchments in each domain are also well represented by REMO. The model has performed well in simulating the inter- and intra- seasonal characteristics of different climate types in different regions. Moreover, the model has a high ability in representing the general characteristics of different climate types as measured by the probability density function (PDF) skill score method. Although REMO seems to perform best over its home domain in Europe (domain of development and testing), the model has simulated quite well the climate characteristics of other regions

with the same set of parameterization options. Therefore, these results lead us to the conclusion that REMO is well suited for long-term climate change simulations to examine projected future changes in all these regions.

G Published Manuscript III

A. F. Carril[1,2,3], C. G. Menendez[1,3], **A.R. C. Remedio**[4], F. Robledo[2], A. Sorensson[1,3], B. Tencer[2], J.-P. Boulanger[5], M. de Castro[6], D. Jacob[4], H. Le Treut[7], L. Z. X. Li[7], O. Penalba[2,3], S. Pfeifer[4], M. Rusticucci[2,3], P. Salio[1,2,3], P. Samuelsson[8], E. Sanchez[6], P. Zaninelli[1,3], (2012). Performance of a multi-RCM ensemble for South Eastern South America. *Climate Dynamics*. doi: 0.1007/s00382-012-1573-z.

Author's contributions: **ARCR** prepared and analyzed observational data and model simulations, performed statistical analysis using box-and-whiskers-plot and revised the paper in response to reviewers' comments. All authors participated in the discussion of results, the writing, and revision process of the manuscript.

[1]Centro de Investigaciones del Mar y la Atmosfera (CIMA), CONICET-UBA, Ciudad Universitaria, Ciudad Autonoma de Buenos Aires, Int. Guiraldes 2160, Pabellon 2, Piso 2, C1428EGA Buenos Aires, Argentina

[2]Departamento de Ciencias de la Atmosfera y los Oceanos (DCAO), FCEN, Universidad de Buenos Aires, Buenos Aires, Argentina

[3]UMI IFAECI/CNRS, Buenos Aires, Argentina

[4]Max Planck Institute for Meteorology (MPI-M), Hamburg, Germany

[5]LOCEAN, UMR CNRS/IRD/UPMC, Paris, France

[6]Universidad de Castilla-La Mancha (UCLM), Toledo, Spain

[7]Laboratoire de Meteorologie Dynamique (LMD), Institut-Pierre-Simon-Laplace et Ecole Doctorale, Sciences de l'Environnementen Ile de France, Paris, France

[8]Swedish Meteorological and Hydrological Institute (SMHI), Norrkoping, Sweden

Abstract

The ability of four regional climate models to reproduce the present-day South American climate is examined with emphasis on La Plata Basin. Models were integrated for the period 1991–2000 with initial and lateral boundary conditions from ERA-40 Reanalysis. The ensemble sea level pressure, maximum and minimum temperatures and precipitation are evaluated in terms of seasonal means and extreme indices based on a percentile approach. Dispersion among the individual models and uncertainties when comparing the ensemble mean with different climatologies are also discussed. The ensemble mean is warmer than the observations in South Eastern South America (SESA), especially for minimum winter temperatures with errors increasing in magnitude towards the tails of the distributions. The ensemble mean reproduces the broad spatial pattern of precipitation, but overestimates the convective precipitation in the tropics and the orographic precipitation along the Andes and over the Brazilian Highlands, and underestimates the precipitation near the monsoon core region. The models overestimate the number of wet days and underestimate the daily intensity of rainfall for both seasons suggesting a premature triggering of convection. The skill of models to simulate the intensity of convective precipitation in summer in SESA and the variability associated with heavy precipitation events (the upper quartile daily precipitation) is far from satisfactory. Owing to the sparseness of the observing network, ensemble and observations uncertainties in seasonal means are comparable for some regions and seasons.

Acknowledgements

A lot of people have helped me along my PhD journey, gave time, inspirations and fruitful discussions. I may not be able to mention all of them but in my heart, I am always indebted to them because they share precious moments with me.

I am deeply grateful for Dr. Daniela Jacob and Dr. Susanne Pfeifer for the knowledge, supervision, and encouragement through the years. Thank you Prof. Hartmut Graßl for the fruitful panel meetings, useful insights, and guidance.

My sincere thanks to Dr. Antje Weitz, Cornelia Kampann, and Wiebke Böhm for their immense support in the International Max Planck Research School on Earth System Modelling. Thank you also for fellow IMPRS PhD candidates from 2009 to 2013, the discussions during retreat and seminars are helpful.

The research leading to these results has received funding from the European Community's Seventh Framework Programme (FP7/2007-2013) under Grant Agreement Nº 212492: CLARIS LPB, A Europe-South America Network for Climate Change Assessment and Impact Studies in La Plata Basin. Thank you Dr. Jose Rozante for sharing the MERGE data. It has been a pleasure working with the CLARIS LPB Family especially with Dr. Silvina Solman, Dr. Patrick Samuelsson, Dr. Enrique Sanchez, Dr. Andrea Carril, Dr. Claudio Menendez, Dr. Iracema Cavalcanti, Dr. Rosmeri da Rocha, Dr. Sin Chan Sou, Dr. Laurent Li. I would like to mention my roommate for life, Stefanie Talento, for the scientific and life integration with the Latin American culture.

I am indebted to the Dr. Stefan Hagemann, Dr. Dmitry Sein, Dr. Diana Rechid, Dr. Christopher Moseley, Julianne Petersen, Thomas Raub, Sherdon Niño Uy, and Ena Caren Edralin for reading my chapters, giving comments, and discussions. A special mention of thanks for Dr. Fahad Saeed for giving me the necessary push especially on the correlation analysis and to Christof Wilhelm for introducing REMO-imove. From Earth to Saturn, my deepest appreciation to Dr. Joseph Pagaran for carefully scrutinizing my chapters.

I am grateful for Daniela for giving me the opportunity to work with great minds in the very dynamic REMO Group. I am thankful for the discussions with my colleagues in the REMO Group.

Thank you Natasha, Suvarchal, Seethala, Ritthik, and Harshi for scientific arguments and deep friendship develop over tea, coffee, and biscuit breaks. Hamburg is a home thanks to various bonding activities organized by Christina, Thomas, Alberto, Christine, Kevin, Julianne, Antje, Swantje, Claas, Bastian, Katrin, and Natalie. I am also grateful for Ivie, Jade, Cheska, Joseph, and Julie for reminding

me of home.

I would also like to thank former colleagues and supervisors at the Manila Observatory, the Jesuits especially Fr. Jett, Fr. Dan, Fr. Su, Fr. Badillo, the Airheads (Faye, Franz, Genie, Grace, Toad, Rolly, Nino, Loric), the abdus salam International Centre for Theoretical Physics Family, the IM2P especially my twin, Dr. Rondrotiana Barimalala for springboarding my interest and passion in learning the atmospheric sciences and for the constant prayers.

I am grateful for the constant companionship of Shantanu. Thank you for the support and encouragement throughout the years. Thank you to Weng, Kai, Niño, Elena, and the Magic Anonymous gang for sharing precious times with me wherever I go.

Without the constant support, prayers, love, and encouragement of my family, I would have not made it. All the blood, sweat, tears, and joy brought by the struggle of this journey, I dedicate this to you Dr. Mama Melodia, Marc Melart, Patrick Art, Phillip Charles, Ena Caren–Perlou–Carper Louren, Clarisse Armie–Jolly Clyde–Jolly Armelle–Luis Alejo, Artemio Emmanuel, Marianne Mae.

This thesis is specially dedicated to my Papa Artemio^{+} who has been and always be an inspiration to strive harder in life and to continue fighting the good fight. *Pang, para ni sa imo!*

I offer thanks and praise to God. All this, for His greater glory.
AM^{+}DG



ISSN 1614-1199